PLASMA POSITION CONTROL IN A TOKAMAK EXPERIMENTAL POWER REACTOR

by

CPT. WILLIAM W. SAYLOR

B.S., United States Military Academy

(1972)

SUBMITTED IN PARTIAL FULFILLMENT

OF THE REQUIREMENTS FOR THE

DEGREE OF

MASTER OF SCIENCE

at the

MASSACHUSETTS INSTITUTE OF TECHNOLOGY

January 1977

Signature of Author.....William W. Saylor, Cpt. CE.....
Department of Nuclear Engineering, January 1977

Certified by.....
Thesis Supervisor

Accepted by.....
Chairman, Department Committee

PLASMA POSITION CONTROL IN A TOKAMAK EXPERIMENTAL POWER REACTOR

by

Cpt William W. Saylor

Submitted to the Department of Nuclear Engineering in partial fulfillment of the requirements for the degree of Master of Science.

Abstract

The plasma position control requirements for a Tokamak experimental power reactor are examined. The design of a candidate plasma position control system is synthesized and the result is tested by computer simulation of a tokamak reactor. The performance is analyzed and recommendations are made for future studies in areas where problems were identified.

Thesis Supervisor: Lawrence M. Lidsky
Associate Professor
Department of Nuclear Engineering

Thesis Advisor: Theodore N. Edelbaum
Lecturer
Department of Aeronautics and Astronautics

ACKNOWLEDGEMENTS

This work was supported by the Charles S. Draper Labratory, Inc under Electric Power Research Institute Contract Number RP546-2.

I wish to thank my thesis advisor Lawrence M. Lidsky and my thesis reader Theodore N. Edelbaum for their understanding and guidance during the completion of this project. I also wish to thank Paul Madden for his help in understanding the control aspects of the problem and Robert Var for his moral and physical support in completing the computer simulation. My wife, Cathy, and Linda Martinez also deserve much thanks for typing this manuscript.

Publication of this thesis does not constitute approval by Draper Labratory or the Electric Power Research Institute of the findings or conclusions contained herein. It is published for the exchange and stimulation of ideas.

Table of Contents

		page
Abstract		2
Acknowledgements		3
Table of Contents		4
List of Figures		6
List of Tables		8
List of Variables		9
I.	Problem Statement	11
	A. Introduction	11
	B. Plasma Equilibrium	12
	C. Previous Position Control Systems	15
	D. Position Control Requirements	19
II.	EPR and MAKO Summary	21
	A. EPR Design	21
	B. MAKO Tokamak Plasma Physics Code	37
III.	Controller Synthesis	43
	A. Introduction	43
	B. Nominal Feedforward System Design	43
	C. Perturbation Feedback Control System	44
	1. System Dynamics	46
	2. Root-Locus Plots and Bode Diagrams	55
	3. Design Prameters	67
	4. Control System Characteristics	68
IV	Controller Operation	72
	A. Analog to Difference Equations	72
	1. EF Coil Current Regulator	72

Table of Contents (Continued)

	page
2. Plasma Position Sensor	74
3. Lead Compensation Network	75
4. Plasma Motion	76
B. Subroutine DRAPER Structure	79
C. Transient Response	83
D. Reactor Shutdown	85
1. Normal Shutdown	85
2. Normal Shutdown with Slightly Enhanced Confinement	88
3. Abort Shutdown with Greatly Enhanced Confinement	88
4. Shutdown with Lead Compensation	94
E. Error Models in Plasma Variables	95
1. Static Estimation Techniques	95
2. Dynamic Estimation	97
3. Constant Error	98
4. Addition of Integrator	100
V. Results and Conclusions	111
A. Introduction	111
B. Plasma Physics	111
C. Controller Design	115
List of References	121

List of Figures

		page
1.	Tokamak Reactor Schematic Diagram	14
2.	Conceptual Controller Design	16
3.	Plan View of ANL-TEPR	22
4.	Ion and Electron Temperatures During Base Case Burn Cycle	25
5.	Ion Density and Refueling Current During Base Case Burn Cycle	26
6.	Safety Factor and Poloidal Beta During Base Case Burn Cycle	27
7.	Primary and Plasma Currents During Base Case Burn Cycle	28
8.	Energy Production During Base Case Burn Cycle	29
9.	ANL-TEPR Magnet Location	30
10.	ANL-TEPR EF Coil LOcation	33
11.	Functional Flow Chart of MAKO	38
13.	Vertical Field Error	45
14.	Static Stability Analysis	48
15.	Neutral Equilibrium Field and Stable Vertical Magnetic Field	50
16.	Open-Loop Response with Negative Static Stability	57
17.	Open-Loop response with Positive Static Stability	58
18.	Root-Locus Plot with Negative Static Stability	60
19.	Root-Locus Plot with Positive Static Stability	61
20.	High Frequency Resonance	62
21.	Perturbation Feedback Control System	64
22.	Compensation Gain Schedule Parameter	65
23.	Closed-Loop Control System Response	69

List of Figures (Continued)

		page
24.	CSDL Candidate Plasma Position Control System	70
25.	Control System Showing Analog Equations	73
26.	Control System Showing Difference Equations	77
27.	Plasma Motion During Controller Operations	80
28.	Flow Chart For Subroutine DRAPER	81
29.	Transient Response	84
30.	Normal Shutdown - Error	86
31.	Normal Shutdown - Plasma Parameters	87
32.	Normal Shutdown with Slightly Enhanced Confinement	89
33.	Normal Shutdown with Slightly Enhanced Confinement	90
34.	Abort Shutdown - Error	92
35.	Abort Shutdown - Plasma Parameters	93
36.	Abort Shutdown with 10% Feedforward Error	99
37.	Integrator Location in Feedback Control System	101
38.	Transient Response with Integrator Added	102
39.	Abort Shutdown with Integrator - Error	106
40.	Abort Shutdown with Integrator - Plasma Parameters	108
41.	Normal Shutdown with Integrator - Error	109
42.	Normal Shutdown with Integrator - Plasma Parameters	110
43.	Proposed X-Ray Position Sensor For ALCATOR C	118

List of Tables

		page
I.	ANL-TEPR Conceptual Design Geometric Parameters	23
II.	TEPR Steady State Plasma Properties at Equilibrium	31
III.	TEPR Burn Cycle Performance	32
IV.	EF Coil System	35
V.	Characteristics of Copper EF Coil Design	35
VI.	Superconducting EF Coil Design	36
VII.	System Dynamics Parameters	49
VIII.	State Variable Matrices	59
IX.	Transfer Functions	63

List of Variables

a	plasma minor radius
a_w	reactor vessel minor radius
B	total magnetic field ($B_t + B_p$)
$B_{eq.}$	equilibrium vertical field required to keep the plasma centered
B_p	poloidal magnetic field
B_t	toroidal magnetic field
B_{to}	toroidal magnetic field at $R = R_0$
B_v	vertical magnetic field inside reactor vessel
B'_v	vertical magnetic field external to reactor vessel
B_{vi}	vertical magnetic field from internal conductors
B_{vz}	z component of vertical magnetic field
I_p	plasma current
I_{vcmd}	component of EF coil current that comes from feedback system
I_{vff}	component of EF coil current that comes from feedforward system
I'_{vff}	input to lead compensation network
I_{vt}	input to EF coil current regulator
I_v	output from EF coil current reguletor
i_w	dipole component of the surface density of current in the wall/ blanket due to the plasma radial motion
k_{ei}	scaling factor relating B'_v to B_v
k_r	gain applied to error in plasma position by feedback control system
k_z	proportionality constant relating EF coil current to B'_v
R	plasma major radius
R_{err}	error in plasma major radius

List of Variables (Continued)

R_f plasma major radius measured by x-ray position detector

V_a Alfven wave velocity

β ratio of plasma thermal energy to magnetic filed energy

β_p ratio of plasma thermal energy to poloidal magnetic field energy

Δ plasma offset from center of reactor vessel

τ_c constant in lead network

τ_b constant in lead compensation network

τ_s time constant associated with low pass filter in x-ray position detector

τ_w time costant for diffusion of fields through reactor vessel

Chapter 1. Problem Statement

A. Introduction

In the search for a source of energy that is inexhaustible and technically and economically feasible to extract, the control of thermonuclear fusion has become one of the main energy options of the future. Within the Controlled Thermonuclear program, magnetic confinement in a tokamak reactor is receiving the greatest amount of funding for research and development. While it could be argued that a tokamak reactor is not the best way to achieve controlled fusion, it is thought that the first reactor to demonstrate the feasibility of fusion as an energy source will be a tokamak type reactor. The Energy Research and Development Agency currently has plans for a tokamak design Experimental Power Reactor (EPR)to be built in the mid 1980's to demonstrate the technical feasibility of producing electric power by the control of thermonuclear fusion.

In a tokamak reactor, the plasma is heated to a high temperature and magnetically confined within a torus shaped structure. The bulk of the energy from the deuterium-tritium fusion reactions is carried away by 14.1 Mev neutrons that give up energy to the reactor by interacting with the blanket materials in the structure that surrounds the plasma. The main plasma energy loss is from particle and energy fluxes that diffuse outward through the plasma and are lost. The plasma also gives off energy in several different types of radiation (bremmstrahlung, cyclotron, and line radiation). In the proposed EPR design submitted by Argonne National Laboratory (ANL), the plasma

temperature is 10 kev (116,000,000°K) and, at an average density of 1.2×10^{20} particles/m^3, the total plasma thermal energy is on the order of 140 MJ. There is also another 150 MJ in the poloidal magnetic field created by the plasma current. For obvious reasons of materials limitations, the plasma must be restrained from touching the walls of the reactor vessel during operation. In previous experimental devices this has not been a problem due to the much lower plasma energies. At the end of each discharge, the plasma has been allowed to dissipate its energy on the device walls. In the EPR, a transfer of the plasma thermal energy to half of the $592m^2$ wall area in a hundredth of a second would cause an average heat load of $50MW/m^2$. Without even considering the magnitude of localized hot-spots, this plasma energy dump exceeds the first wall design limitation of 1-2 MW/m^2 by a factor of 25. The poloidal magnetic field energy will be safely transferred back to the EF and OH coils as long as the plasma maintains a stable, conducting configuration. It is not possible to predict exactly what damage this would or would not do to the reactor, but it should be prevented from happening. For this reason, an effective, reliable system for controlling the plasma position must be an integral part of the EPR.

B. Plasma Equilibrium

In a tokamak there are three forces acting on the plasma which tend to move it away from an equilibrium condition - internal pressure, diamagnetic, and an $\vec{I}_p \times \vec{B}$ force. All three forces show up in

equation (1). Simply put, the plasma ring acts as a current conductor and there is an outward hoop force. Since the toroidal magnetic field falls off from the major axis as 1/R, the total magnetic field $(B_t + B_p)$ at the inside of the plasma is greater than the total force at the outside of the plasma and there is a pressure gradient which also has an outward net force. There must be a vertical magnetic field applied that interacts with the plasma and gives a $\vec{I}_p \times \vec{B}_v$ force inward. The plasma will be centered in the reactor when the inward and outward forces are equal. Figure (1) shows this schematically.

The calculation of the vertical field required for equilibrium has been done by Mukhovatov and Shafranov[1]; Greene, Johnson and Weimar[2]; and several others. From Shafranov's paper, the vertical magnetic field must equal (MKS units);

$$B_v = B_{eq} = \frac{\mu_o I_p}{4R}\left\{\ln\frac{8R}{a} + \beta_p + \frac{1i}{2} - \frac{3}{2}\right\} \qquad (1)$$

This magnetic field will keep the plasma centered in the reactor horizontally. Reference 2 showed that B_v should be less than B_{eq} where $R < R_o$ and B_v should be greater than B_{eq} where $R > R_o$ in order to insure radial stability.

Yoshikawa[3] has shown that the vertical magnetic field can provide stability against vertical displacement if it is concave towards the axis of symmetry. This is true when[4]:

$$\frac{\partial B_{vr}}{R B_v} < 0 \qquad (2)$$

The problem of controlling the vertical displacement of the

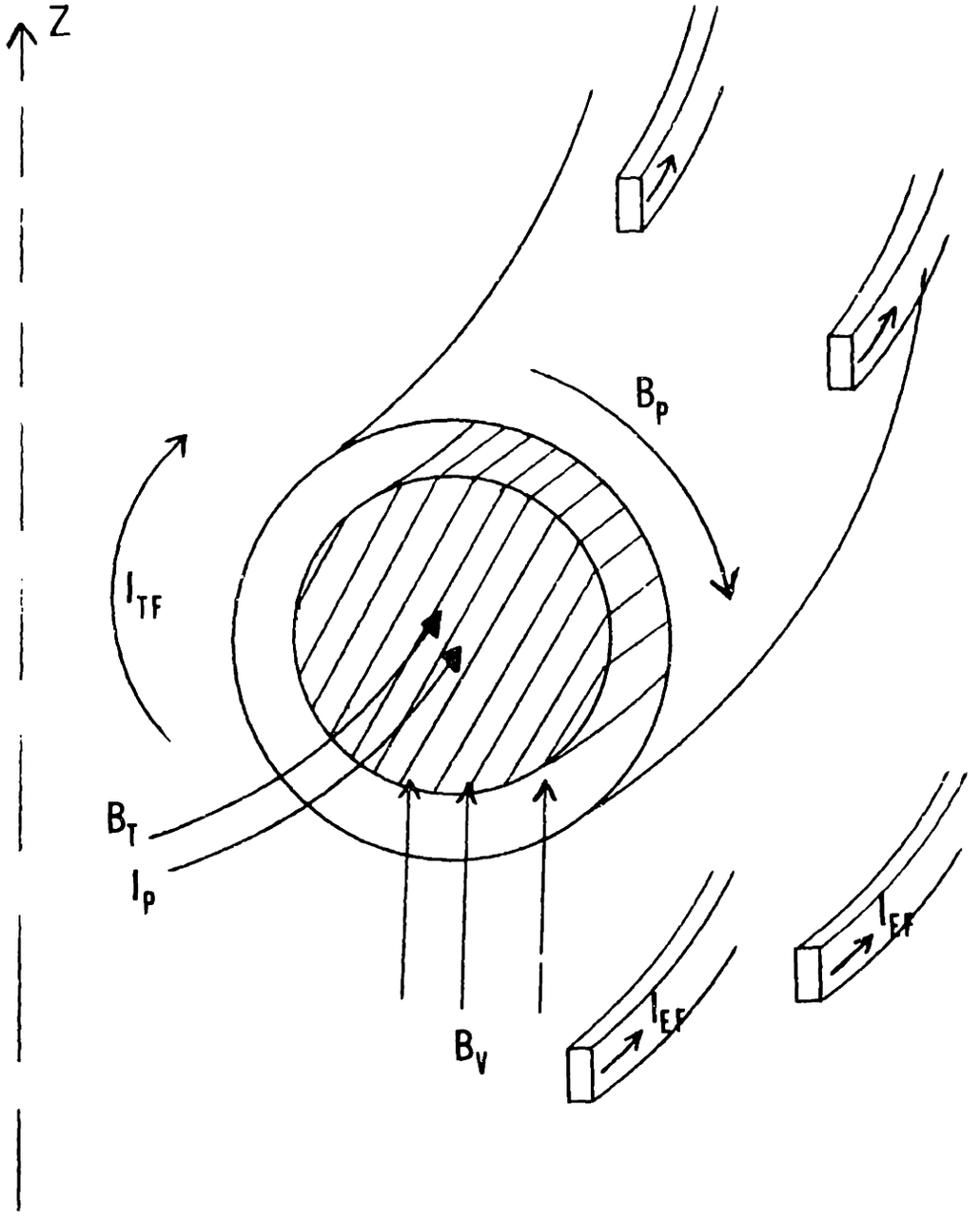

Figure 1 Tokamak Schematic Diagram

plasma will not be considered here since proper design of the vertical magnetic field coils will provide the necessary curvature to keep the plasma vertically centered. The system for controlling the plasma radial position must be able to determine the required vertical magnetic field by measuring or estimating certain plasma parameters and then applying this vertical magnetic field to the plasma.

C. Previous Position Control Designs

Before describing the position controller in detail, it would be worthwhile to give a brief review of some presently operating control systems. Figure (2) is a conceptual diagram of the CSDL candidate plasma position controller design. A variety of sensors are used on the reactor to determine as many of the plasma variables as possible. Some variables can be measured directly in real time and some variables must be estimated by assuming linear (or linearized) relationships with the variables that can be directly measured. These measured and estimated variables are fed into the reactor control system, which will control as many of the plasma and reactor characteristics as required. A fault diagnostic system will in all probability be included in the reactor control system to detect and predict abnormal reactor operation. The variables that are needed for the plasma position control system will constitute the input to a feedforward vertical field algorithm that is designed to keep the plasma correctly positioned. Some measured variables will also detect errors in the plasma position and they will be used in a feed-

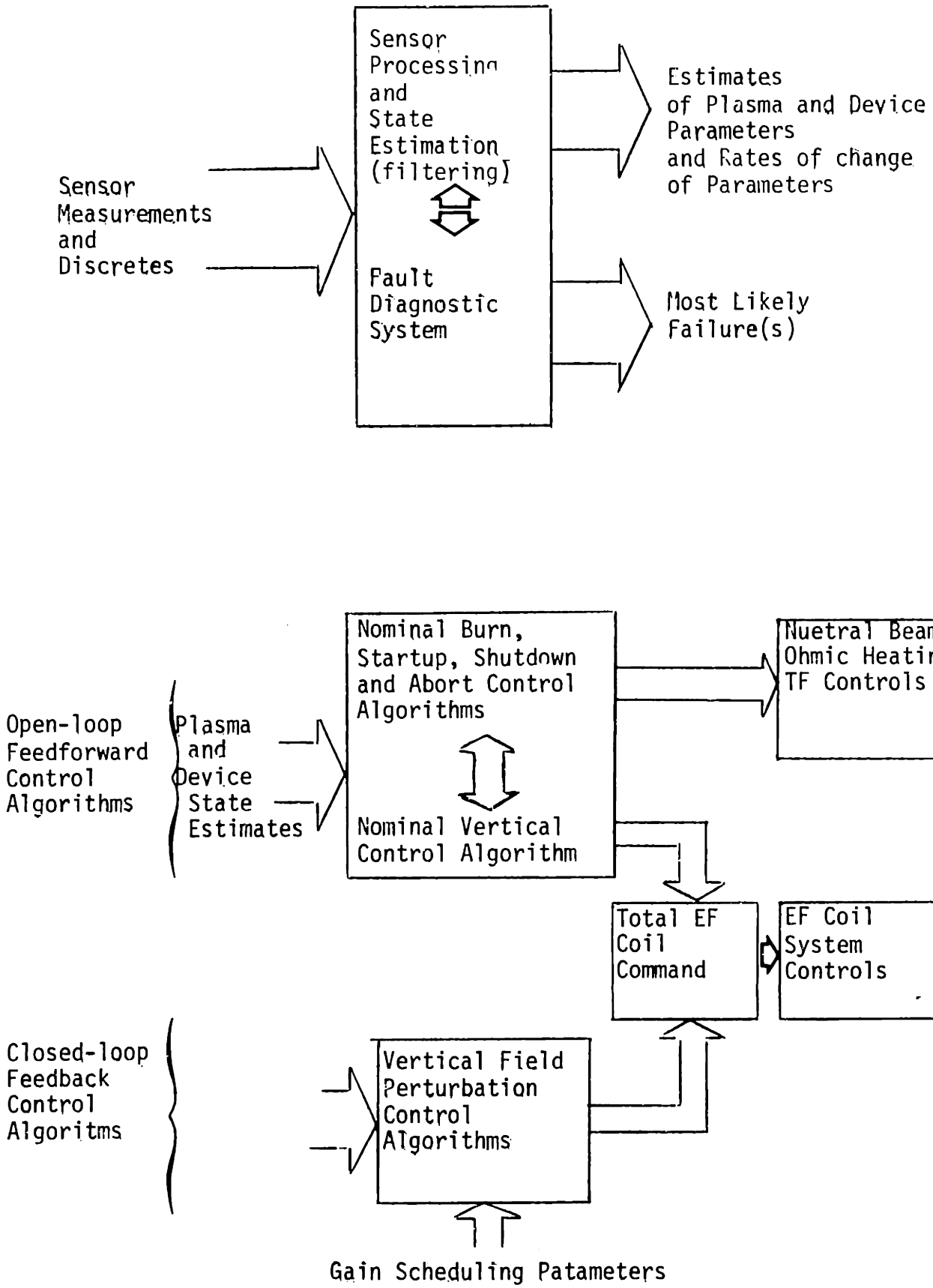

Figure 2 Conceptual Controller Design

back vertical field perturbation control system which will correct for any errors in the plasma position. Proper design of a control system of this type, in which the nominal vertical field is not pre-programmed, should be more flexible than previous control systems and should allow for satisfactory operation over a wider range of reactor operating conditions - including unpredicted reactor aborts.

References 9, 10, 11, and 12, describe proposed and actual plasma position controllers for the ORNL ORMAK tokamak (9 and 10); the plasma position controller used on the CLEO-TOKAMAK at Culham Laboratory (11); and the plasma position controller used on PLT at PPPL (12).

Miskell's proposed plasma control is a complicated system that has an optimized (minimization of a specific quadratic criterion index) feedforward nominal control and a perturbation full-state feedback structure. The actual position of the plasma is not measured, but must be inferred by solving the classical Shafranov equations[1] that relate the magnetic axis offset to the strength of signals picked up by coils placed on the surface of the reactor vessel. It was assumed that the coefficient of asymmetry of the poloidal field, ($\Lambda = \beta_p + \frac{li}{2} - 1$), was a time dependent control variable that could be controlled by neutral beams, or some other form of energy input. This implies that active control of poloidal beta and internal inductance is possible. However, an active control of these parameters would strongly couple a plasma position control system to control of the plasma burn cycle dynamics by varying plasma temperature, plasma density, and/or plasma current. It is possible that such a system would keep the

plasma from a desired operating regime in order to control the plasma position. The plasma position control should be independent of any other possible plasma parameter control systems. The same state variables used in the nominal feedforward system were used in the feedback system, with an extended Kalman filter to estimate the unmeasured variables.

The actual control system employed on ORMAK is considerably simpler. The ORNL tokamak uses a pre-programmed nominal feedforward vertical field current with a feedback current that is a function of the outer poloidal flux. The pre-programmed current is a result of ramping the vertical field current proportional to the plasma current. The feedback current required for a 60 msec controlled plasma discharge is about ± 25% of the nominal feedforward current. The pre-programmed current can be modified between discharges after post-shot data analysis.

The CLEO tokamak plasma position control system uses magnetic pick up coils located outside the vessel to infer the plasma position. The system then applies the signals to a predetermined feedback algorithm that supplies a vertical field coil current. The control algorithm used assumes a constant value of β_p and li/2 - which is not a bad assumption for that machine. This control system has increased discharges from 110 msec to 200 msec.

The PLT at PPPL also uses a pre-programmed nominal control signal and a feedback control signal. The feedback control signal comes from an estimate of the actual plasma position that is obtained by measuring

the vertical field outside the reactor vessel; estimating $\beta_p + li/2$; and solving Shafranov's equation for the plasma offset. This control system can also be adjusted between plasma discharges to improve performance.

D. Position Control Requirements

While these control systems may be adequate for the small experimental machines with short discharges, none of them may be readily extended with confidence to a large power reactor. A reliance on pre-programmed nominal vertical fields is not acceptable on a machine that can suffer extensive damage from one aborted run that had not been "pre-programmed". Many of the plasma parameters should be able to change from burn cycle to burn cycle. If the burn cycle is impurity limited, different impurity levels would lead to different burn cycle lengths with different plasma characteristics. The plasma position control system must be able to respond to the actual plasma position and not what it is predicted to be. The control system should also be able to control plasma position during an abort due to machine failure or plasma perturbation. It is with these ideas in mind that the control system of figure (2) was designed.

This study will examine the CSDL candidate plasma position control system and attempt to verify its operation by the use of computer modeling. This control system is different from previous systems in that the feedforward nominal current is not pre-programmed and the plasma position is directly measured with an x-ray detector.

Recommendation will be made for further study and refinement.

Chapter 2. EPR and MAKO Summary

A. EPR Design

The reactor design for the tokamak EPR was done by the Argonne National Laboratory for ERDA under contract W-31-109-Eng-38. The version used in this control study is ANL/CTR-75-2. The design process is open-ended so that there are continual reviews and updates. Later versions of the design should not effect the methodology used to design the position control system. Figure (3) shows a general plan of the overall design of the reactor. Table (1) gives the basic design dimensions.

The main objective of this EPR is to prove the engineering feasibility of a tokamak fusion power reactor. Both circular and noncircular plasma cross sections were considered in the design. The circular cross section option was studied in greater detail and that is the one used in this control study. Because of uncertainties in the plasma physics, the design and operating parameters are predicated on certain assumptions. It was assumed in the design[5] that trapped ion mode transport was too pessimistic by an order of magnitude. Confinement was assumed to be fifteen times greater than that predicted by trapped ion mode transport. This leads to an operating regime of $Te = Ti \cong 10kev$ at a density of $ni = 5.6 \times 10^{19}$ ions/m^3. Tokamaks are inherently non-steady state devices with the burn cycle being limited by the available machine volt-seconds that provide the stabilizing plasma current. Other factors such as levels of impurity build-up may also be limiting factors in the length of the burn cycle.

Figure 3 Plan View of ANL-TEPR

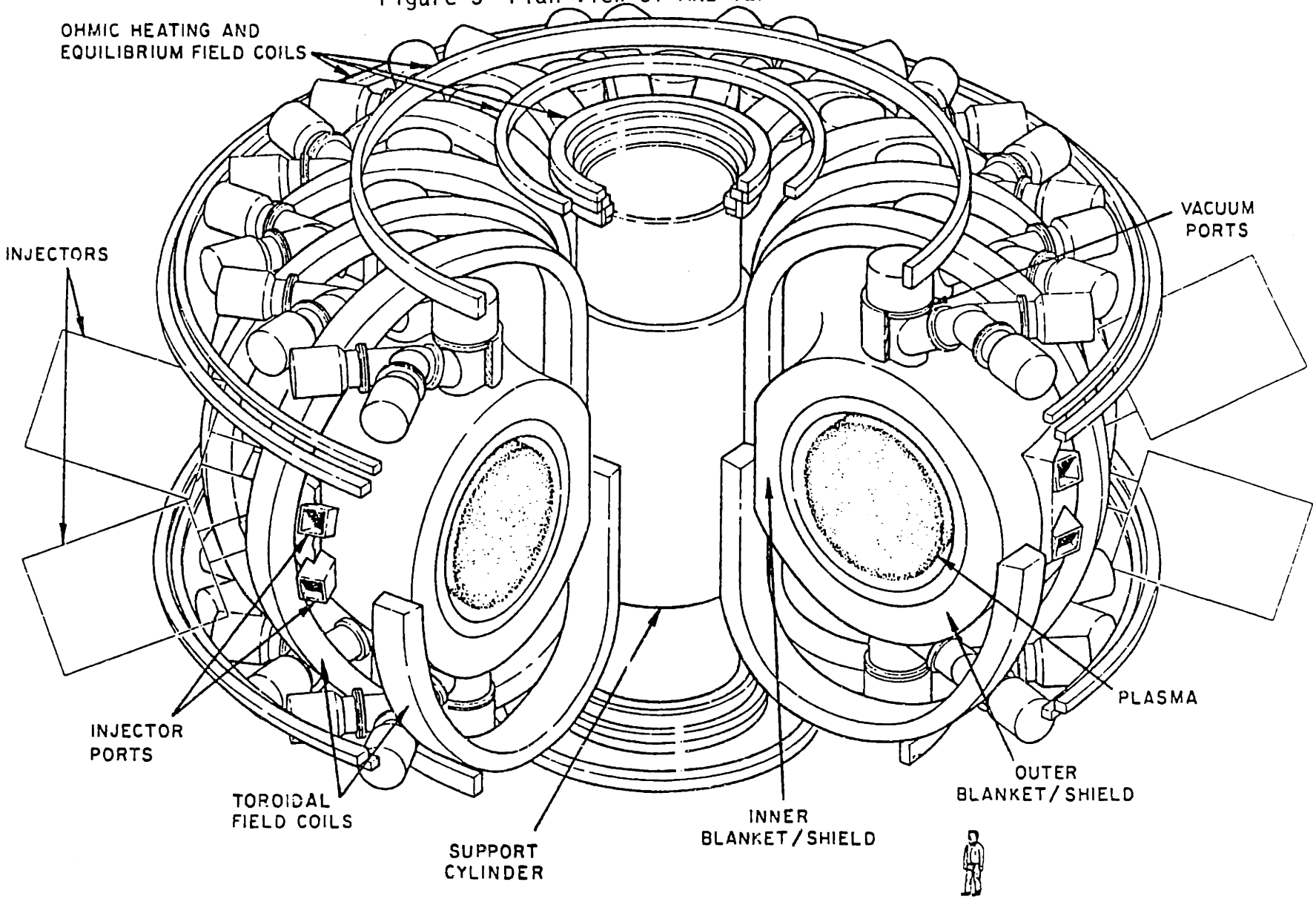

TABLE I

ANL-TEPR Preliminary Conceptual Design Geometrical Parameters

Central core radius, r_v	1.8 m
Thickness of TFC + OHC + Support cylinder, Δ_m	1.05 m
Blanket + shield thickness, inside, $\Delta_B^{in} + \Delta_S^{in}$	1.0 m
Toroidal-field coil minor bore, R_{bore}	7.7 m
Toroidal-field coil major bore, Z_{TFC}	11.9 m
Circular Plasma	
Plasma radius, a	2.1 m
First-wall radius, $r_w = a + \Delta_v$	2.4 m
Major radius, R	6.25 m
Aspect ratio, A = R/a	2.98
Plasma volume	544 m^3
Toroidal vacuum-chamber volume	711 m^3
First-wall area	592 m^2
Blanket + shield thickness, outside, $\Delta_B^{out} + \Delta_S^{out}$	1.3 m[(a)]

a. Blanket and shield thickness = 1.3 m. The space available within the toroidal-field coil is 1.9 m for the circular plasma and 3.5 m for the noncircular plasma.

A nominal burn cycle length of twenty seconds was chosen to illustrate typical operating conditions during the burn cycle. Figures (4,5,6,7,8) show various plasma parameters during the entire burn cycle and tables (2,3) show the characteristics of the plasma in the flat top region.

At the start of each burn cycle, deuterium and tritium gas are introduced into the vessel and ionized. The plasma current is ramped up to 4.5 MA in one second. The current provides the initial heating to the plasma in the form of Joule heating. Neutral beams of deuterium are used to heat the plasma to operating conditions in 4 seconds. At this point ignition of the D-T mixture should result and an unspecified means of refueling more D-T is used to keep the plasma at a quasi-steady state during the burn cycle. Five seconds before the end of the burn cycle the refueling rate is dropped to allow the density to decrease by a factor of one hundred. One second before the end of the burn cycle the plasma current is ramped down to finish the run.

The location of the different magnet systems and associated magnetic fields are shown in figure (9). All three magnet systems: toroidal field (TF), ohmic heating (OH), and equilibrium field (EF), are made of a superconducting material - niobium titanium - and operated at $4.2^{o}K$. They are all fully stabilized with copper to prevent damage from thermal transients.

The equilibrium field is the field that must be controlled in order to control the plasma position. Figure (10) and Table (4) show

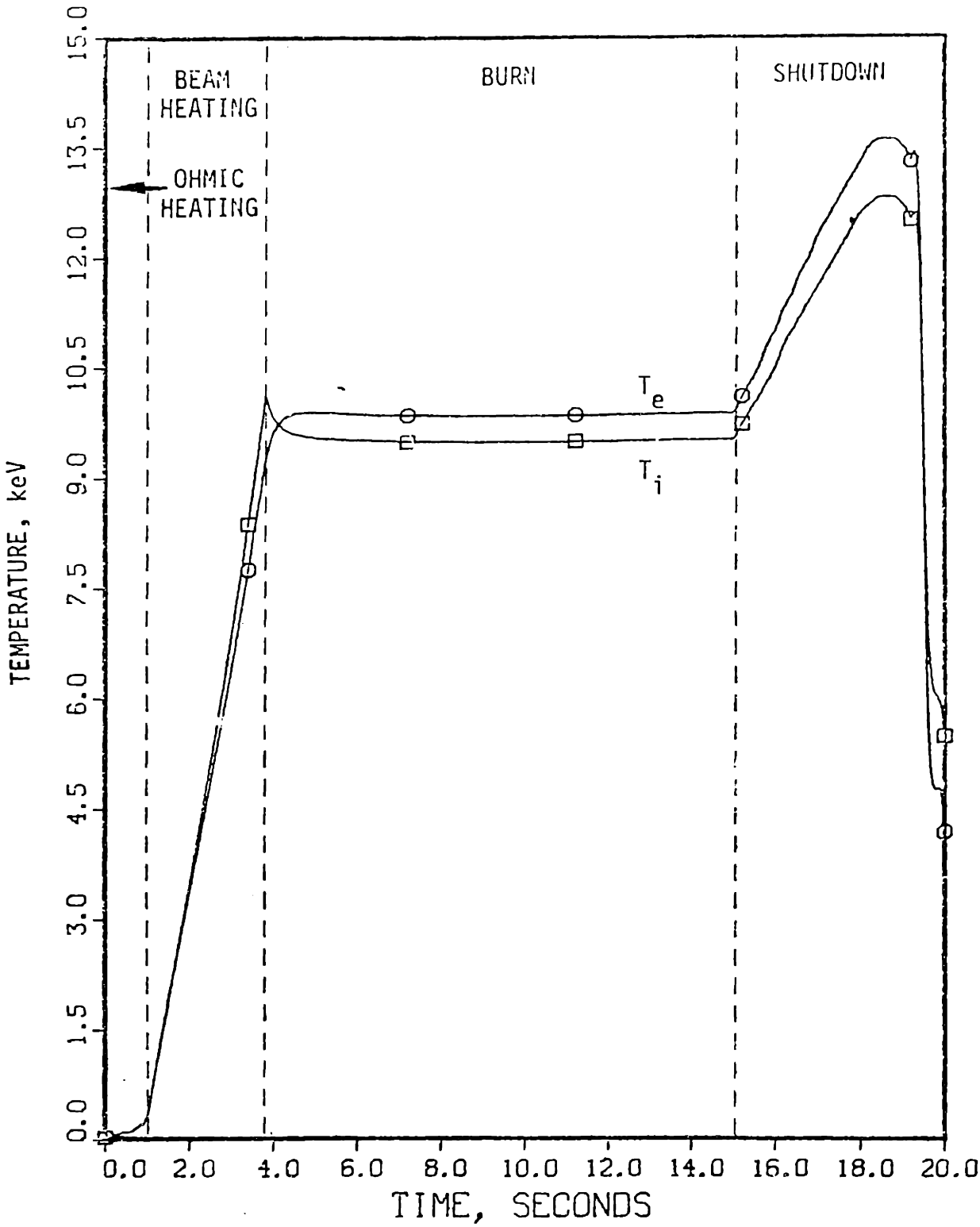

Figure 4 Ion and Electron Temperatures During Base-Case Burn Cycle

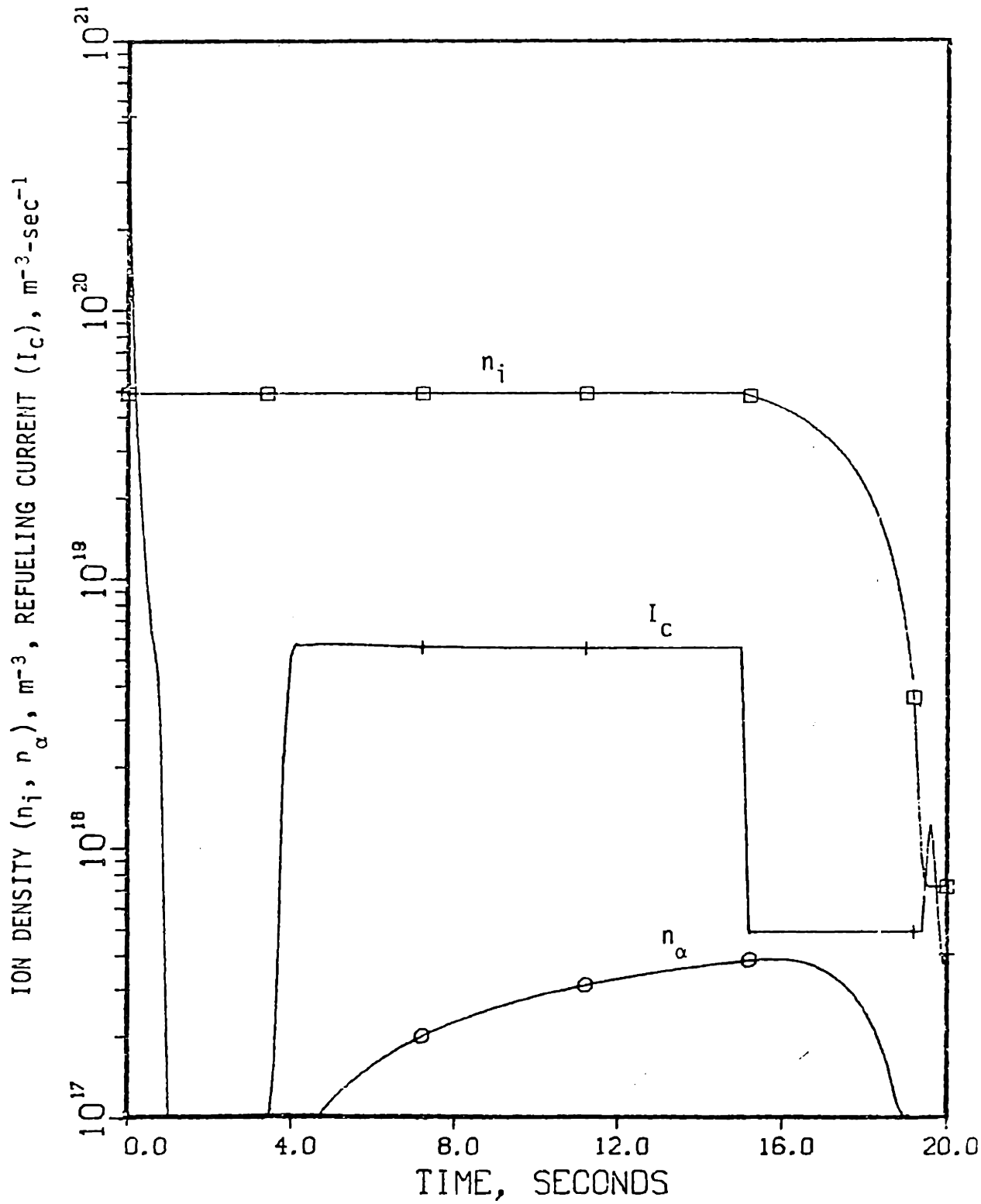

Figure 5 Ion Densities and Refueling Current During Base-Case Burn Cycle

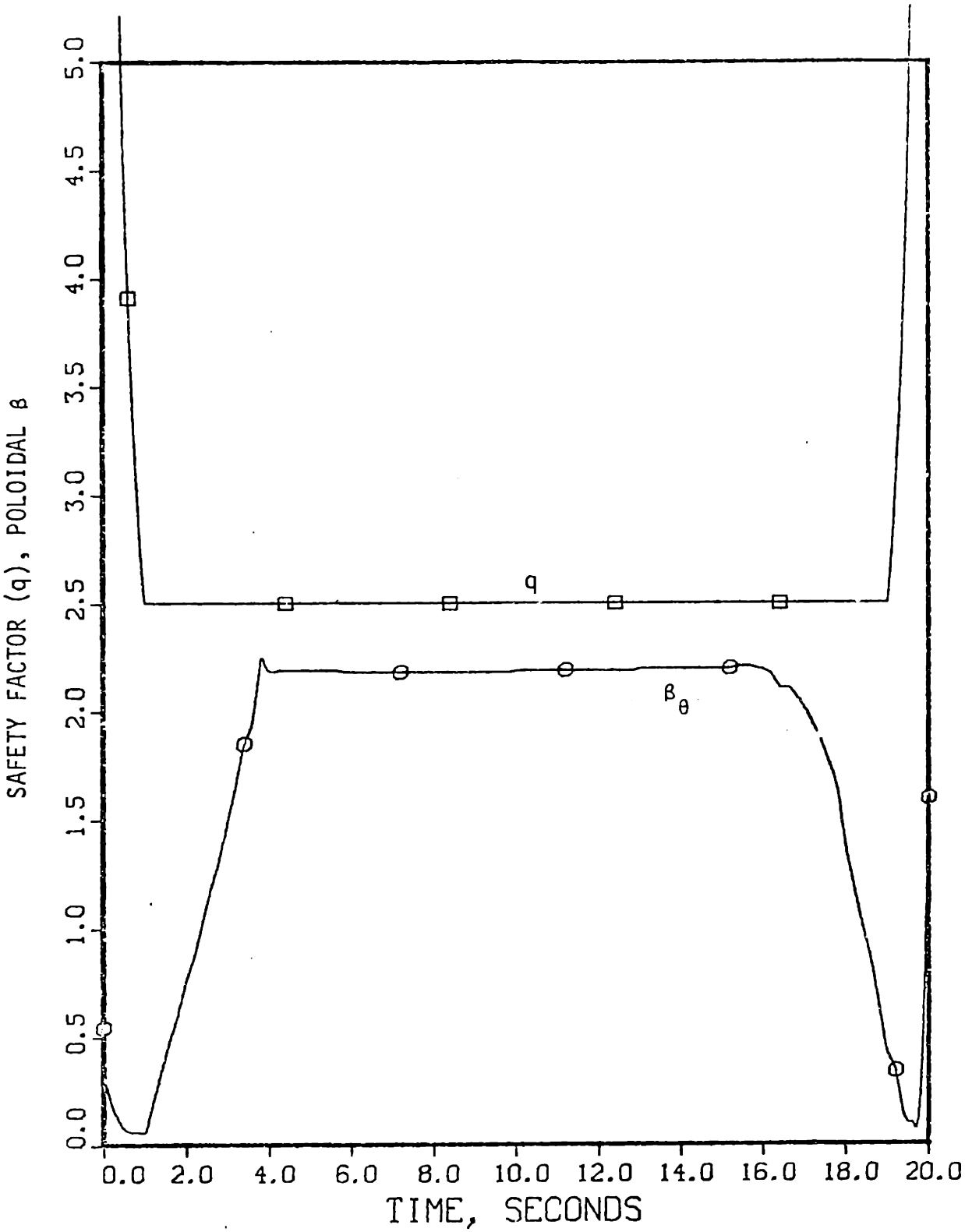

Figure 6 . Safety Factor, q, and Poloidal Beta, β_θ, During Base-Case Burn Cycle

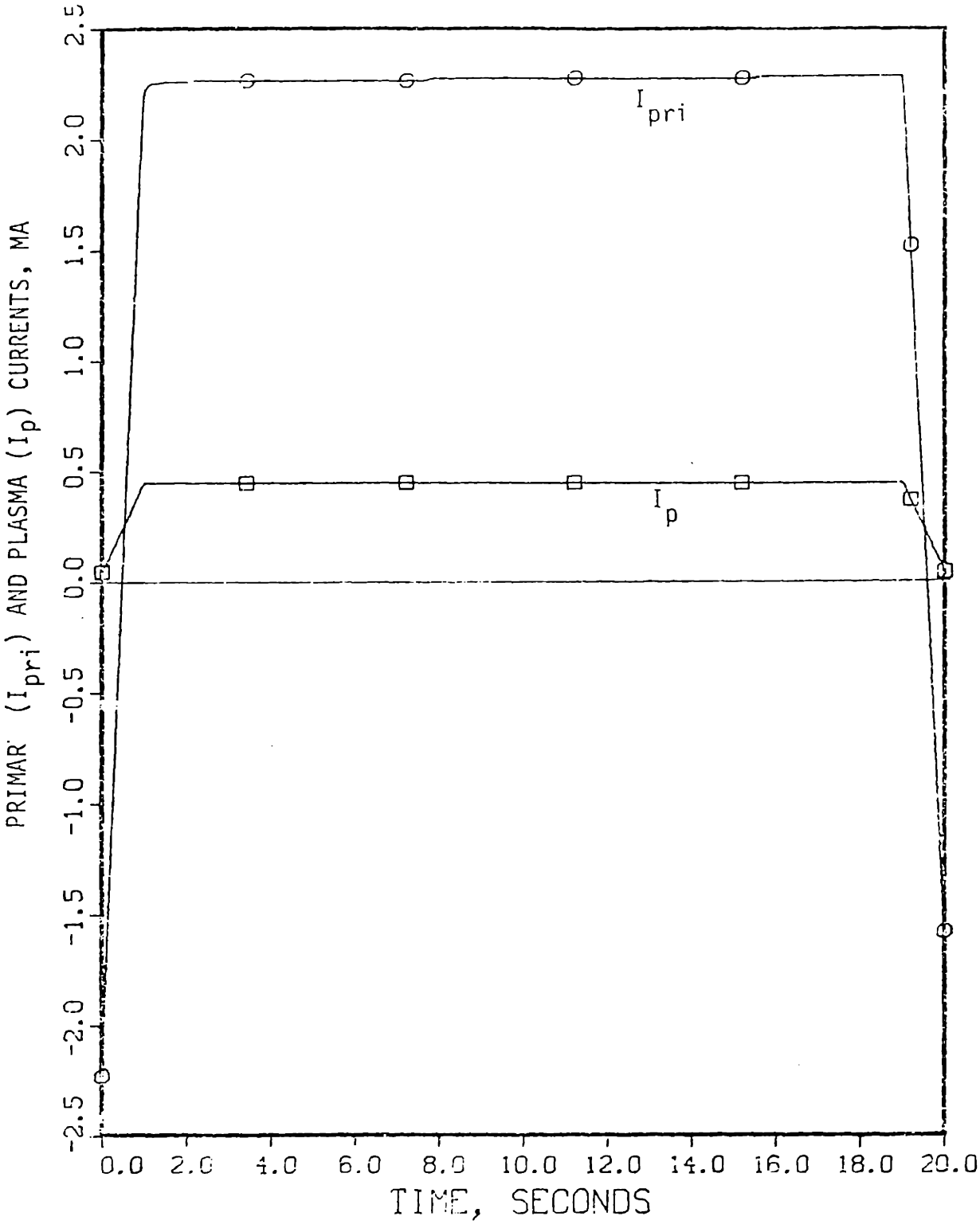

Figure 7 Primary and Plasma Currents During Base-Case Burn Cycle (Primary current in MA-turns.)

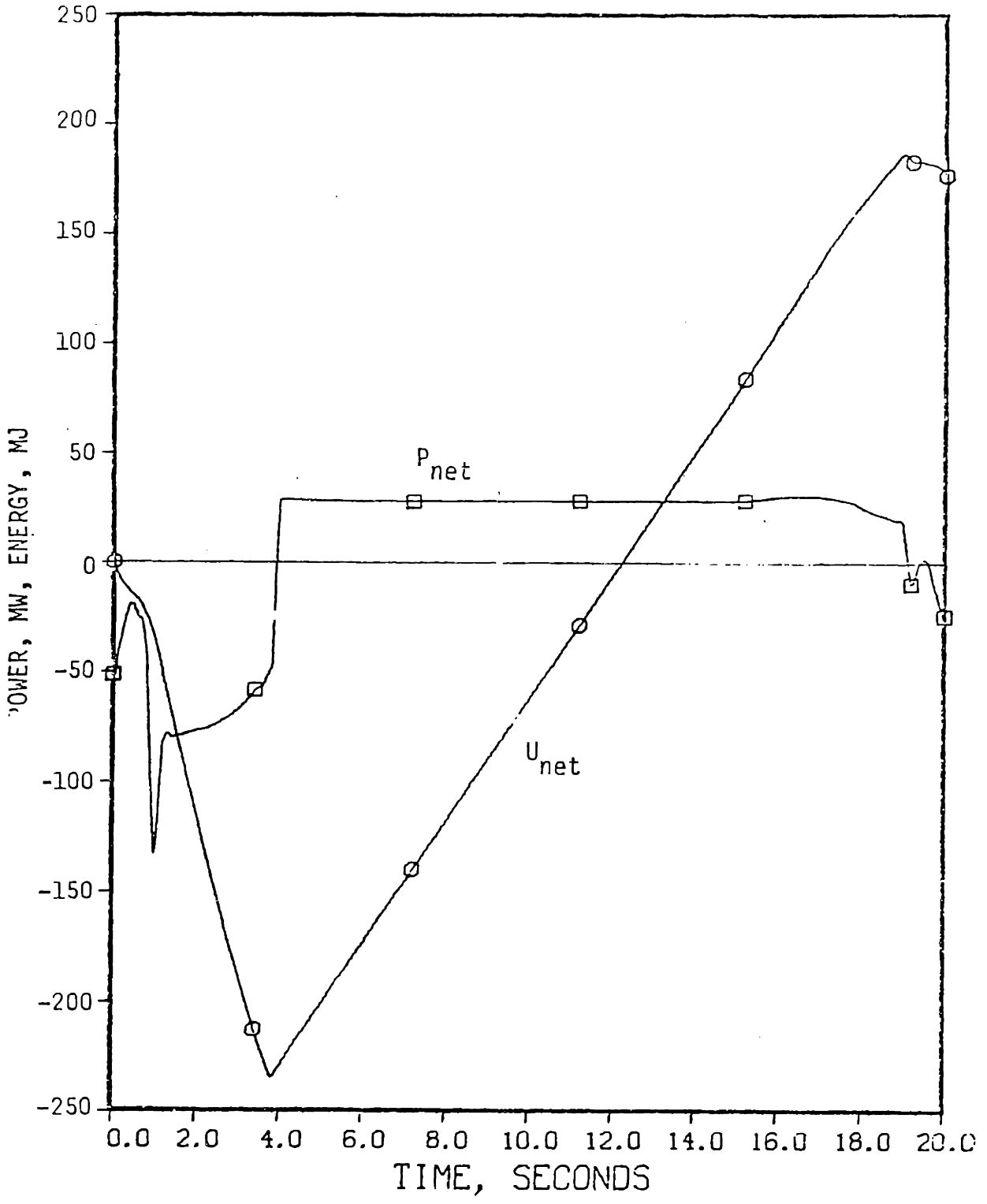

Figure 8 Instantaneous Net Electrical Power and Cumulative Net Electrical Energy During Base-Case Burn Cycle

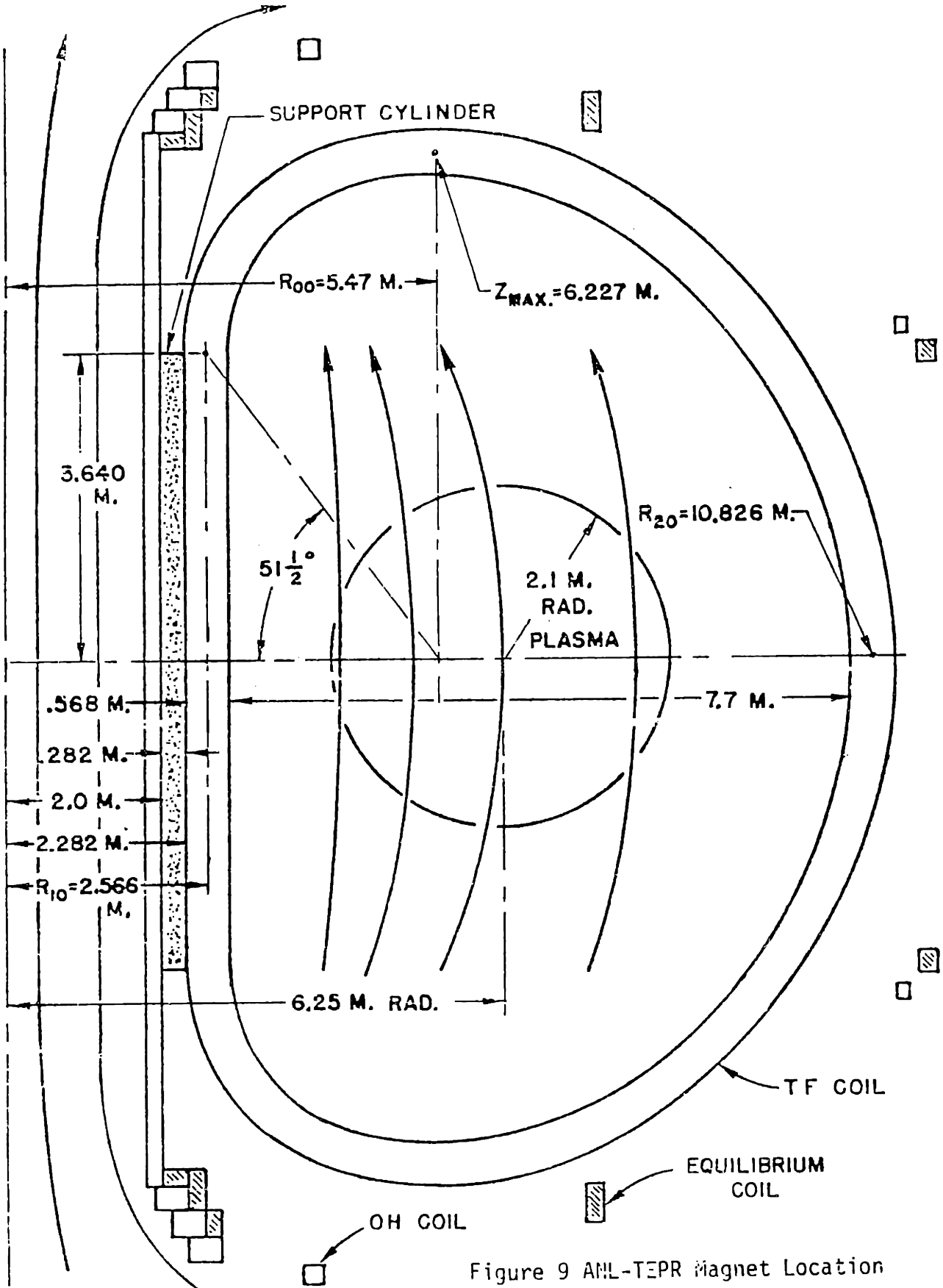

Figure 9 ANL-TEPR Magnet Location

TABLE II

TEPR Steady-State Plasma Properties at Equilibrium

Parameter	Circular Plasma = 1
Pressure ratio, β_Θ	2.2
Safety factor, q(a)	2.5
Density, n_i (m^{-3})	0.56×10^{20}
Temperature, T_i (keV)	9.6
T_e (keV)	10.0
Confinement, n (sec/m^3)	6.2×10^{20} (15 x TIM)
Plasma current, I_p(MA)	4.8
Toroidal field, B_t (kG)	34
Power, P_T (MWt)	129
Neutron wall load, P_w (MW/m^2)	0.16

the exact position and amount of current that each of the EF coils carry. Notice that EF coils 1, 2, and 3 are there to decouple the EF coils from the OH coils. They accomplish this by generating small vertical fields in the negative Z direction. EF coils 4 and 5 actually generate the vertical control field. The curvature of the field is sufficient to satisfy the criteria of equation (2) and control vertical motion.

The ideal location for the EF coils would be between the first wall and the blanket. This would reduce the flux diffusion time and

TABLE III

TEPR Burn Cycle Performance - Circular Plasma

Burn Cycle	
Current-rise phase (sec)	1
Beam-heating phase (sec)	∿3
Burn phase (sec)	20-50
Shutdown phase (sec)	5
Exhaust & Replenishment phase (sec)	∿15
Neutral-Beam Requirements	
Startup - 40 MW @ 180 keV for ∿8 sec	
Burn * - 23 MW @ 180 keV for 20-50 sec	
Plasma Driving-System Requirements	
$\Delta\phi$ (volt-sec)	∿100
Peak power (MWe)	∿1000
Energy (MJ)	∿300

Reactor Performance (B_{max}^{TFC} = 70 KG)	$n\tau$ = 15 x TIM	$n\tau$ = TIM
Electrical power, $\overline{P}_E$ (MWe)	∿25	∿25
Net electrical power, $\overline{P}_{NET}$ (MWe)	15-20	∿-17

* Required if τ_e = TIM.

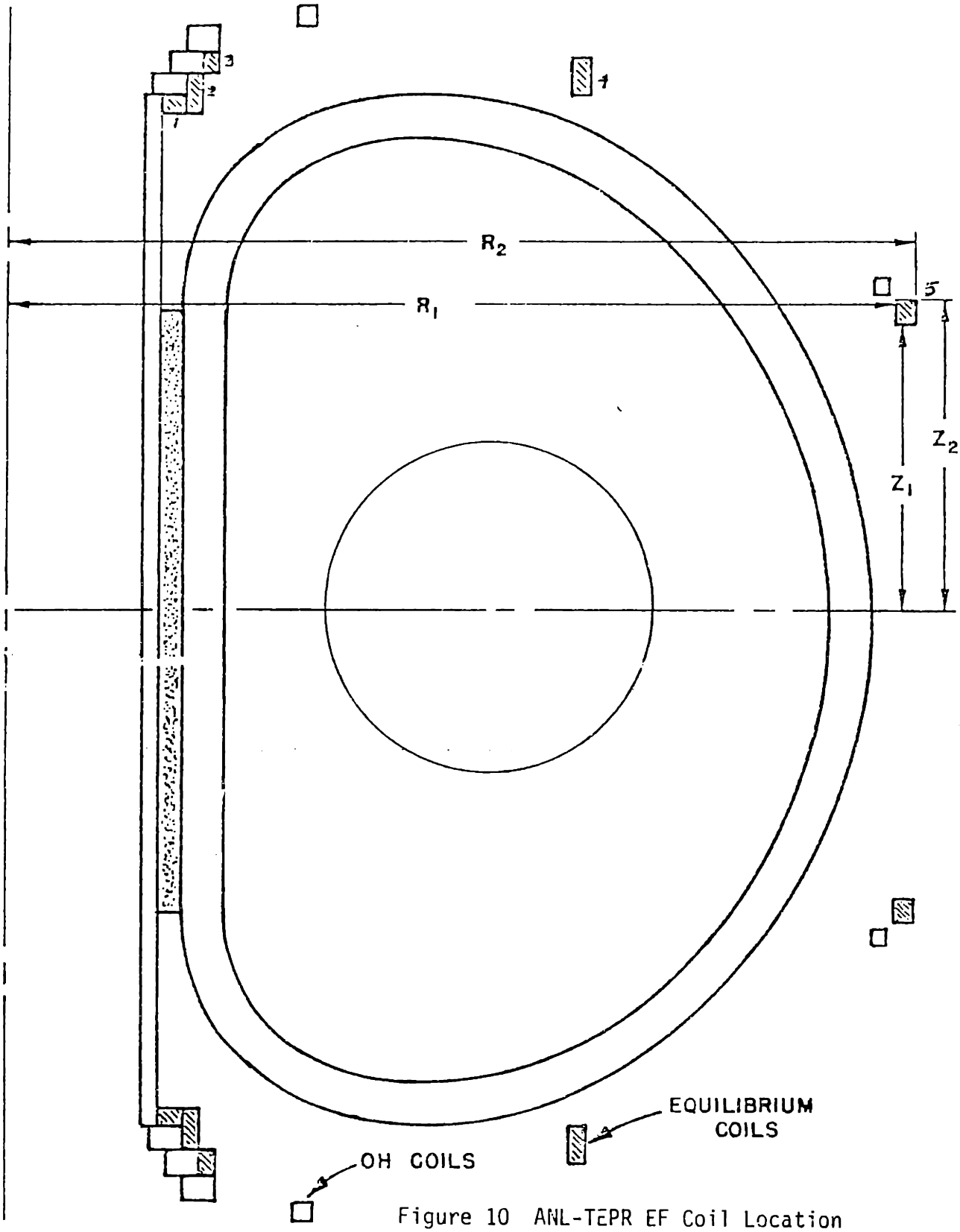

Figure 10 ANL-TEPR EF Coil Location

the total ampere-turns required. However, the temperature and neutron flux in that area preclude such a location. Placing the EF coils on the outside of the TF coils is the simplest materials solution and most accessible location. This location also allows a choice to be made between superconducting magnets and conventional copper magnets. Table (5) shows the dimensions of the EF coils if they were made of copper. The total power consumed of 92MW would be almost four times the net power production of the EPR. This is the main reason superconductors seem to be the system to use.

The EF coils were designed to be made of a multiple strand cable with the filaments being composed of niobium-titanium, copper, and cupro-nickel. The complete design characteristics are shown in table (6). The short twist-pitch and small filament size allow for fast charging of the EF coils. When cooled to $4.2^{o}K$, the EF coils have an average power dissipation of 777W during a complete 35 second fusion cycle[6]. There was no specific EF coil current regulator included in the ANL design. For purposes of the control study, an EF coil current regulator was assumed to exist with the same dynamic properties as the twelve phase controlled rectifier type used on PLT[7].

The wall penetration time for the vertical magnetic field to diffuse inside the reactor vessel was not included in the ANL/CTR-75-2. However, in conversations with the ANL staff, CSDL has determined that the calculated wall penetration time is calculated to be 20 msec.

This is a summary of all the important aspects of the ANL EPR design that effect the design and operation of the plasma position con-

TABLE IV

Equilibrium-Field Coil System

Coil No.	R_1 (cm)	R_2 (cm)	Z_1 (cm)	Z_2 (cm)	Central Field (Gauss)	Conductor Peak Field (KG)	Coil-Pair Conductor Length (A-m)
1	200	230	± 630	± 650	- 261	37	37×10^6
2	230	250	± 630	± 580	- 492	32.5	69×10^6
3	250	270	± 680	± 710	- 287	18	45×10^6
4	720	745	± 640	± 695	2192	32	291×10^6
5	1180	1210	± 362	± 390	1732	25	285×10^6

TABLE V

Characteristics of Copper Equilibrium-Field Design

	Coil Number				
	5	4	3	2	1
No. of layer/coil	13	22	10	15	10
Turns/layer/coil	10	10	9	10	10
Conductor outside dimension (cm)	6.063	5.075	3.617	4.031	3.498
Conductor inside dimension (cm)	4.483	4.079	2.456	2.126	2.413
dc voltage (V)	2600	4494	1000	1000	1000
Power (MW)	24	41	9	9	9
Q (gallons/min)	2022	3500	778	778	778
Copper Weight (tons)	400	254	25	57	21

TABLE VI

Superconducting Equilibrium Coils

Superconductor/Stabilizer	NbTi/Cu & cupro-nickel
Average current density	2300 A/cm^2
Equilibrium field	3.0 KG
Peak field	$\sim$ 37 KG
Ampere turns	10×10^6
Conductor length	727×10^6 amp-m
Field rise in conductor	37 KG/sec
Stored energy	90 MJ
Operational current	15,000 A
Inductance	0.8 H
Power supply voltage	37.7 KV
Volt-sec to plasma	37 volt-sec

15,000 A Cable:

Composite diameter	0.6mm
Composite operational current	61.7 A at 4.2^oK
Composite critical current	123.4 A at 4.2^oK
Composite composition	NbTi/Cu/Cu-Ni = .23/.57/.20
Twist pitch	6 mm
Matrix resistivity	10^{-6} Ω-cm
Filament diameter	5 μm
Number of filaments in composite	3307
Number of composites in cable	243

trol system. It is by no means a summary of the complete reactor design.

B. MAKO Tokamak Plasma Physics Code

The computer code, "MAKO", used as a model for the plasma physics is a code developed by Scientific Applications, Incorporated (SAI) for Draper Laboratories. The code is designed to be used as a vehicle for testing various fusion reactor control procedures.

MAKO is a zero-dimensional code that deals with plasma properties averaged over the entire plasma volume. There is no spatial resolution and no assumptions are made that are dependent on the dynamics of profile distributions. MAKO starts with a set of initial conditions and moves forward in time by solving a set of differential equations that describe: ion and electron temperatures; fast particle (beam particles and fusion generated alpha particles) energy densities; particle (ion, electron, alpha and impurity) densities; and toroidal voltage. The exact equations in each case are listed in reference (23).

Figure (11) is a flow chart of the MAKO program. BLKDTA is a subroutine that merely sets all the initial conditions. MAKO reads an input data set at this time which allows the user to change almost all parameters between data runs without recompiling the program. The user can input: reactor and plasma geometry, initial temperatures and densities for all particles, plasma current profile, neutral beam current and voltage profiles, refueling profiles,

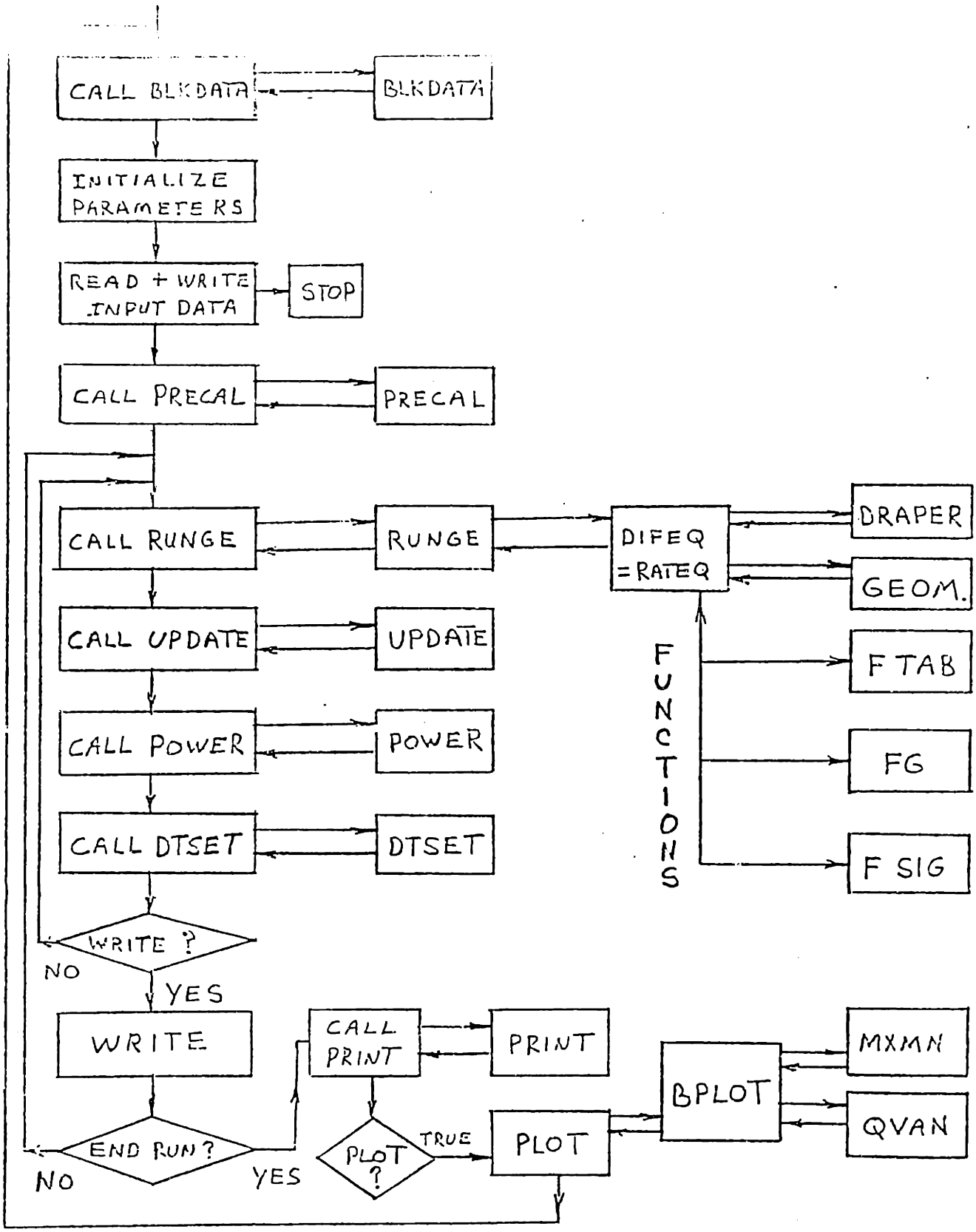

Figure 11 Function Flow Chart For MAKO

microwave heating profile, and a variety of variables that control the use of the plasma position control system. The user can also change a transport coefficient multiplication factor, neutral beam cutoff points as a function of ion temperature or poloidal beta, deuterium-tritium ratio in the plasma or refueling supply, and the amount and type of impurity particles present in the plasma.

After the initialization procedure, MAKO goes to subroutine PRECAL. A change was made in the original code here. Now the input temperatures and densities and plasma current are used to calculate beta, poloidal beta, toroidal voltage and initial particle energies.

In subroutine RUNGE, a first order Runge-Kutta integration is done to update the ion, electron, alpha and impurity densities and energies. A first order Runge-Kutta integration technique, instead of a higher order integration technique, saves computing time and is made accurate by strict constraints on the size of the time step allowed between cycles. Some changes in the code were made here to allow more flexibility. The dynamic limits on the time step preclude using the code during startup (.1kev to 1kev, plasma current less than 1MA) unless the user can afford large amounts of computer time to cover a small amount of burn cycle time during startup. Since the model does not accurately model diffusion physics in the low temperature region, it is not worth the computing time. When the plasma current is started at a low value (less than 1MA), and large time steps (5 msec) are used, the ion and electron temperatures will go negative before the ohmic heating input can balance transport

losses. Therefore a limit of .05kev was put on all temperatures so that an attempt could be made at modeling startup without using an inordinate amount of computer time. A similar limiter was used with any densities that start out low; i.e., any wall impurity that starts at zero and builds up during the burn cycle. The results obtained this way are in reasonable agreement with the ANL design.

In subroutine RATEQ all the terms that comprise the differential equations are calculated and added together. The functions FTAB, FG, and FSIG, are for calculating input variable time profiles from a tabular entry and for empirical calculations of the Maxwellian averaged D-T fusion cross sections. A change was made here in the original MAKO code to make the Maxwellian averaged D-T fusion cross sections agree with the values listed in "The Barn Book".[8]

At this point, subroutine DRAPER, which includes the plasma position control system, is entered. DRAPER will be described in detail in the chapter on the control system. When the position control is not used, the plasma geometry and position remain constant. DRAPER also includes the plasma position dynamics.

Subroutine GEOM takes the output from DRAPER and calculates a new volume, aspect ratio, plasma perimeter, and plasma total inductance.

Subroutine UPDATE updates ion and electron temperatures, amount of impurity ionization and a z-effective for the plasma.

POWER is a subroutine that calculates the total powers and power densities for all the input and output energies. The Q of the reactor,

ratio of cumulative energy out and cumulative energy in, is also calculated here.

In subroutine DTSET, the time step for the next cycle is calculated as a function of several dynamic factors. The time step is less than one tenth of the product of the wall time constant and the aspect ratio. The time step is smaller than the time required to produce a ten percent change in plasma energy or plasma major radius. When the position controller is used, the time step is also limited by a "sample speed" that reflects the sampling speed for the various diagnostics in the control system. This minimum sampling speed insures numerical stability of the difference equations that model the controller and diagnostic functions.

The code will keep going through this cycle until it reaches a predetermined cycle number or time stopping point. The program may also be abnormally terminated if any of the following happen: Kruskal-Shafranov limit exceeded, poloidal beta exceeds aspect ratio (or any other constant), toroidal voltage exceeds Dreicer condition and runaway electrons are produced, or the plasma moves beyond previously specified limits.

Because the computer code is zero dimensional, no attempts have been made at estimating how some of the plasma averaged parameters might be changing during the burn cycle. An example of this would be a change in the total plasma inductance or the plasma internal inductance as the radial distribution of plasma current changed. While a one dimensional code with spatial resolution would be more desirable

to use, a zero-dimensional code seems sufficient for verifying and improving a basic design for a position controller. The postulated control design would then be applied to a one dimensional code to determine any plasma profile effects on the position controller.

Chapter 3. Controller Synthesis

A. Introduction

As indicated in Chapter 1, the present generation control systems are probably not extendable to a large power reactor. This chapter describes a synthesis procedure that can be used to develop a candidate plasma position control system.

B. Nominal Feedforward System Design

The nominal vertical feedforward current control system has to generate an equilibrium field that will keep the plasma at a commanded radius. As indicated previously in equation (1), the magnitude of the vertical field is:

$$B_v = B_{eq} = \frac{\mu_o I_p}{4R}\left[\ln\frac{8R}{a} + \beta_p + \frac{li}{2} - \frac{3}{2}\right] \quad \text{Tesla}$$

There are several assumptions implicit in this formula. The plasma is assumed to be circular and toroidal effects on the asymmetry of field distribution are neglected. This is true as long as $a/R \ll 1$. In the case of the EPR, $a/R = .336$. Since .336 is not $\ll 1$, there will be an error introduced that will effect the magnitude of B_{eq}. This will be a constant bias error that will not effect the dynamics of the control system. A more accurate expression than equation (1), which includes first and second order toroidal effects, is only appropriate when using a one or two dimensional plasma physics code that has spatial resolution. These conditions allow the deriva-

tion of the equilibrium formulae without assuming any particular current or pressure distribution in the plasma[1]. The assumption is also made that the effects of diamagnetism in the plasma column are small. This is true when $B_{to}^2 >> B_i^2$, where B_i is the diamagnetic field in the plasma caused by the plasma current. In the EPR, B_{to} = 11.56 Tesla^2 and B_i^2 = .184 Tesla^2.

To generate the proper nominal vertical field; plasma current, major and minor radii, poloidal beta, and internal inductance must be known. Plasma current, major radius, and minor radius can all be quickly and accurately measured in real time (a description of the diagnostic techniques used is given in chapter 4). However, there is presently no way to measure directly or accurately estimate the values of poloidal beta and internal inductance at any time other than an ideally stable situation. It will be shown later that a simple static estimation technique is unstable during shutdown and does not lead to good control. Whatever estimation technique is arrived at will introduce errors in the nominal vertical field which must be corrected by the perturbation feedback controller without using exessive amounts of energy. The feedback control system will be designed to provide a satisfactory response for a given error in the vertical field. Figure (15) shows the percent error in the vertical field magnitude as a function of percent error in the estimation of poloidal beta and internal inductance.

C. Perturbation Feedback Control System

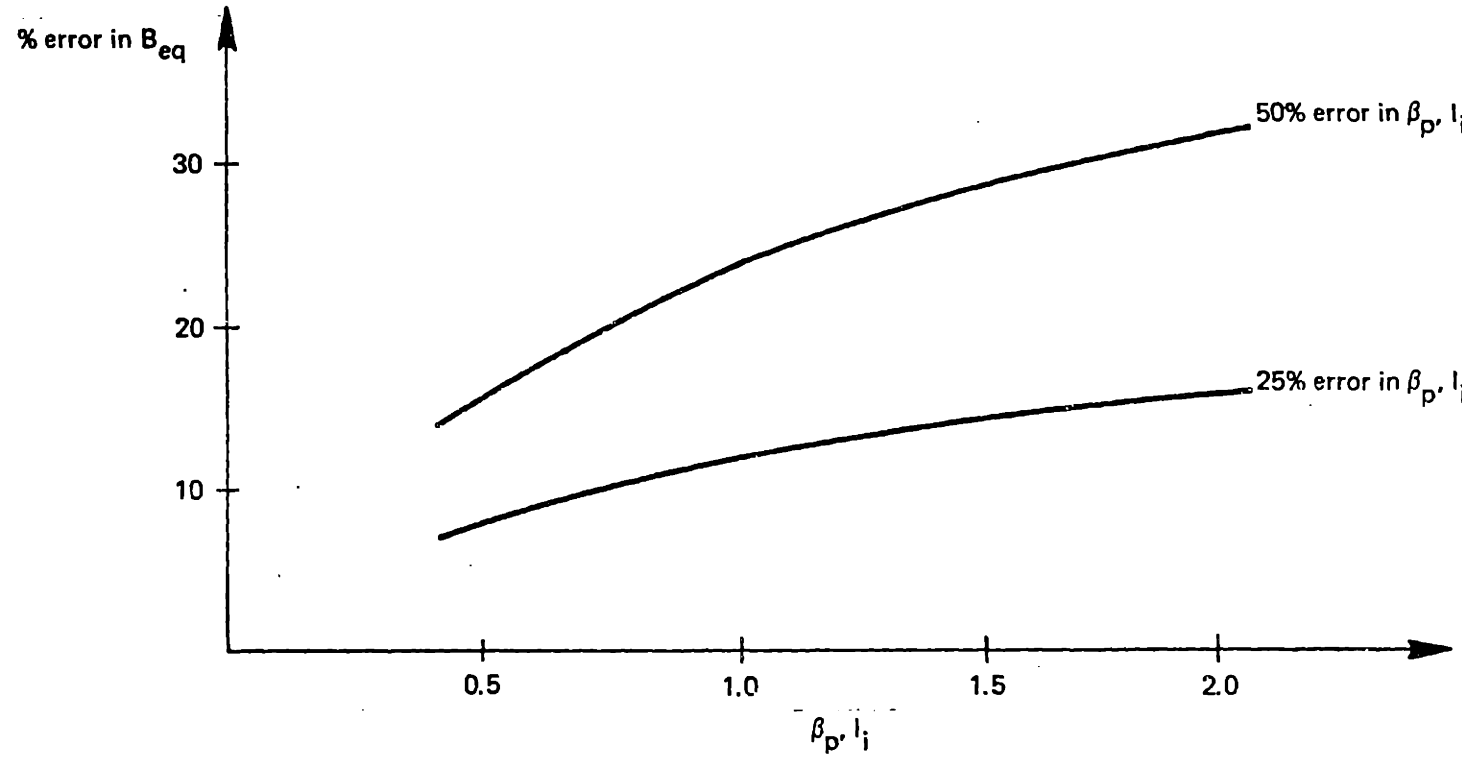

Figure 13 Vertical Field Error

The basis for the design parameters of the perturbation feedback control system are a series of equations that describe the dynamics of the macroscopic plasma motion, vertical field diffusion time, and the vertical field coil current regulator. The biggest problem in describing the system mathematically is the uncertainty in various aspects of plasma physics, notably appropriate transport coefficients, which could have an important effect on the plasma dynamics. However, as the physics become more accurately modeled, the same controller synthesis procedures should still be applicable and would only lead to a modification of the basic design. The equations used will be consistent with using a zero-dimensional plasma physics model.

The system equations used do not have time varying coefficients. It is obvious that many of the parameters of the plasma, such as plasma current, plasma mass, and equilibrium field gradient, vary with time. But if the control system dynamic characteristics are much faster than the dynamic characteristics of the time changing plasma parameters, then a synthesis method based upon a constant coefficient "frozen" approximation is satisfactory. In this case, the diagnostics can respond in less than one msec and the EF coil current regulator can respond in tens of msec. The plasma characteristics vary over a period of seconds. An approximation of the time varying plasma characteristics can be made by scheduling the system gain to one or more dominanat parameters that can be accurately measured.

1. System Dynamics

The dynamic equations used in designing the CSDL candidate plasma

position feedback controller are described below in MKS units:[7]

$$M\frac{d^2r}{dt^2} + I_p\left(\frac{\partial B_v}{\partial r} - \frac{\partial B_{eq}}{\partial r}\right) r + \left(\frac{\mu_o I_p}{2}\right) i_w = I_p B_v \qquad (3)$$

This describes the small motion dynamics of the plasma when it is perburbed about its operating point by changes in the vertical field. Static stability is determined by the sign of the expression:

$$\left(\frac{\partial B_v}{\partial r} - \frac{\partial B_{eq}}{\partial r}\right) \qquad (4)$$

A negative sign on this expression will give a positive (unstable) acceleration in equation (3) and a positive sign will give negative (stable) acceleration provided; in each case, the perturbation in r is positive. A plot of equation (4) can be made over the entire predicted operating regime. This is shown in figure (14), using the values from table (7). The value of $\partial Bv/\partial r$ is found by taking the gradient of the vertical field from figure (15) and scaling it with the vertical field current. $\partial B_{eq}/\partial r$ is the derivative of Shafranov's equation. If poloidal flux is conserved, the minor radius changes with a change in the major radius:

$$\frac{a}{a_o} = \left(\frac{R}{R_o}\right)^{\frac{1}{2}} \qquad (5)$$

This gives an equilibrium field gradient of:

$$\frac{\partial B_{eq}}{\partial r} = -\frac{\mu_o I_p}{4\pi R^2}\left[\ln\frac{8R}{a} + \beta_p + 1i/2 - 2\right] \qquad (6)$$

If it is assumed that a divertor or mechanical limiter keeps the minor radius constant, then the value of the equilibrium field gradient

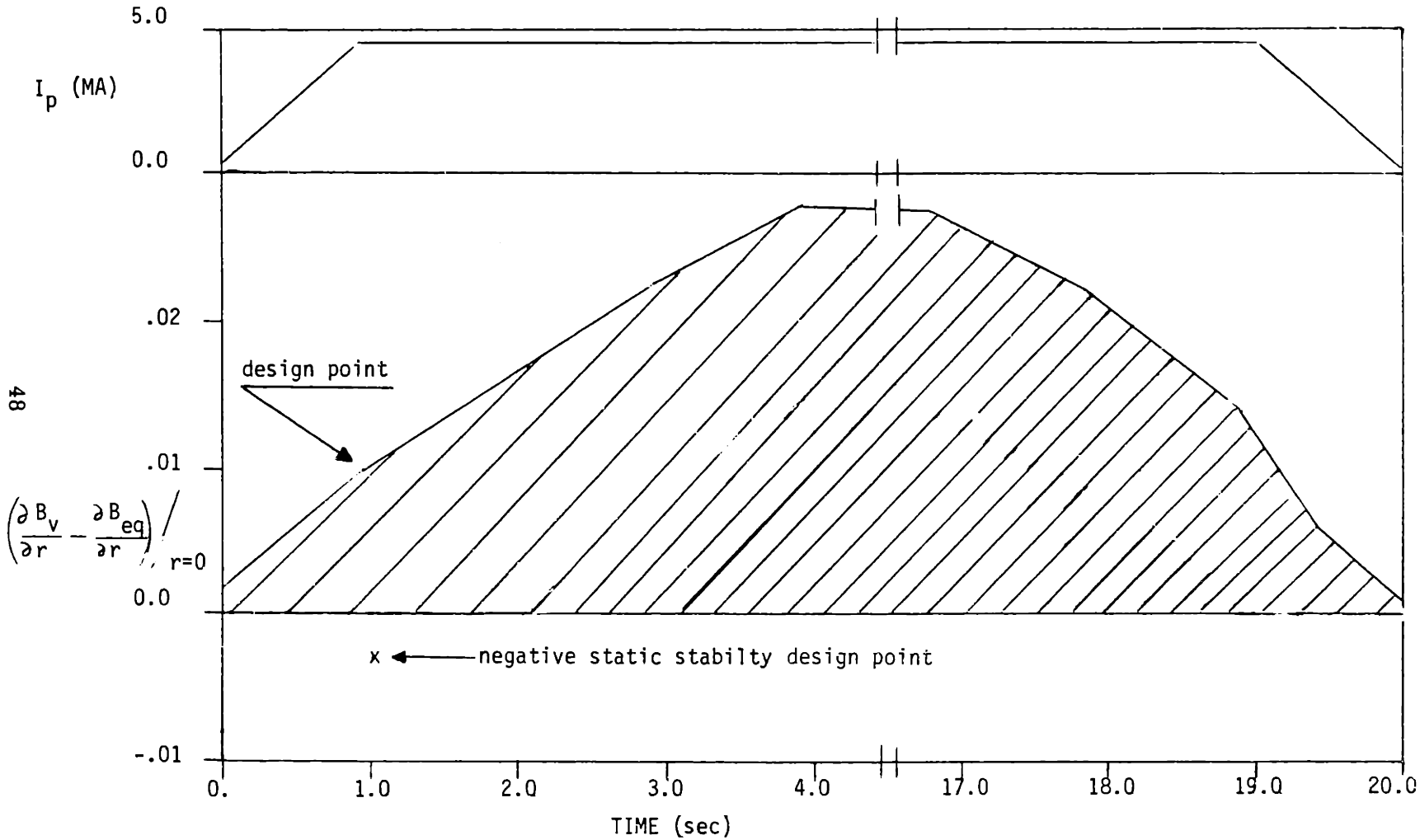

Figure 14 STATIC STABILITY ANALYSIS

TABLE VII

TIME (s)	I_p (MA)	β_p	B_{eq}(T)	$\frac{\partial B_v}{\partial r}$(T/m)	$\frac{\partial B_{eq}}{\partial r}$(T/m)	$\frac{\partial B_v}{\partial r} - \frac{\partial B_{eq}}{\partial r}$ (T/m)
0.0	0.50	0.50	.0194	-.0010	-.0025	.0015
0.5	2.65	0.05	.0835	-.0042	-.0100	.0060
1.0	4.80	0.05	.1513	-.0077	-.0180	.0100
2.0	4.80	0.75	.2051	-.0104	-.0270	.0160
3.0	4.80	1.50	.2627	-.0133	-.0360	.0230
4.0	4.80	2.20	.3164	-.0161	-.0445	.0280
.	.	.	.	.	.	.
.	.	.	.	.	.	.
.	.	.	.	.	.	.
17.0	4.80	2.00	.3010	-.0152	-.0420	.0270
18.0	4.80	1.40	.2550	-.0130	-.0350	.0220
19.0	4.80	0.50	.1860	-.0094	-.0240	.0140
19.5	2.65	0.05	.0840	-.0042	-.0100	.0060
20.0	0.50	1.60	.0300	-.0015	-.0040	.0020

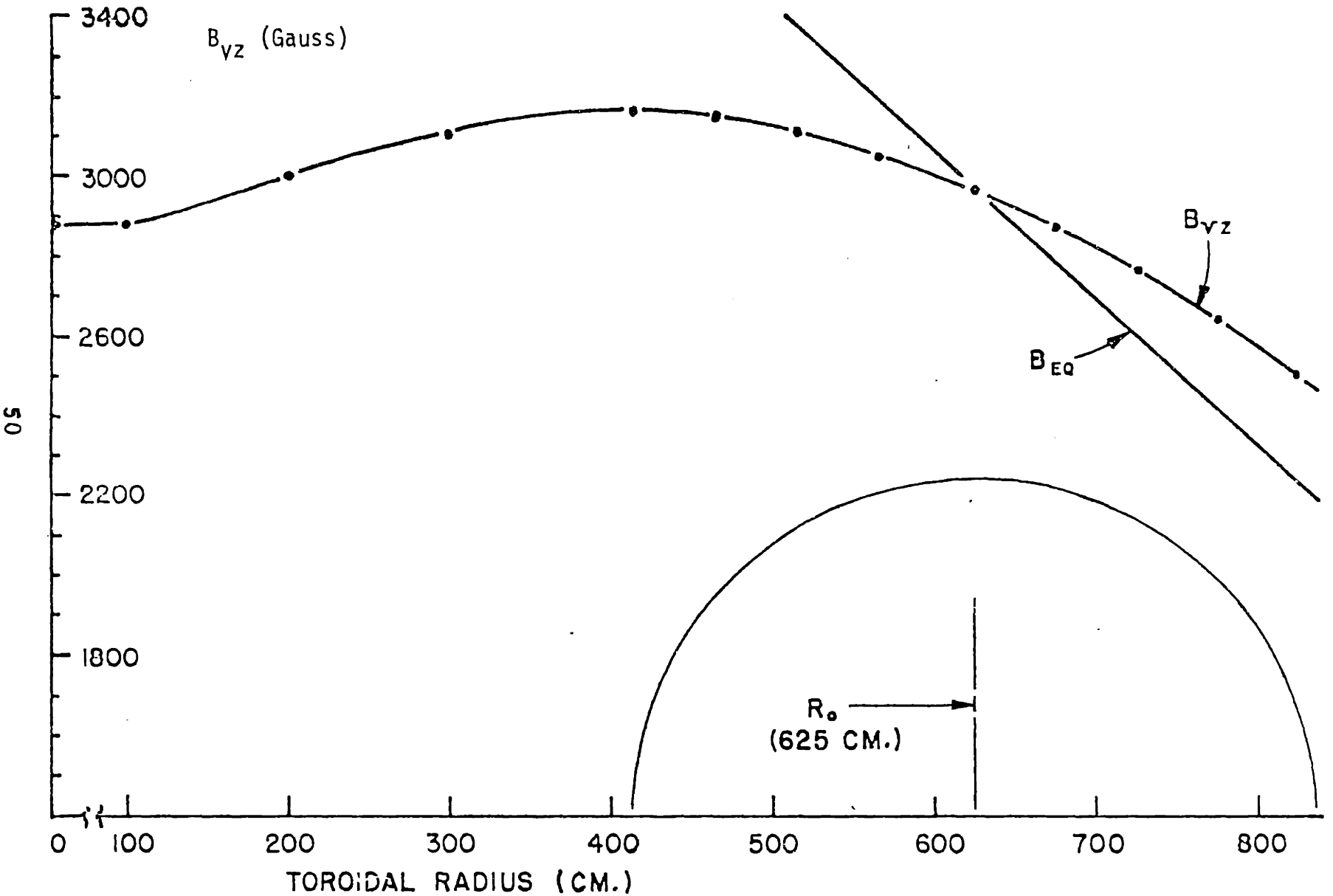

Figure 15 The Neutral Equilibrium Field B_{EQ} and the Stable Vertical Field B_{VZ}

is:

$$\frac{\partial B_{eq}}{\partial r} = -\frac{\mu_o I_p}{4\pi R^2}\left[\ln\frac{8R}{a} + \beta_p + li/2 - 2.5\right] \qquad (7)$$

Equation (6) is more conservative in the sense that it will give less positive static stability. Equation (6) was used to obtain the plot in figure (14) from the values in table (7). Figure (14) shows that the system always has positive static stability. The design point used for the feedback control system is shown on figure (14). This is a point of reduced static stability and should lead to a conservative design.

The equation describing the dynamics of the dipole component of the surface density of current in the wall due to plasma motion is:

$$\frac{di_w}{d_t} + \left(\frac{1}{\tau_w}\right) i_w = \frac{I_p}{\pi a_w^2}\frac{dr}{dt} \qquad (8)$$

The driving force for the motion of the current induced in the wall is the motion of the magnetic field that surrounds, and moves with, the plasma. Despite the seeming complexity of magnetic field diffusion through a complicated wall/blanket structure, references [13, 1] indicate that a first order differential equation is sufficient to describe experimental tokamak devices. The actual design of the wall/blanket and surrounding structure suggests a distributed parameter system model. However, a simple lumped parameter model has been substituted here, based on the experimentally observed characteristic of a single dominant time constant in existing tokamak devices. Complicated power reactor structures will warrant examination of this model

in the future.

The equation that describes the inward diffusion of the vertical magnetic field is:

$$\frac{dB_v}{dt} = \frac{K_{ei}(B_v^1 - B_v)}{\tau_w} \qquad (9)$$

This can be easily derived from equations (173) and (174) in Shafranov's paper. All the terms in (174) disappear because there are no internal conductors. This result is also used later in the modeling of the plasma motion during the operation of the plasma position controller. As in equation (8), a first order differential equation is used to describe the diffusion of a magnetic field through the structure of the reactor. A similar lumped parameter model is used. Notice that the wall time constants for equations (8) and (9) are the same. This implies that the rate of field diffusion outward is the same as the rate of field diffusion inward. This is probably not true since there are different distributed currents in each case that drive the different diffusion. The only way to accurately determine the differences in the diffusion times will be by experimental measurements on the reactor after it is built. Order of magnitude errors or less in the estimation of the diffusion times will probably not change the requirements for the controller dynamic response. Unequal diffusion times will probably necessitate a lead and/or lag compensation network in the feedforward path. Therefore this assumption of equal diffusion times will not effect the basic control system synthesis procedure.

The EF coil current regulator is modeled as follows:

$$\frac{d^2I_v}{dt^2} + 2\rho\omega_n\frac{dI_v}{dt} = \omega_n^2(I_{vcmd} - I_v) \qquad (10)$$

As mentioned previously, this model comes from measurements of the current regulator presently in use on the PLT. That system approximates a second order system with a natural frequency of 150 Hz and a damping coefficient of .8.

The radial position sensor is modeled as:

$$\frac{dr_s}{dt} = \frac{r-r_s}{\tau_s s} \qquad (11)$$

The time constant, τ_s, is the lag of a low pass filter used to remove hard x-ray noise in the position detector. A one msec lag was used in this study. Data from ALCATOR[14] indicates that the time constant may be even less with improved techniques.

The vertical field magnitude at the outside of the reactor vessel is related to the magnitude of the EF coil current by a scaling factor:

$$B_v^1 = K_z I_v \qquad (12)$$

The internal on axis vertical field strength is related to external vertical field strength at the coil by the proportionality constant:

$$Bv = K_{ei}B_v^1 \qquad (13)$$

The plasma position detector used identifies the hotspot in the plasma. This hotspot is the magnetic flux surface center and corresponds to the peak of the density and temperature distributions within the

plasma. This magnetic flux center is usually not the geometric center of the plasma. The hotspot is the point that has to be controlled since 50% of the plasma energy is contained within the center 10% of the plasma volume when Gaussian temperature, density, and current profiles are assumed.

There are no equations included that describe the motion of the magnetic flux center within the plasma. This is because the diffusion of the magnetic field within the plasma is very slow. The one-fluid approximation for magnetic field diffusion through a stationary plasma is:[24]

$$\nabla^2 B - \frac{4\pi\sigma}{c^2} \frac{\partial B}{\partial t} = 0 \quad \text{(cgs)} \tag{14}$$

This has a solution of the form:

$$B \propto e^{-t/t_m} \tag{15}$$

where:

$$t_m = 4\pi\sigma L^2/c^2 \tag{16}$$

A magnetic gradient as small (sharp) as 10cm still gives $t_m \sim 8.7$ sec. This is the characteristic time for changes in the magnetic flux surface distribution within the plasma.

The magnetic Reynold's number[24] ($R_m = 4\pi\sigma L V_o/c^2$) characterizes magnetic field diffusion through a moving plasma. R_m for a 2.1 meter minor radius plasma moving at 1 m s^{-1} is $\sim$1820. This number implies that the field lines are "frozen" into the plasma and move as the plasma moves. The motion of the magnetic flux surface is so slow that it can be neglected in the control system design.

Modern control theory can be used to combine all the dynamic equations into one state variable matrix equation of the form:

$$\left[\Phi\right] = \left[\ F\ \right] \cdot \left[\ x\ \right] + \left[\ G\ \right] \cdot \left[\ u\ \right] \qquad (17)$$

F is the 7 x 7 state matrix with the seven columns representing the values of seven state variables ($v, r, i_w, B_v, \dot{I}_v, I_v, r_s$) and the seven rows are the seven model equations (3, 8, 9, 10, 11, 12, 13). The state variables used determine the dynamic behavior of the system. x is the state vector composed of the seven state variables. G is the control disturbance matrix that represents the disturbances in the dynamic equations. u is the control vector which is composed of the state variables used to control the system. In this case, I_{vcmd} is the only control state variable. Putting the dynamic equations in a state variable matrix equation form allows the use of standard matrix algebra techniques to solve coupled differential equations. This modern control theory approach is necessary for an accurate description of the control problem in a multiple-input–multiple-output dynamic system.

2. Root-Locus Plots and Bode Diagrams

A standard computer program was used to develop root-locus plots and Bode diagrams from equation (17). A computer program was also used to evaluate the classical transfer functions associated with the state variable representation. A parametric study was done at two points on the burn cycle to see the effect of positive and negative static stability on the open loop response of the system. One study was done at the design point indicated on figure (14) and another study was done at

point "x" on figure (14). Point "x" corresponds to negative static stability. Point "x" was chosen to allow for variations in $\partial B_v / \partial r$ from possible changes in the EF gradient and to allow for variations in $\partial B_{eq} / \partial r$ from changes in the nominal operating characteristics of the plasma during startup or shutdown. Figure (16) is a Bode diagram of the open loop response of the system dynamics at the point of negative static stability. Figure (17) is a Bode diagram of the open loop response of the system dynamics at the design point of reduced positive static stability. Table (8) shows the values used in equation (17) for the case of negative static stability. For the open loop response for negative static stability, the negative phase margin was very small at very low frequencies.

Figures (18) and (19) show root-locus plots of the same points. Figure (18) is for negative static stability and figure (19) is for positive static stability. It is clear here that the system dynamics dominate over whether or not the system is positively or negatively statically stable. The only difference caused by the static stability value is the root at s = -.44 on figure (18) and the root at s = +.92 on figure (19). These roots would only be noticed at very low gains and very low frequencies.

One pair of roots is not shown on figures (18) or (19) since it is off the scale. These points occur at $25.46 \pm j4.92 \times 10^5$ on figure (18) and at $24.78 \pm j1.83 \times 10^6$ on figure (19). These roots are very lightly damped ($\zeta = 5.18 \times 10^{-5}$, $\zeta = 1.35 \times 10^{-5}$) and have very high natural frequencies ($\omega_n = 4.92 \times 10^5$ rad s^{-1}, $\omega_n = 1.83 \times 10^6$ rad s^{-1}).

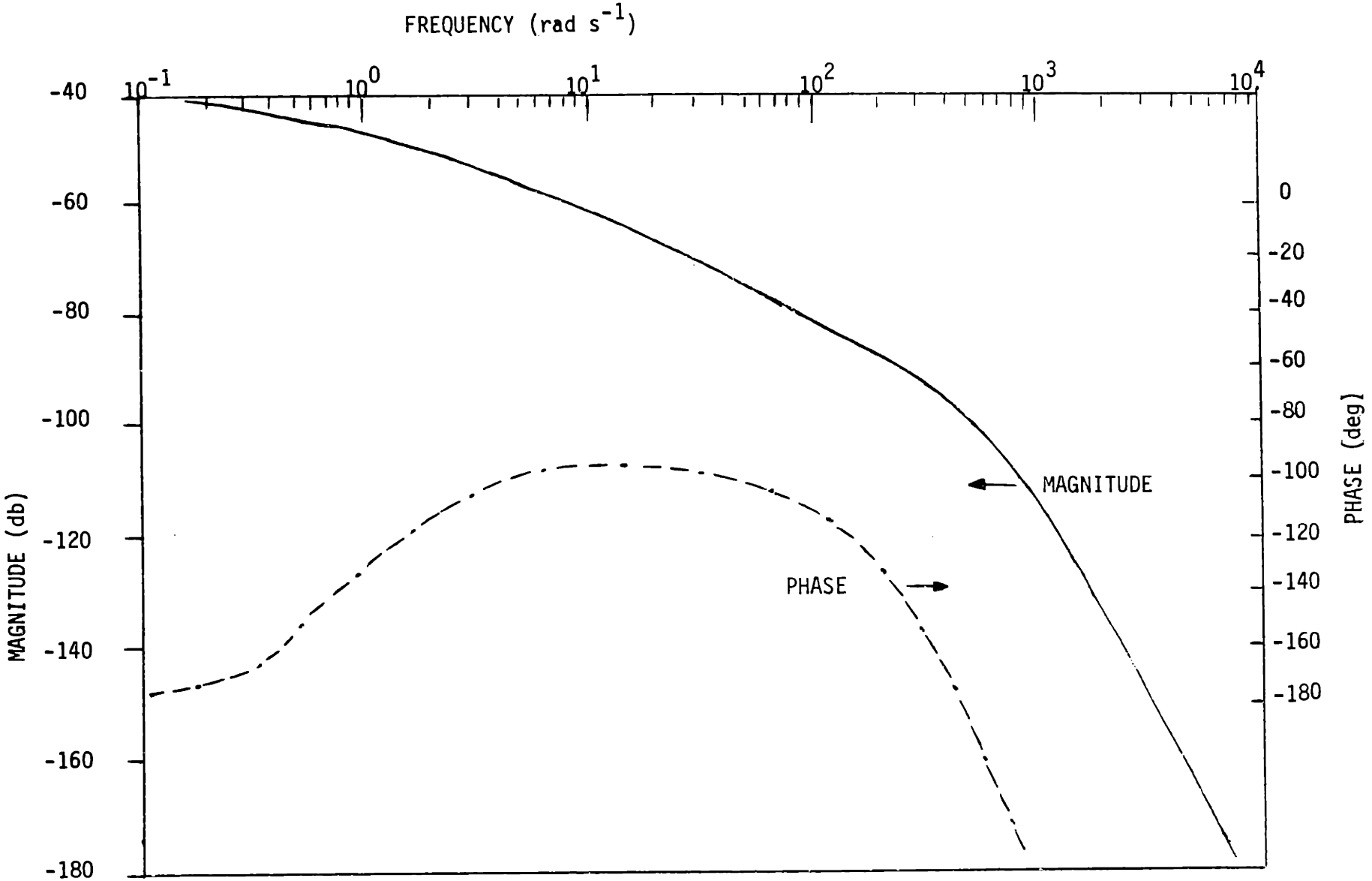

Figure 16 Open-Loop Response With Negative Static Stability

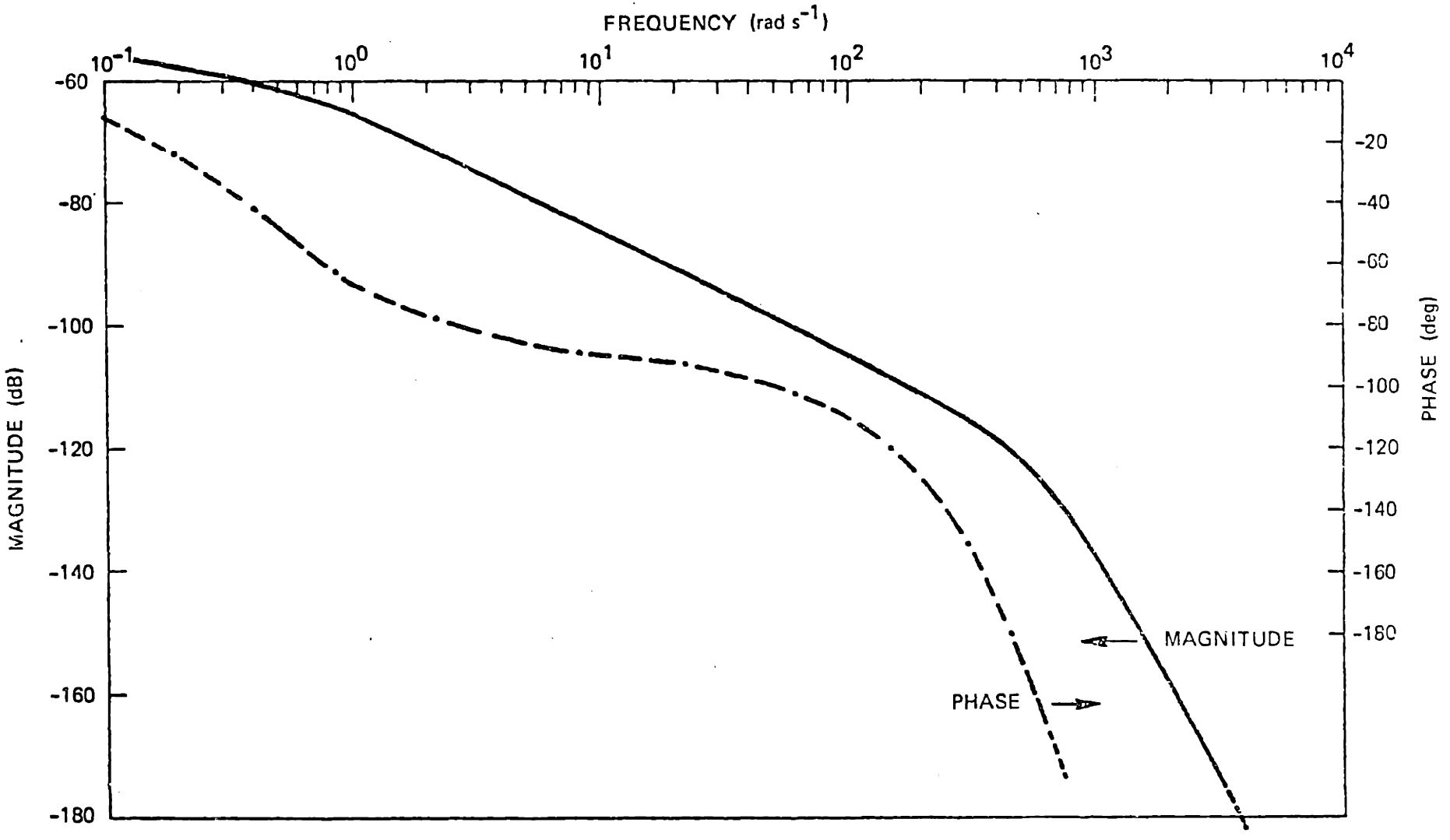

Figure 17 Open-Loop Response With Positive Static Stability

TABLE VIII

$$F = \begin{array}{c} \begin{matrix} v & r & i_w & B_{vz} & \dot{I}_v & I_v & r_s \end{matrix} \\ \begin{bmatrix} 0 & -4.44 \times 10^{9} & -9.31\ 10^{5} & 1.48\ 10^{12} & 0 & 0 & 0 \\ 1.0 & 0 & 0 & 0 & 0 & 0 & 0 \\ 2.65\ 10^{5} & 0 & -.5\ 10^{2} & 0 & 0 & 0 & 0 \\ 0 & 0 & 0 & -.5\ 10^{2} & 0 & 1.84\ 10^{-3} & 0 \\ 0 & 0 & 0 & 0 & -1.01\ 10^{3} & -3.95\ 10^{5} & 0 \\ 0 & 0 & 0 & 0 & 1.0 & 0 & 0 \\ 0 & 1\ 10^{3} & 0 & 0 & 0 & 0 & -1.\ 10^{3} \end{bmatrix} \end{array}$$

$$x = \begin{bmatrix} v \\ r \\ i_w \\ B_{vz} \\ \dot{I}_v \\ I_v \\ r_s \end{bmatrix} \quad G = \begin{bmatrix} 0 \\ 0 \\ 0 \\ 0 \\ 3.95\ 10^{5} \\ 0 \\ 0 \end{bmatrix} \quad u = \begin{bmatrix} I_{vcmd} \end{bmatrix}$$

System matrices corresponding to equation (17) and the parameter values of Table 7

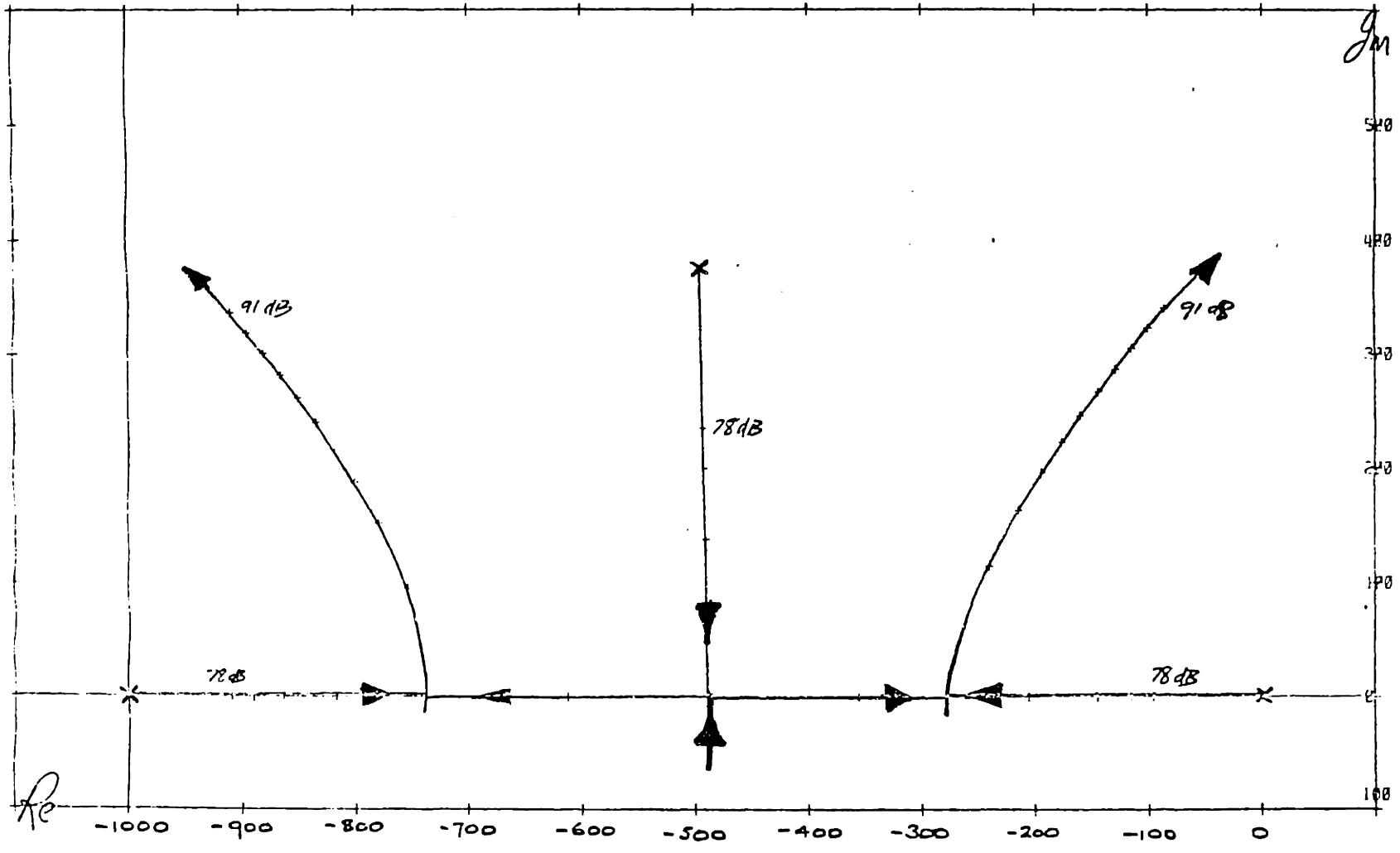

ROOT-LOCUS PLOT FOR LOW MAGNITUDE NEGATIVE STATIC STABILITY

Figure 18

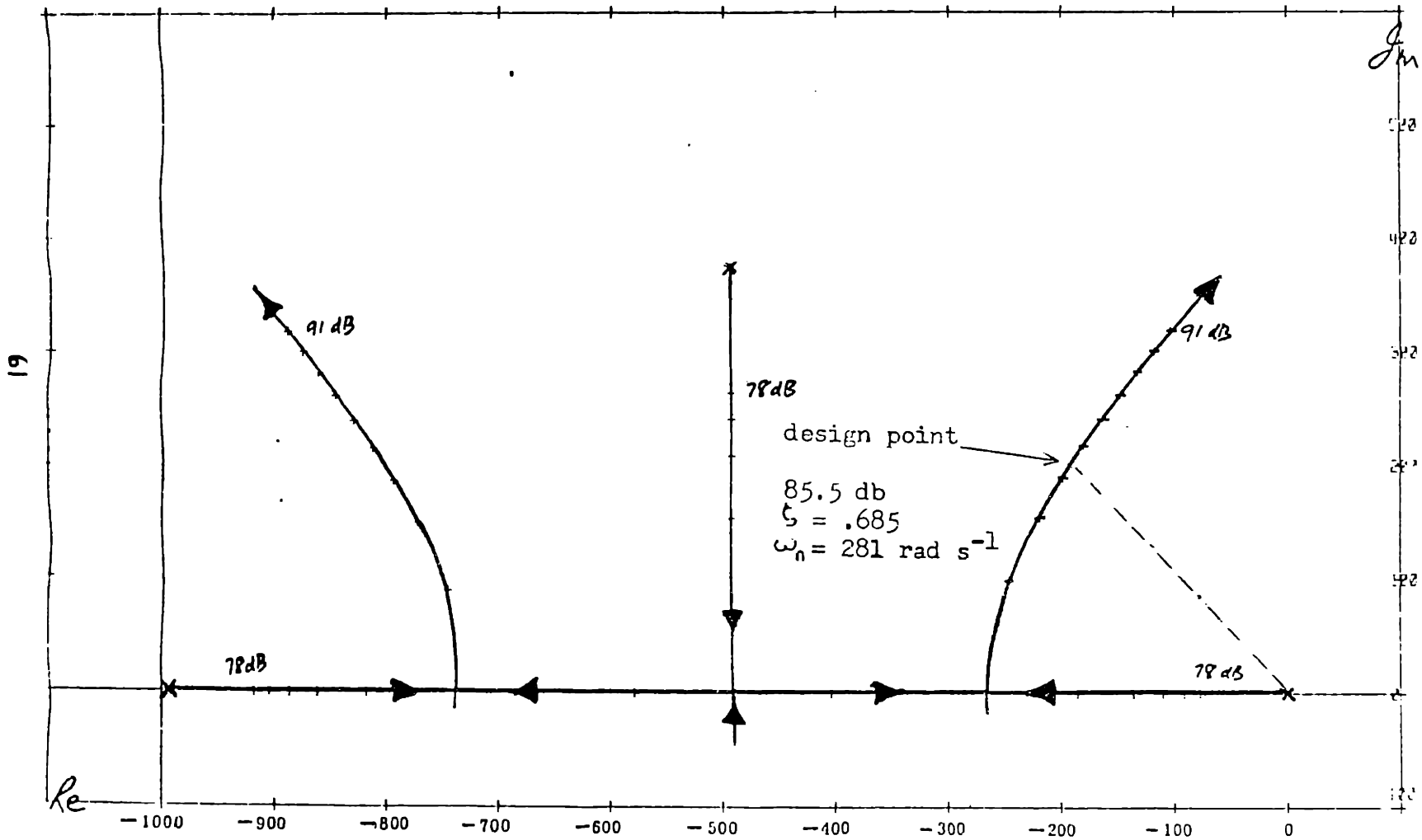

Figure 19 ROOT-LOCUS PLOT FOR POSITIVE STATIC STABILITY

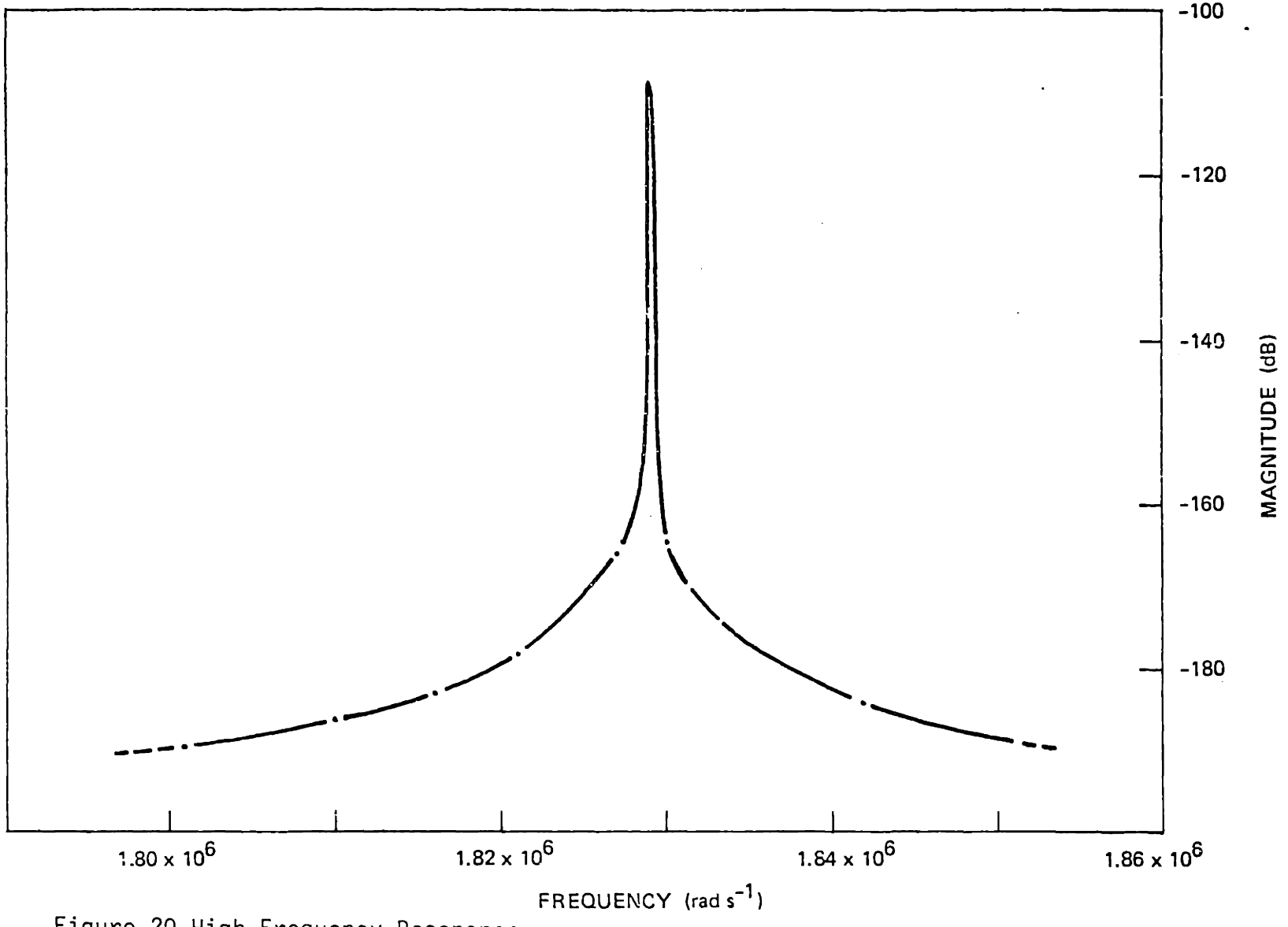

Figure 20 High Frequency Resonance

TABLE IX

OPEN LOOP CHARACTERISTICS

A. Negative Static Stability

$$G(s) = \frac{r(s)}{I_{vcmd}(s)} = \frac{7.66\ 10^{14}}{(s-.92)(s^2+50.92s+2.42\ 10^{11})(s^2+1010s+3.95\ 10^5)}$$

$$H(s) = \frac{r_s(s)}{r(s)} = \frac{1000}{s + 1000}$$

$$K_{DC} = -8.708\ 10^{-3}$$

B. Positive Static Stability

$$G(s) = \frac{r(s)}{I_{vcmd}(s)} = \frac{7.66\ 10^{14}}{(s+.44)(s^2+49.56s+3.35\ 10^{12})(s^2+1010s+3.95\ 10^5)}$$

$$H(s) = \frac{r_s(s)}{I_{vcmd}(s)} = \frac{1000}{s + 1000}$$

$$K_{DC} = 1.316\ 10^{-3}$$

C. Closed Loop Response

$$\frac{K_r\ G(s)}{1 + K_r\ G(s)\ H(s)} =$$

$$\frac{(1.443\ 10^{19})(s + 1000)}{(s+1000)(s+.44)(s^2+49.56s+3.35\ 10^{12})(s^2+1010s+3.95\ 10^5) + 1.443\ 10^{22}}$$

$K_r = 1.884\ 10^4$ A/m

$$\text{Steady State Error} = \frac{100}{1 + K_r K_{DC}} = 3.88\%$$

Bandwidth = 300 rad s^{-1} Cutoff Frequency = 145 rad s^{-1}

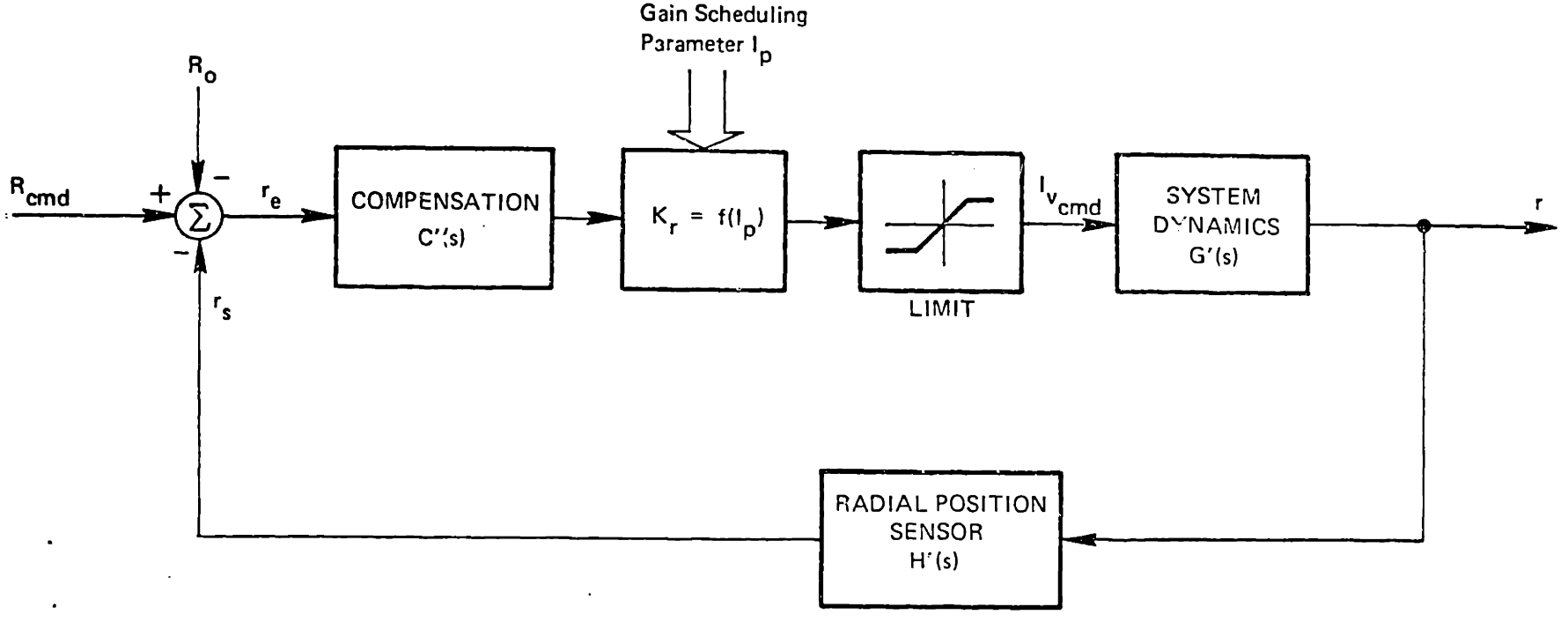

Figure 21 Perturbation Feedback Control System

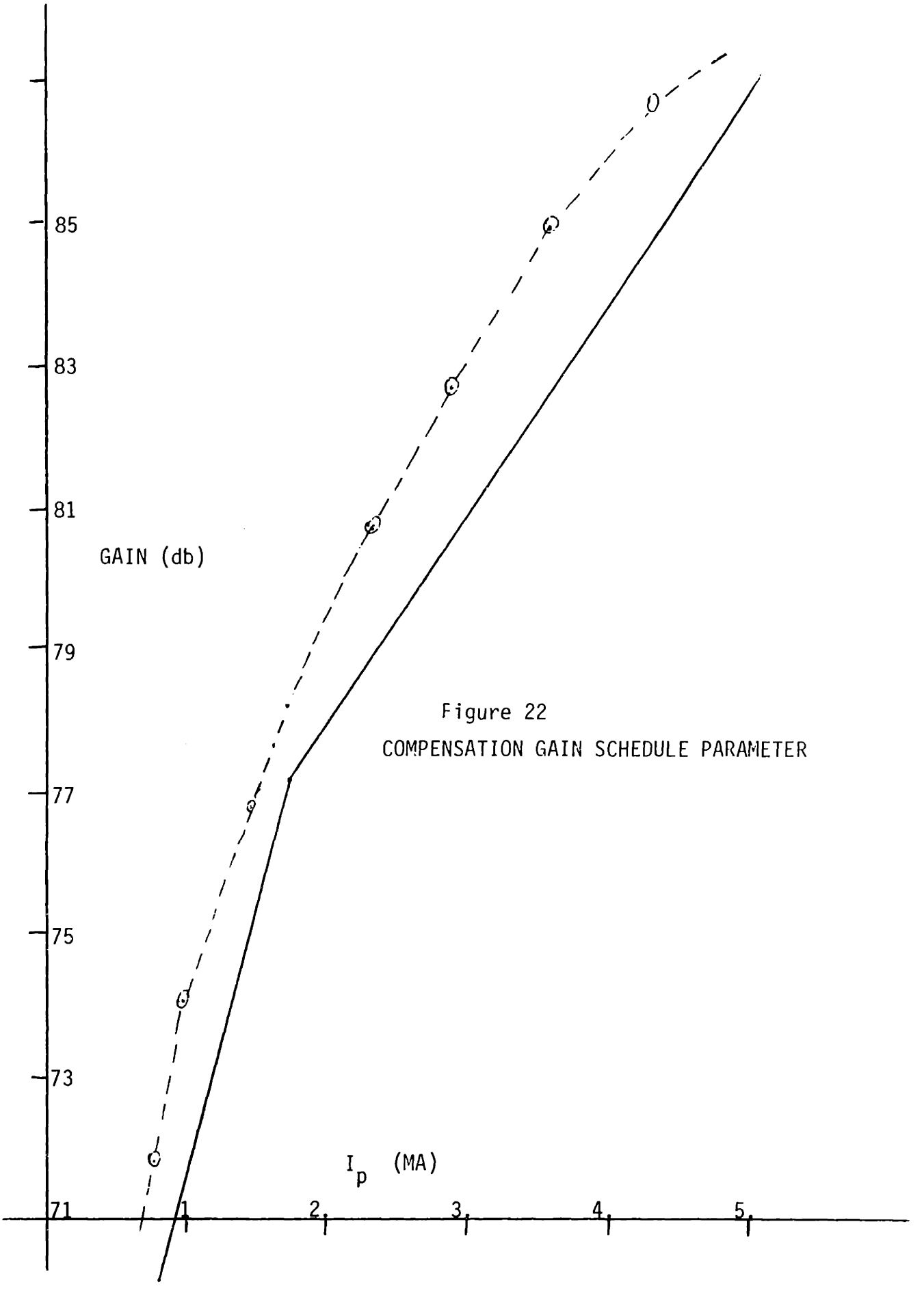

Figure 22

COMPENSATION GAIN SCHEDULE PARAMETER

Neither of these two points are on the Bode diagrams. An example of the attenuation of these points that is provided by the system dynamics is shown in figure (20). This shows the attenuation of the high frequency root of the positive static stability case to be -110 db. The high frequency dynamics of the plasma are a result of the low inertia of the plasma column. The controller design bandwidth need not be extended to try and control this high frequency resonance. The Foucault currents created by the motion of the plasma tend to provide a stabilizing vertical field until they decay with a time constant of τ_w. Table (9) shows the transfer functions for the cases of positive and negative static stability.

While this high frequency resonance causes no problems for the control system, the effect on possible plasma microinstabilities must be examined. A disturbance of the plasma at a frequency near the ion cyclotron frequency, ω_{ci} ($\omega_{ci} = eB/m_i c \sim 1.3 \times 10^8$ rad s^{-1}), can cause an Alfven wave which will propogate parallel to the magnetic field and radiate disturbances in a perpendicular direction. The velocity of the wave, V_a ($V_a = B/\sqrt{4\pi n m_i}$), would be $\sim 6.6 \times 10^6$ m s^{-1}. Any Alfven wave created by the plasma motion would be attenuated proportional to[24]:

$$\omega_i \propto \exp\left[\frac{-B^2}{8\pi n \kappa T_i}\frac{\omega_{ci}^2}{\omega_r^2}\right] \qquad (18)$$

For the EPR nominal design this is:

$$\omega_i \propto \exp(-1.186 \times 10^5) \sim 0 \qquad (19)$$

The problem of Alfven waves should not exist since the high frequency motion waves will be effectively damped.

3. Design Parameters

Figure (21) shows the basic design of the perturbation feedback controller. All that needs to be determined now are the gain, compensation, and limits necessary for a desired closed loop operation. Using the design point of figure (14) and the root-locus plot of figure (19), it should be possible to specify the damping coefficient and natural frequency desired. Such a point is shown on figure (19). At a gain of 85.5 db, the dominant roots of the system will have a damping coefficient of .7 and a natural frequency of about 280 rad s^{-1}. The actual system will be slightly different from this since there are other roots that have different damping coefficients and natural frequencies at that specific value of gain. These dominant roots are located at $-505 \pm j374$.

This analysis of the plasma dynamics has identified the three major parameters that effect the position control design. The three variables are: plasma mass, plasma current, and the magnetic static stability. The parametric study showed that magnetic static stability has very little effect on the system design parameters and that the plasma mass had only a negligible effect on the system response. Assuming negative static stability caused only a very slight degradation of system characteristics when compared to the case of positive static stability. For that reason, only plasma current was included as a gain scheduling parameter for the perturbation feedback control system.

Figure (22) is a plot of the gain schedule used in the feedback system. The dotted curve represents the values of the gain that were

obtained by taking the nominal ANL/EPR values of the plasma parameter at various "frozen" design points over the nominal burn cycle and calculating the appropriate gain. The solid line is the gain schedule that was used in the feedback control system. This is slightly conservative design in that the gain used is always slightly less than the gain calculated from the nominal plasma characteristics. This should insure stability without degrading the closed loop performance. It should be noted that the resulting gain schedule is approximately proportional to $1/I_p$.

4. Control System Characteristics

Figure (23) is a Bode diagram of the closed loop response of the feedback control system when operated at the positive static stability design point of figure (14). The cutoff frequency is approximately 145 rad s^{-1} and the bandwidth is 300 rad s^{-1}. Table (9) has the closed loop transfer function used for this diagram. The bandwidth appears sufficient to control the important system dynamics. There appear to be no resonances in the operating regime of the controller. The steady state error is 3.88%. The response seems good enough to warrant no phase compensation in the feedback system.

Figure (24) is a diagram of the CSDL candidate plasma position control system with both the feedforward and feedback systems included. Notice there is a lead compensation network included in the feedforward system. While there are large lags included in this system, they tend to cancel each other out. This is because the simple lumped parameter model for inward and outward field diffusion in the reactor vessel uses the same wall time constant in each case. For this reason, the network

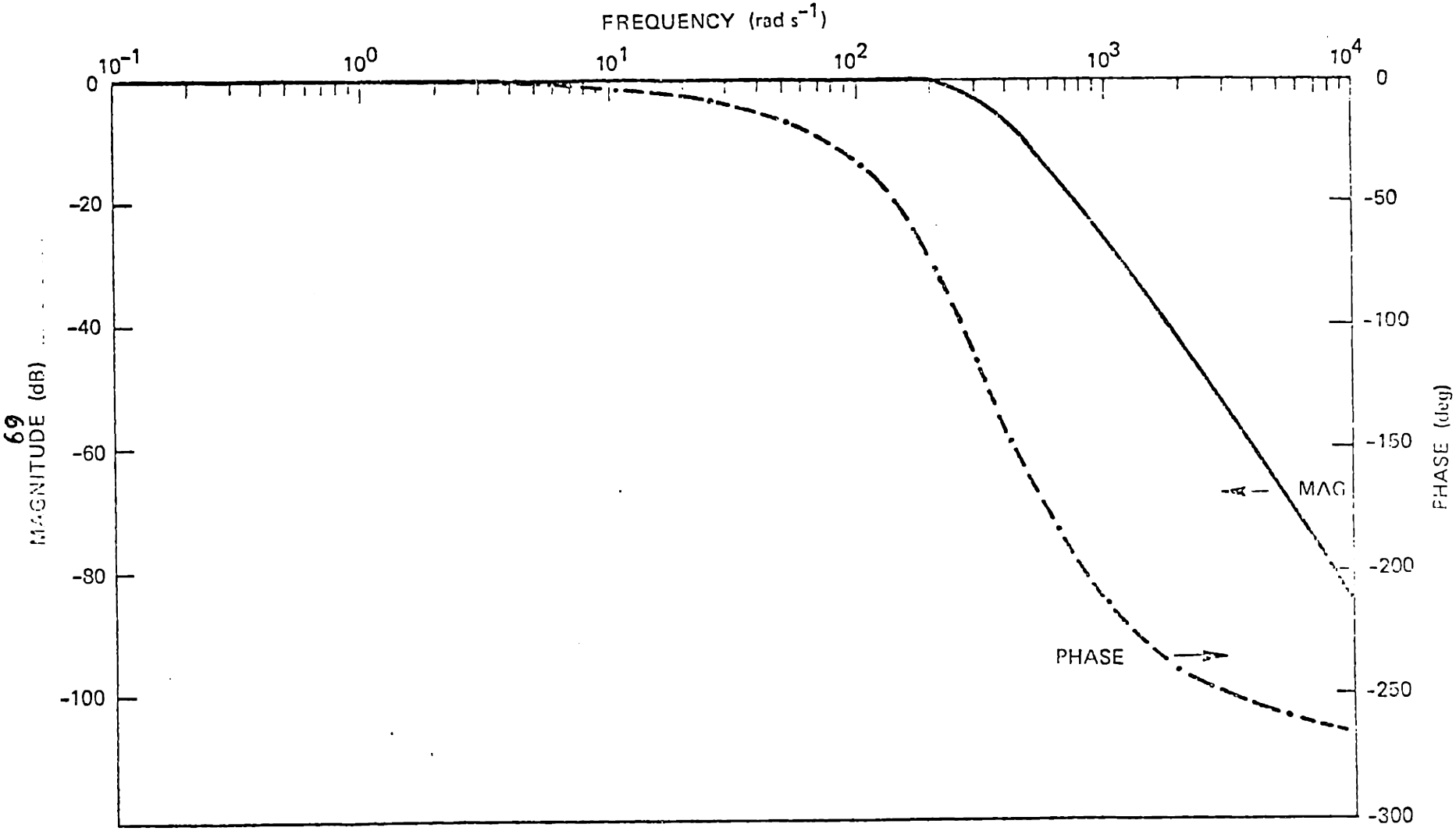

Figure 23 CLOSED LOOP CONTROL SYSTEM RESPONSE

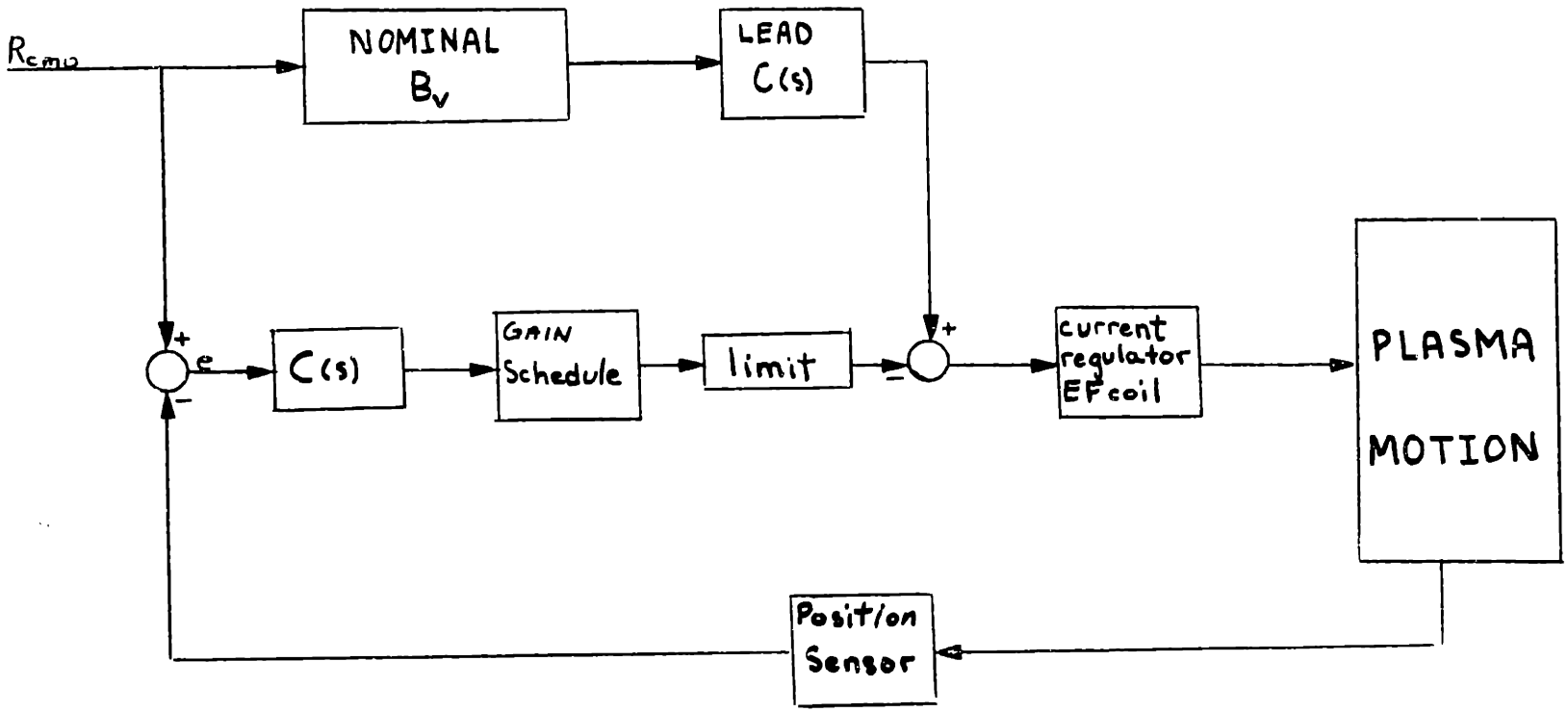

Figure 24 CSDL CANDIDATE PLASMA POSITION CONTROL SYSTEM

may possibly degrade the performance of this system. Experimental measurements on a completed reactor structure will be needed to determine or not any lead, or even lag, compensation is required in a final controller design. The results of the application of this controller to the plasma model are in chapter 4.

Chapter 4. Controller Operation

A. Analog Equations to Difference Equations

Before the plasma position controller model was applied to the plasma physics model, the analog equations of chapter 3 were put in the form of difference equations to simulate the digital operation of the controller. Figure (25) shows the controller with analog equations.

A z-transform can be used to relate a continuous time Laplace transform to a function that is sampled at discrete time periods. If the sampling frequency, F_s, is equal to 1/T; then the z-transform is defined to be:[27]

$$z \equiv e^{Ts} \tag{20}$$

where T is the sampling interval. The z-transformed equation can then be written in difference equation form to model the discrete sampling rate of the continuous equation.

1. EF coil current regulator. For the EF coil current regulator the equations are:

$$\frac{I_v}{I_{vt}} = \frac{\omega_n^2}{s^2 + 2\rho\omega_n s + \omega_n^2} \tag{21}$$

$$s^2 I_v = -2\rho\omega_n s I_v + \omega_n^2 (I_{vt} - I_v) \tag{22}$$

Or, in derivative form:

$$\ddot{I}_v = -2\rho\omega_n \dot{I}_v + \omega_n^2 (I_{vt} - I_v) \tag{23}$$

Let:

$$\dot{I}_v = y \tag{24}$$

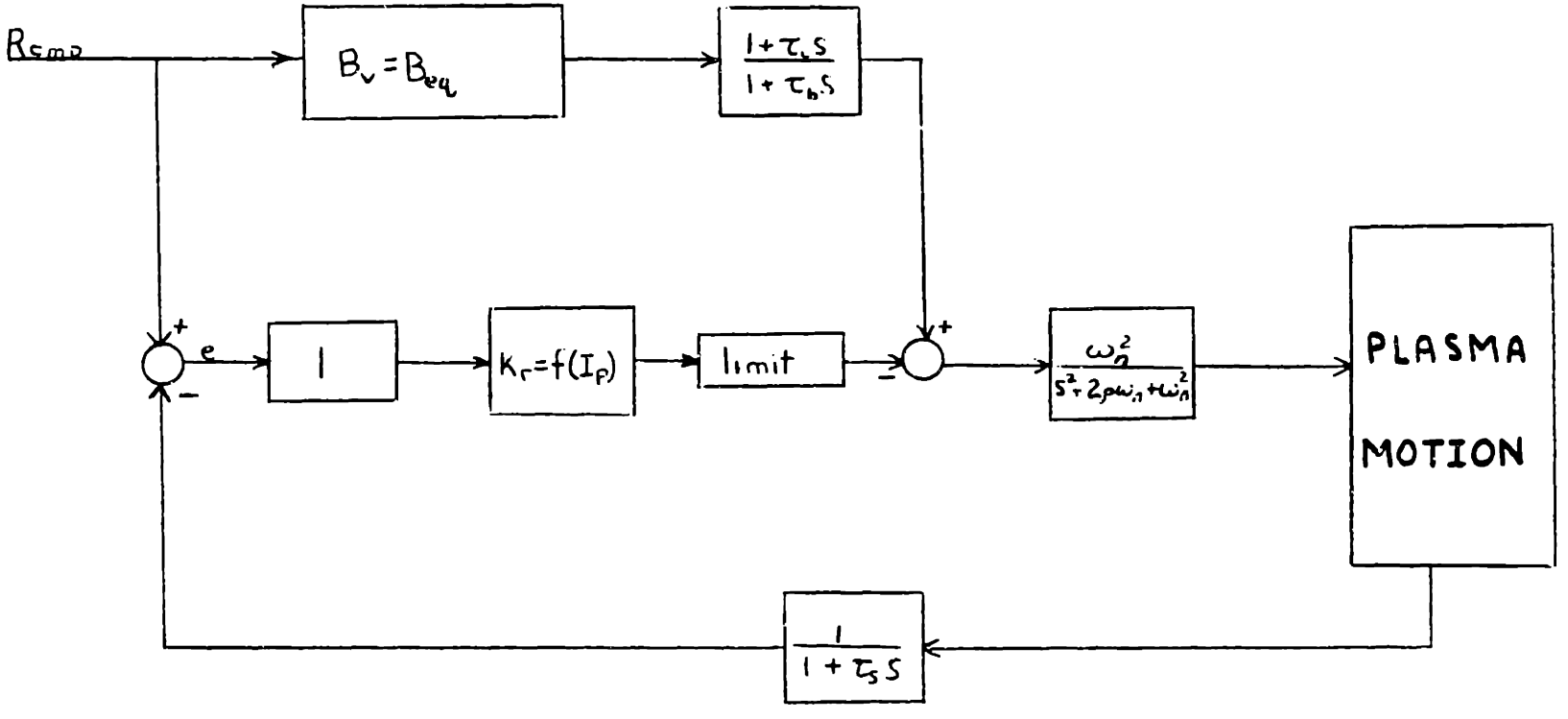

Figure 25 CONTROL SYSTEM SHOWING ANALOG EQUATIONS

Then:

$$\dot{y} = -2\rho\omega_n y + \omega_n^2(I_{vt} - I_v) \tag{25}$$

From equation (24):

$$\frac{I_v}{y} = \frac{1}{s} \tag{26}$$

and from equation (25):

$$\frac{y}{(I_{vt} - I_v)} = \frac{\omega_n^2}{2\rho\omega_n + s} = \frac{\omega_n/2\rho}{1 + s/2\rho\omega_n} \tag{27}$$

Transforming equation (26) gives:

$$\frac{I_v(k)}{y(k)} = \frac{Tz^{-1}}{1 - z^{-1}} \tag{28}$$

which reduces to:

$$I_v(k) = I_v(k-1) + Ty(k-1) \tag{29}$$

Transforming equation (27) gives:

$$\frac{y(k)}{(I_{vt}(k) - I_v(k)} = \frac{\omega_n/2}{1 - z^{-1}e^{-2\rho\omega_n T}} \tag{30}$$

which reduces to:

$$y(k) = \left[I_{vt}(k) - I_v(k)\right](\omega_n/2\rho)(1 - e^{-2\rho\omega_n T}) + y(k-1)e^{-2\rho\omega_n T} \tag{31}$$

Equations (29) and (31) describe the EF coil current regulator. Equation (31) must be solved first each cycle through the controller to obtain the present value of y(k).

2. Plasma position detector. For the x-ray position detector the transform is as follows:

$$\frac{R_f}{R} = \frac{1}{1 + \tau_s s} \tag{32}$$

The transform is:

$$\frac{R_f(k)}{R(k)} = \frac{1}{1 - z^{-1}e^{-T/\tau_s}} \tag{33}$$

which reduces to:

$$R_f(k) = R(k)(1 - e^{-T/\tau_s}) + R_f(k-1)e^{-T/\tau_s} \tag{34}$$

3. Lead compensation network. The transform is:

$$\frac{I_{vff}}{I'_{vff}} = \frac{1 + \tau_c s}{1 + \tau_b s} \tag{35}$$

Breaking this into two parts gives:

$$\frac{x_2}{I'_{vff}} = \frac{1}{1 + \tau_b s} \tag{36}$$

$$\frac{x_1}{I'_{vff}} = \frac{\tau_c s}{1 + \tau_b s} \tag{37}$$

Taking the transforms gives:

$$\frac{x_2(k)}{I'_{vff}(k)} = \frac{1 - e^{-T/\tau_b}}{1 - z^{-1}e^{-T/\tau_b}} \tag{38}$$

$$\frac{x_1(k)}{I'_{vff}(k)} = \frac{(\tau_c/\tau_b)}{1 - z^{-1}e^{-T/\tau_b}} (1 - z^{-1}) \tag{39}$$

These equations reduce to:

$$x_2(k) = I'_{vff}(1 - e^{-T/\tau_b}) + x_2(k-1)e^{-T/\tau_b} \quad (40)$$

$$x_1(k) = \left[I'_{vff}(k) - I'_{vff}(k-1)\right](\tau_c/\tau_b) + x_1)k-1)e^{-T/\tau_b} \quad (41)$$

The sum of these two equations gives the feedforward current.

$$I_{vff} = x_1(k) + x_2(k) \quad (42)$$

Figure (26) shows the model of the plasma position controller with the difference equations.

4. Plasma motion. A model of the plasma motion must be added at this time. From Shafranov[1], the displacement of the plasma is described to be:

$$\Delta = \Delta_0 - \left[\frac{2\pi a_w^2}{\mu_o I_p}\right](B_0 + B_1) \quad (43)$$

B_0 is defined to be the true balancing vertical field inside the vessel:

$$B_0 = B_{vi} + B_v \quad (44)$$

B_{vi} is the vertical field due to the internal conductors in Shafranov's paper. Since there are no internal conductors in the EPR:

$$B_0 = B_v \quad (45)$$

The penetration of the vertical field through the reactor vessel is:

$$\frac{dB_v}{dt} = \frac{B'_v - B_v}{\tau_w} \quad (46)$$

The Laplace transform is:

$$B_v = \frac{B'_v - B_v}{\tau_w s} \quad (47)$$

B_1 represents the amount of additional displacement that occurs as the vertical field leaks through the reactor vessel. This leakage field is:

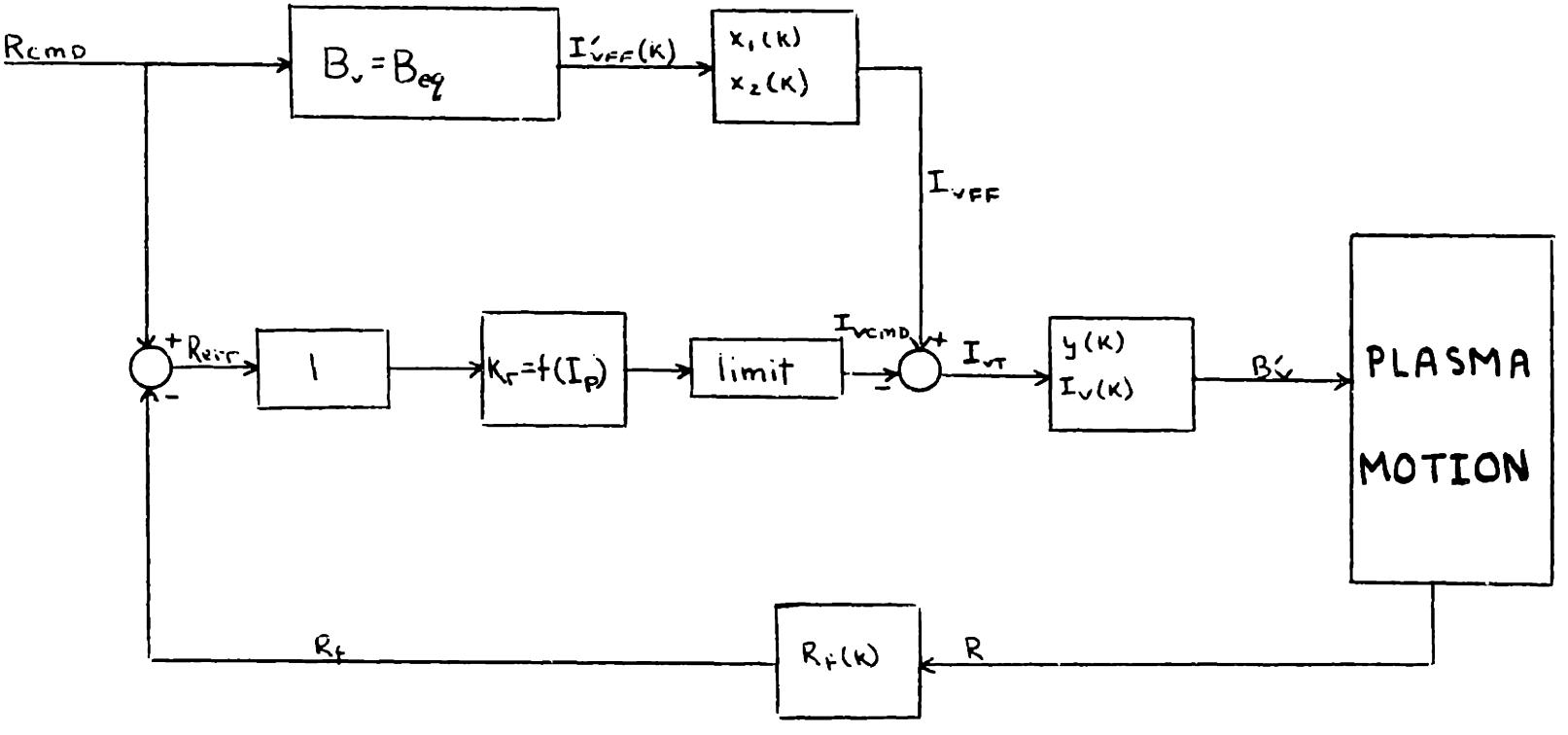

Figure 26 CONTROL SYSTEM SHOWING DIFFERENCE EQUATIONS

$$\frac{dB_1}{dt} = -\frac{1}{\tau_w}(B_{eq} - B_0) = -\frac{1}{\tau_w}(B_{eq} - B_v) \qquad (48)$$

Making a Laplace transform:

$$B_1 = \frac{B_v - B_{eq}}{\tau_w s} \qquad (49)$$

Substituting into equation (43) gives:

$$\Delta = \Delta_0 - \frac{2\pi a_w^2}{\mu_0 I_p} \frac{B_v - B_{eq}}{\tau_w s} \qquad (50)$$

Δ_0 is the displacement of the plasma in an ideally conducting casing. In an ideally conducting casing, the equilibrium field required would be generated by the Foucault currents caused by an offset of the plasma of Δ_0 meters. The magnitude of the offset is:

$$\Delta_0 = \frac{a_w^2}{2R}\left[\ln(a_w/a) + (1 - a^2/a_w^2)(\beta_p + li/2 - 1/2)\right] \qquad (51)$$

This formula is applicable when $\Delta_0 \ll a_w$. The magnitude of Δ_0 during the flat top region of the burn cycle is .3 m. This is much smaller than the vessel minor radius of 2.4 m. In a real tokamak where the casing is deliberately not a perfect conductor, this offset has a decay time of the wall time constant. In an EPR, unlike a small experimental device, the burn cycle length is approximately one thousand times longer than the wall time constant. As a result, this ideal casing offset is only important as an initial condition to the controller operation and does not show up in the dynamics of the plasma motion. Equation (51) becomes inac-

curate at high poloidal betas when the magnetic flux surfaces in the plasma are severely deformed. Substituting into equation (50) with equation (51) gives the following equation for the offset of the plasma during the controller operation:

$$\Delta = \frac{a_w^2}{2R}\left(\ln(a_w/a) + (1 - a^2/a_w^2)(\beta_p + li/2 - 1/2)\right) - \left(\frac{2\pi a_w^2}{\mu_o I_p}\ \frac{B_v - B_{eq}}{\tau_w s}\right) \qquad (52)$$

This gives a plasma major radius of:

$$R = R_w + \Delta \qquad (53)$$

where R_w is the major radius of the reactor vessel. Putting equation (52) into difference form gives:

$$\Delta(k) = \Delta(k-1) + (T/\tau_w)\frac{2\pi a_w^2}{\mu_o I_p}(B_v - B_{eq}) \qquad (54)$$

with the initial conditions being set by equation (51). Figure (27) shows the model of the plasma motion used in this study.

B. Subroutine DRAPER Structure

The equations that describe the controller operation and plasma motion are included in subroutine DRAPER in the MAKO computer code. A complete listing is available by request. Figure (28) shows a flow chart of DRAPER. The code enters DRAPER every cycle and checks for operation of the plasma position controller. If the code is not in use, the plasma position remains constant and the vertical magnetic field is set equal to the equilibrium field. If the position controller is being used, the

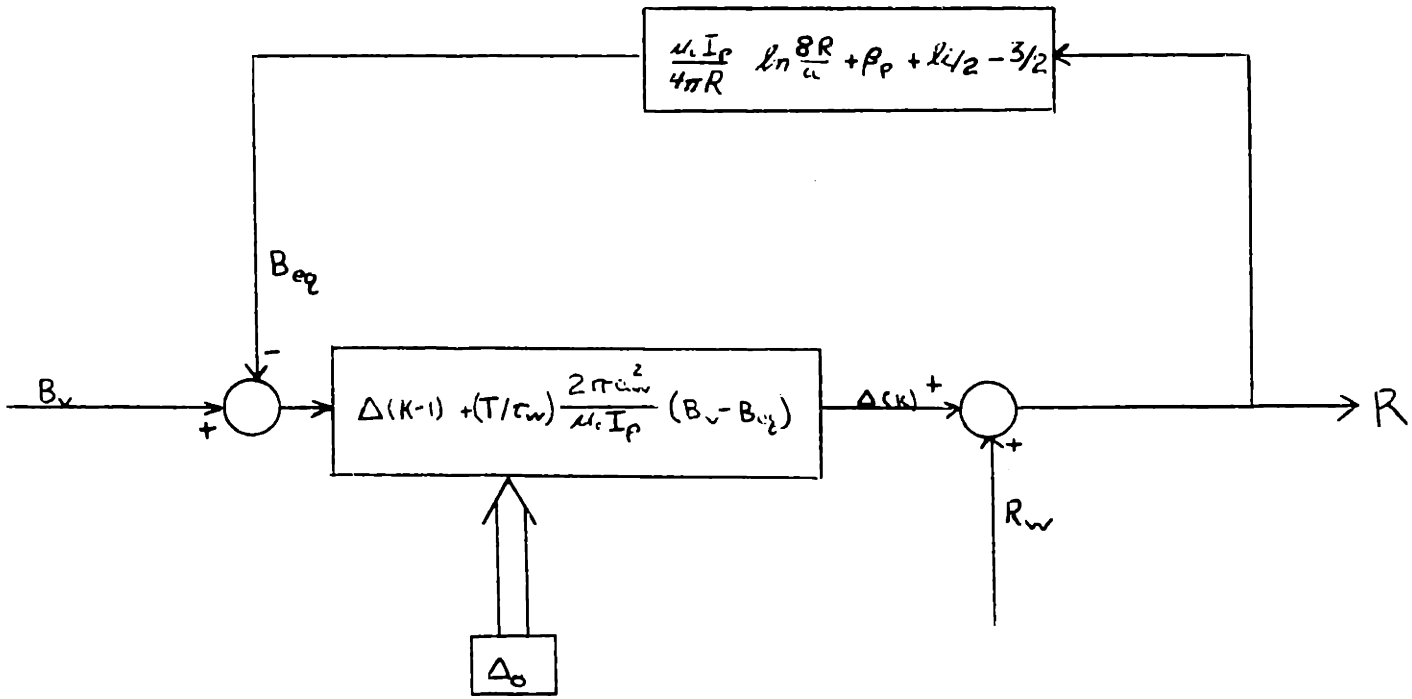

Figure 27 PLASMA MOTION DURING CONTROLLER OPERATION

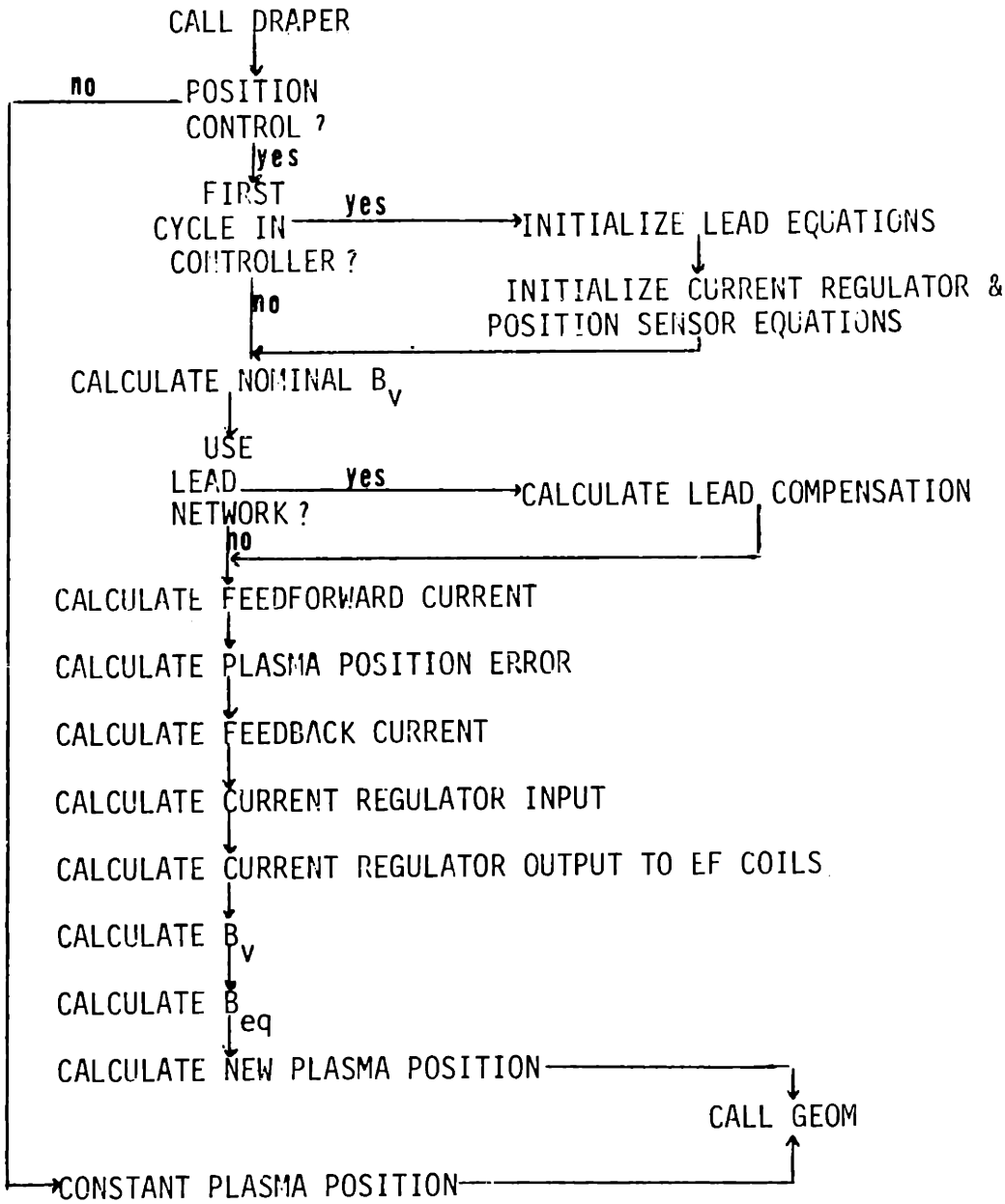

Figure 28 FLOW CHART FOR SUBROUTINE DRAPER

code checks to see if it is the first cycle the controller is used.

The code initializes all the equations in the first cycle the controller is used. This is accomplished by evaluating the equation in the lead network for 400 time steps and the equation in the EF coil current current regulator and position detector for 50 time steps. This allows the position controller to start with zero error in the plasma position. With a .4msec time step, it was found that 400 loops of the lead network were needed to get rid of any transients. 50 loops of the EF coil current and position detector equations were sufficient to get zero initial error.

After this one time initialization procedure, the controller calculates a new nominal vertical magnetic field strength. If lead compensation is included, it is calculated at this time. A value of the nominal feedforward EF coil current is then calculated. The position error is measured and the gain schedule is used to determine the gain on the feedback loop. Then a feedback EF coil current is calculated. This is added to the feedforward current to give the value of the input to the EF coil current regulator. The present value of the EF coil current is calculated which gives magnitude of the external vertical field. The vertical field is applied to the plasma motion equations and a new offset and plasma position is calculated.

C. Transient Response

The first runs to check the operation of the controller were done with perfect knowledge of all variables. There was no error or noise in the feedforward or feedback loops. A transient response was done during the normal operating regimes for these conditions and the results are shown in figure (29). A unit step input was applied to the control at t=0, to drive the plasma to a radius of 6.26m from 6.25m. Curve 1 is the response of the feedback system only. The graph shows a maximum overshoot of 22.5% and a rise time of 8.2 msec. The steady state error is 5.% with feedback only. Curve 2 shows the system response with lead compensation included in the feedforward system. Curve 3 shows the response with no lead compensation. The response with lead compensation is worse than the response with no lead compensation. This should be expected in this case since, as mentioned in Chapter 3, the only lags in the model cancel each other. The lead compensation only slightly improves the rise time from 8msec to 7msec, but more then doubles the maximum or overshoot to 37.6%. The lead compensation increases the 2% settling time from 24msec to 29msec.

In chapter 3, it was shown that the gain schedule was designed to give a damping coefficient of approximately .7 and a natural frequency of 280 rad s^{-1} for the feedback system. Using second order system equations and curve 1, the damping coefficient for the feedback system is .45 and the natural frequency is 560 rad s^{-1}. There are a few reasons for the differences from the design parameter. First, the equations are only for

Figure 29 TRANSIENT RESPONSE

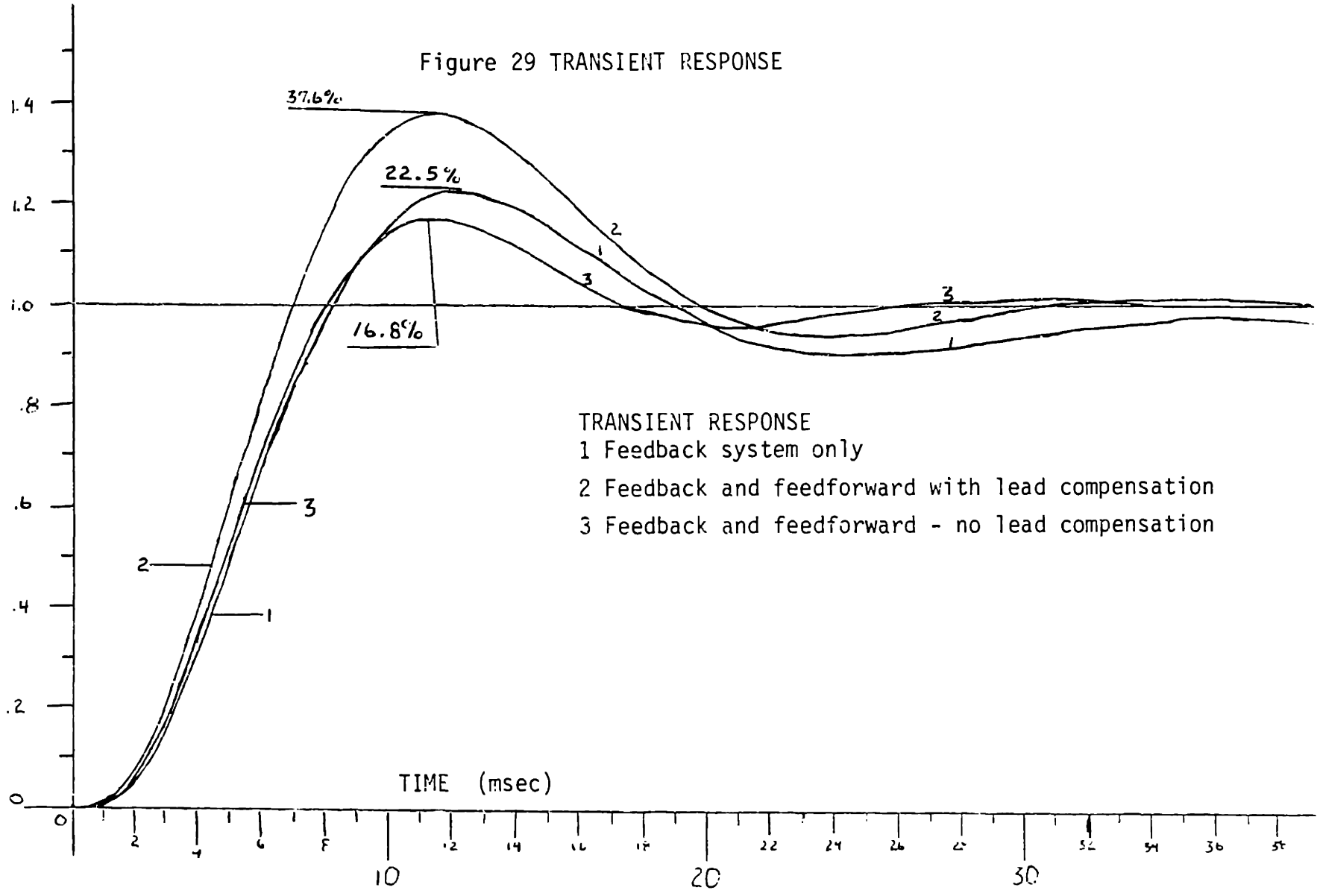

small pertrubations around the operating point. Any large perturbation will introduce non-linearities into the system and make the characteristics different than predicted by linear control theory. Secondly the system is only an approximate second order system. The non-dominant roots have an effect on the system response. The 5% steady state error is close to the predicted 3.88% steady state error. The response of the system in curve 3, with feedforward and no lead compensation, seems sufficient. The maximum feedback current needed is only 2.15% of the nominal feedforward current.

D. Reactor Shutdown

1. Normal Shutdown

The plasma position controller was then applied to three different shutdown scenarios that provide a wide range of possible operating conditions. The first case approximates a normal shutdown where the plasma current is ramped down from 4.5MA to 1 MA in 1 sec. when: ni = 1.67×10^{18} particles/m^3, Ti = 5.96 Kev, and β_p = .128.

The particle and energy loss rate was equal to that predicted by trapped ion mode. Figure (30) shows the result of the shutdown. The maximum error was less than .06cm and the maximum perturbation feedback current was only .22% of the nominal feedforward current. The value of the required equilibrium field ranged from .14 Teslas to .05 Teslas. Figure (31) shows the range of the main parameters I_p and β_p. The difference between the supplied vertical field and the required equilibrium field was less than .001 Tesla during this shutdown. The plasma

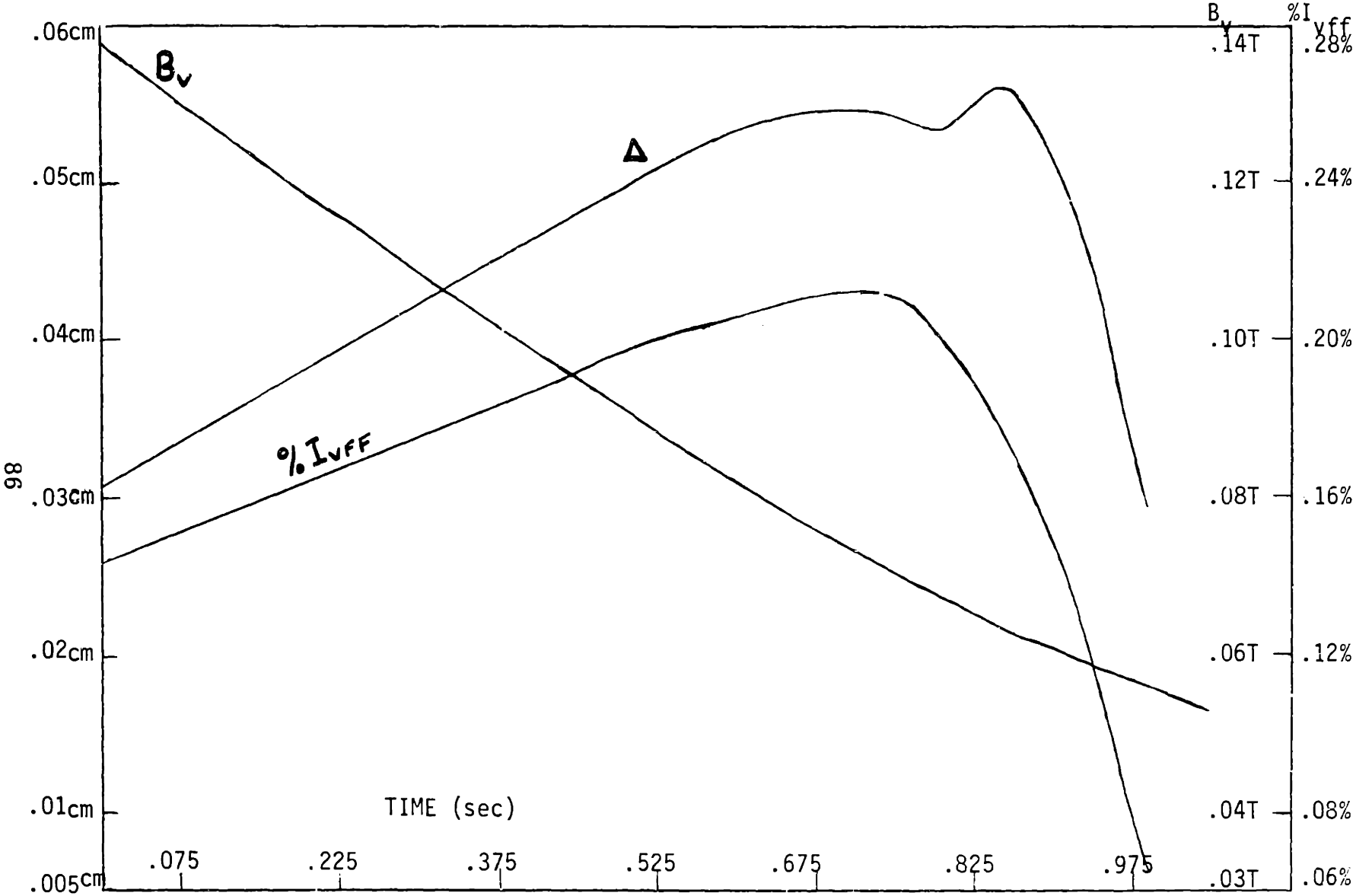

Figure 30 NORMAL SHUTDOWN (τ_e = TIM)

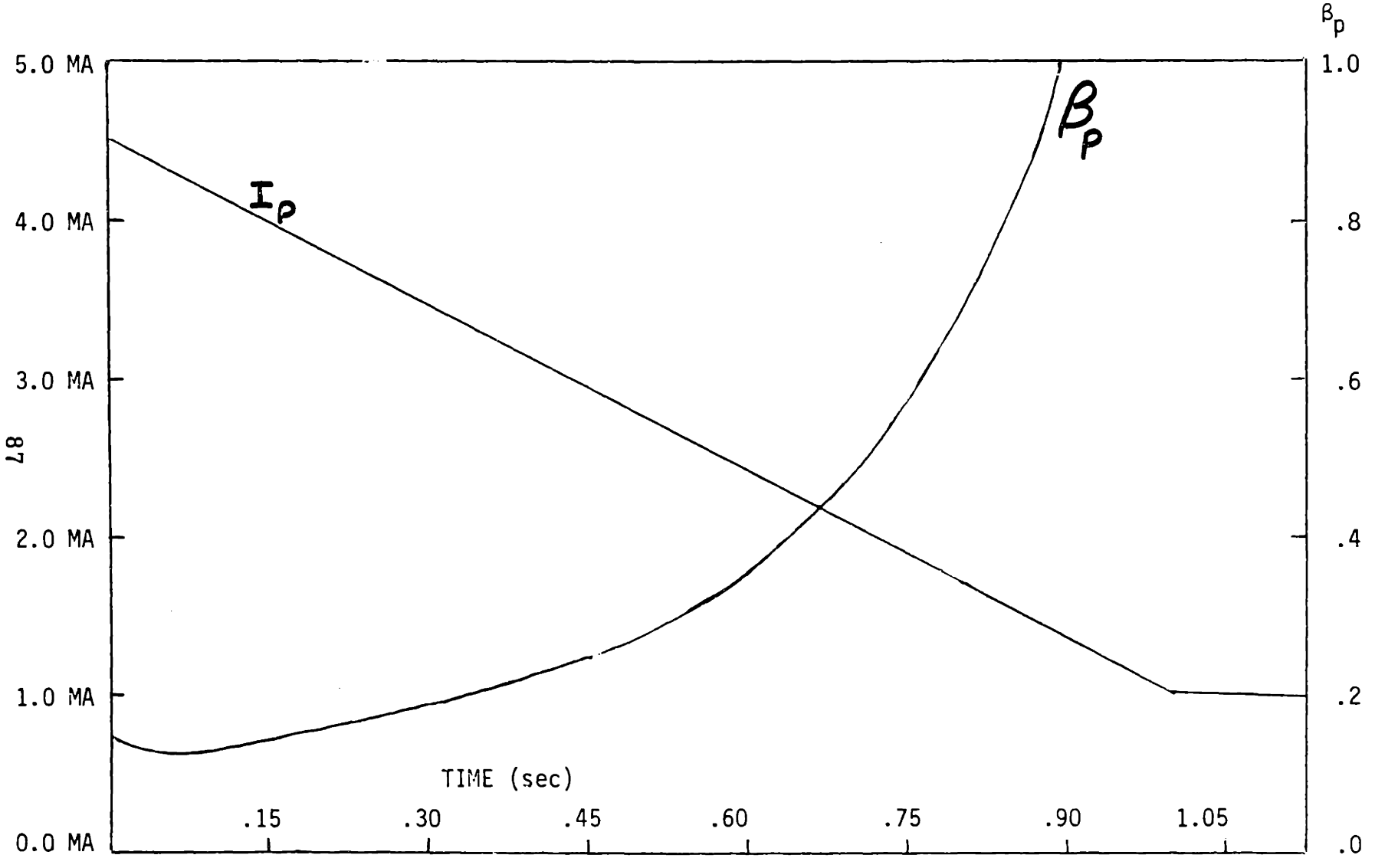

Figure 31 NORMAL SHUTDOWN (τ_e = TIM)

energy decreases from 6.8 MJ to 5.3 MJ during shutdown. Perfect plasma variable knowledge was used in this case.

2. Normal Shutdown with Slightly Enhanced Confinement

The second shutdown corresponds to a slightly worse condition for the controller where ni = 4 x 10^{18} particle/m^3, Ti = 10.0 Kev., and β_p = .421. It was assumed here that confinement was five times better than trapped ion mode transport. The plasma energy at the start of the shutdown was 15.5 MJ and decreased to 13.5 MJ after .81 second. The results are shown in Figure (32) and (33).

In this case, the maximum position error was less than .04 cm and the perturbation feedback current was never more .13% of the nominal feedforward current. As in case 1, the supplied vertical field was always within .001 Tesla of the required vertical field. Both these two cases show that the control system is very good with perfect variable knowledge. This should be expected when there are no errors in the feedforward path.

3. Abort Shutdown with Greatly Enhanced Confinement

The third case used for verifying the basic controller design was with the following plasma parameters at the start of shutdown: ni=6.7 x 10^{19} ion/m^3, Ti = 7.0 Kev, β_p = 2.55, plasma energy = 133 MJ. The particle and energy confinement was assumed to be 15 times greater than trapped ion mode predictions. This case is expected to approximate the worst case abort mode. A possible reactor failure (loss of superconductivity in the TF magnets, damaged TF or OH power supplies, loss of coolant accident, etc) might necessitate the ramping down of the plasma

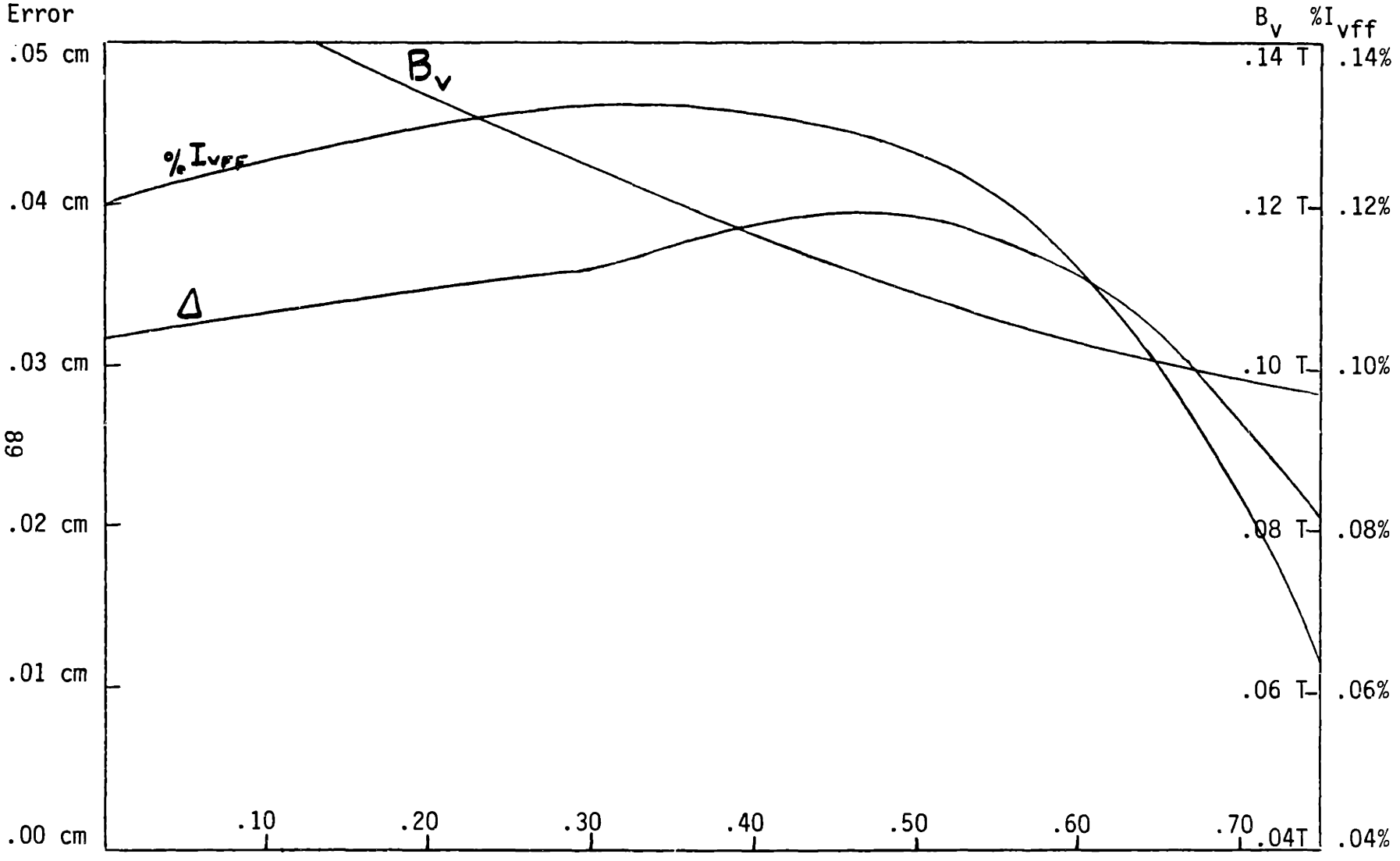

Figure 32 NORMAL SHUTDOWN (τ_e = 5 x TIM)

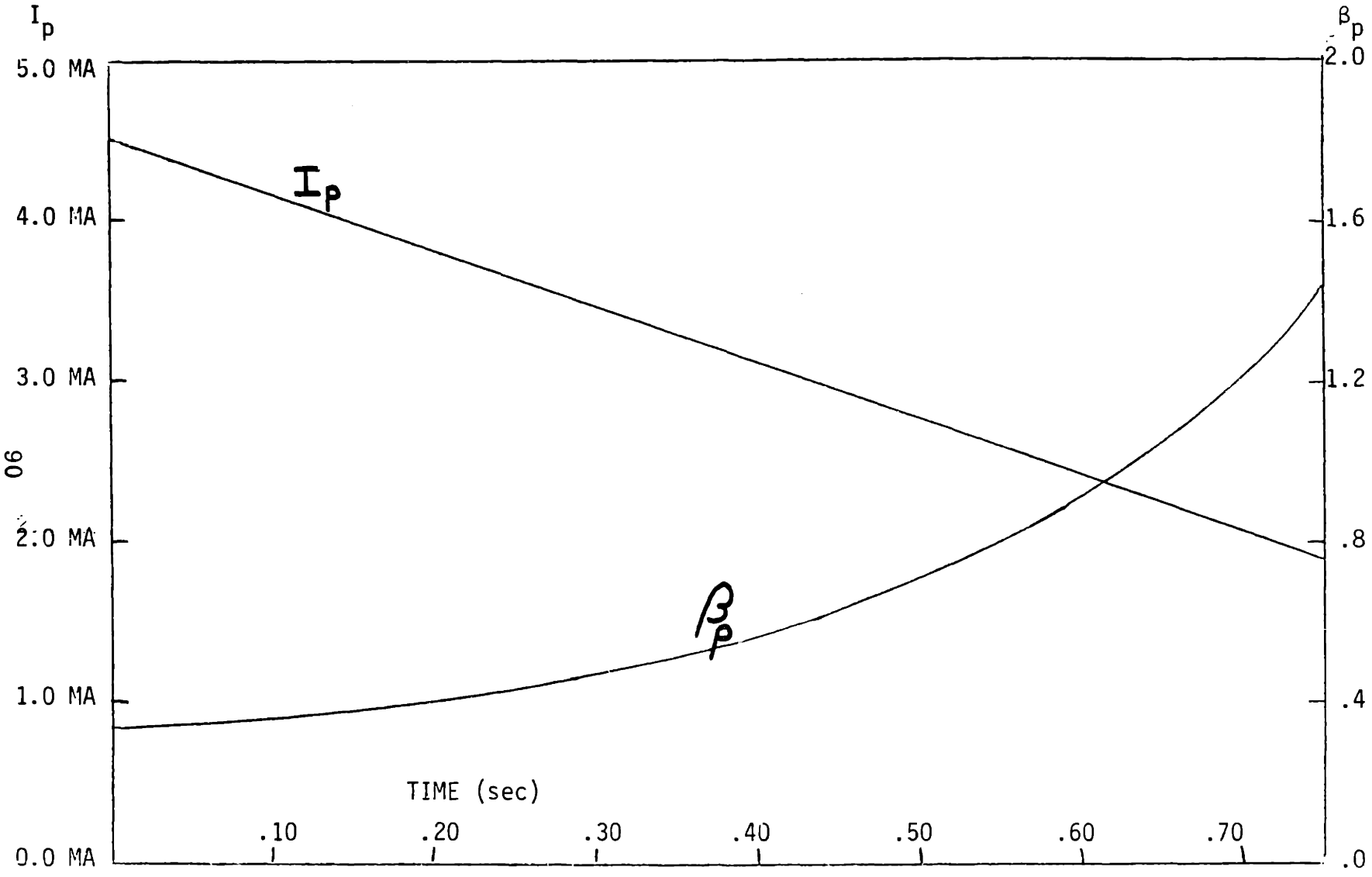

Figure 33 NORMAL SHUTDOWN (τ_e = 5 x TIM)

current in the flat top region of the burn cycle. There was no injection of impurities or neutral gas to speed up the energy losses. The current was ramped from 4.5MA to 1MA in one second. Chapter 5 will discuss the problems of ramping the current in this manner. Figure (34) and (35) show the results. With perfect variable knowledge the error is less than .25cm after .65 seconds and the perturbation feedback current is only .2% of the nominal feedforward current. On figure (35) it can be seen that beta poloidal has been increased from 2.5 to 10 after .7 seconds. Since this value is much greater than the aspect ratio 2.98, serious questions are raised about the stability of the plasma. Because the computer model is zero dimensional, it is not possible to determine the shape of the magnetic flux surfaces and find out if and when a separatrix has occured inside the plasma and caused a disruptive instability. Recent work by Clarke and Sigmar indicates that configurations of arbitrarily high poloidal beta may exist in equilibria for a time on the order of the poloidal skin penetration time.[15] From reference 15 the poloidal skin penetration time is:

$$\frac{1}{\tau_{poi}} = \frac{1}{\psi}\frac{\partial \psi}{\partial t} \simeq \frac{\eta}{4\pi a^2} \qquad (55)$$

where ψ is the poloidal magnetic flux and η is the plasma resistivity. However, in their work, Clarke and Sigmar achieve high beta poloidal beta by the fast injection of energy, and allow the plasma current to increase with increasing plasma pressure. The situation during shutdown is much different. In a zero dimensional model, poloidal beta is defined as:

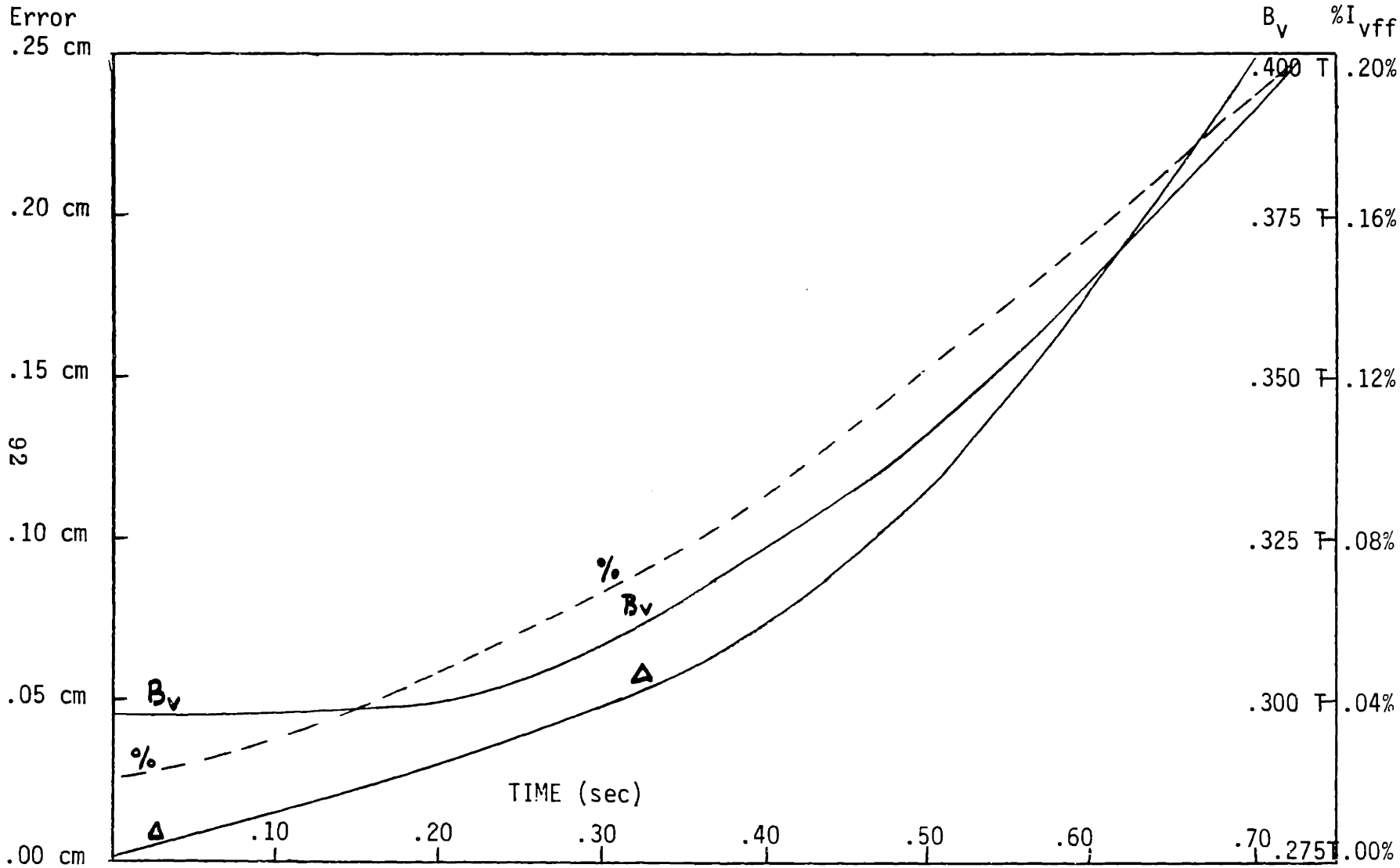

Figure 34 ABORT SHUTDOWN (τ_e = 15 x TIM)

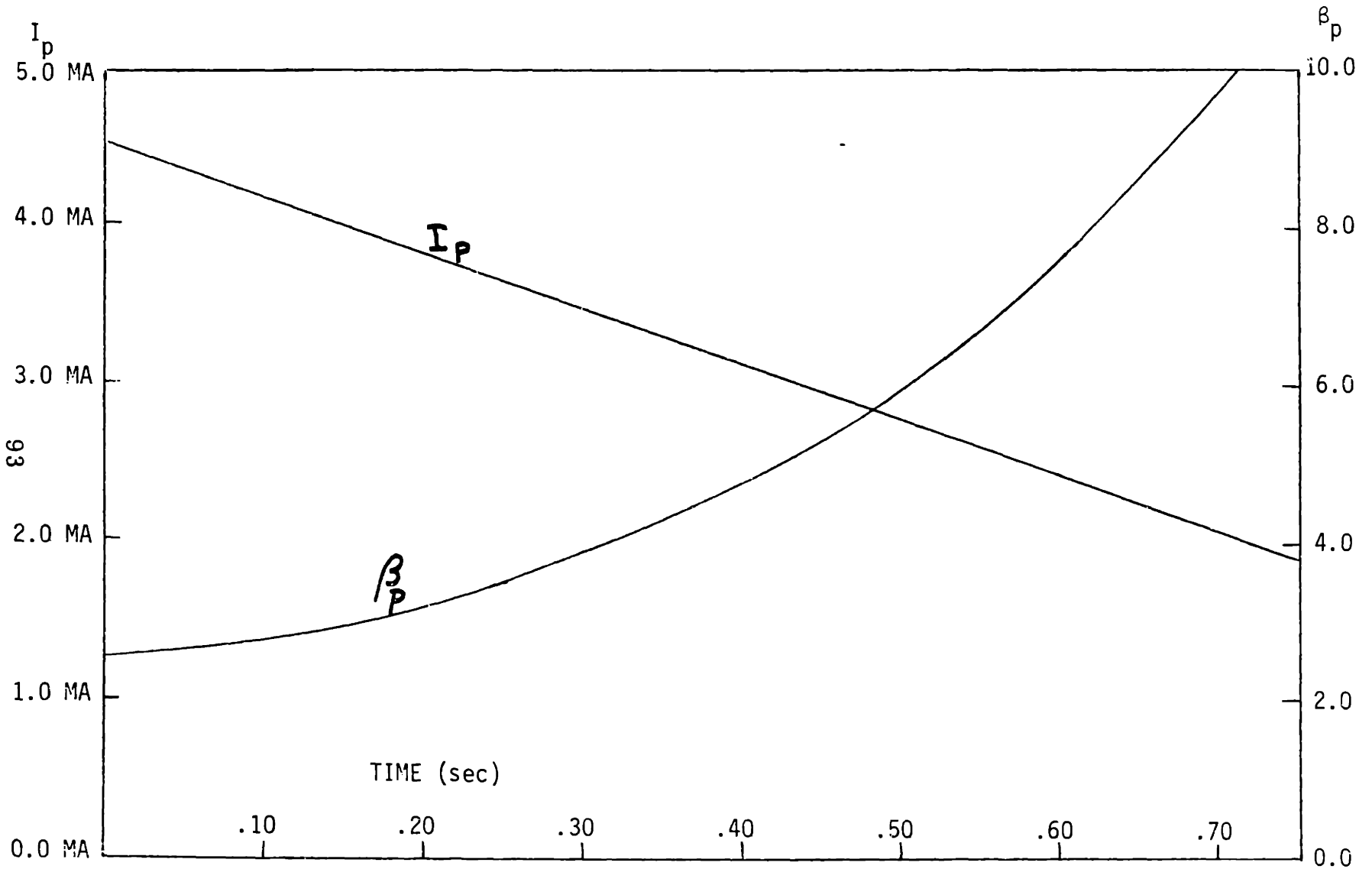

Figure 35 ABORT SHUTDOWN (τ_e = 15 x TIM)

$$\beta_p = \beta \left(\frac{B}{B_p}\right)^2 \tag{56}$$

where:

$$\beta_p = \frac{\mu_o I_p}{2\pi a} \tag{57}$$

since B remains almost constant during shutdown, β_p scales as:

$$\beta_p \simeq \frac{\beta}{I_p^2} \tag{58}$$

The reason for the sudden increase in β_p during shutdown is the fact that β will decrease slowly with enhanced confinement (15 x TIM), while the plasma current decreases very rapidly. The question of plasma stability and limits to poloidal beta during shutdown must be studied in much greater detail with a one or two dimensional plasma physics code to resolve the problem. For the sake of this study, it was assumed that case 3 would then be a conservative estimate of the worst possible abort shutdown that the plasma position controller would have to control. Figure (34) shows that the magnitude of the required vertical field increases by over 50% in .7 seconds. With perfect variable knowledge the supplied vertical field was within .002 Tesla of the required vertical field.

4. Shutdown with lead compensation

During the three previous cases there was no lead compensation in the feedforward system. Case 3 shutdown, abort, was attempted with lead compensation parameters of τ_c = 20 msec and τ_b = 4 msec (DC gain = 5). This increased the plasma position error by a factor of ten to 2.5 cm. The

gain on the lead compensation network had to be reduced to almost unity (τ_c = 20 msec, τ_b = 16 msec) in order to get the same plasma position error as with no lead compensation.

E. Error Models in the Plasma Variables

The operation of the plasma position controller, with perfect variable knowledge, on these three cases verified the basic controller design. At this point it is necessary to introduce models for errors in the measurement of the plasma variables that make up the inputs to the feedforward and feedback control systems. Conversations between the CSDL staff and AS&E have indicated that the error that could be nulled out with proper calibration. This error would then also be negligible compared to the error in the estimate of β_ρ and li/2. Later models of the control system should include the appropriate noise and error models for the diagnostics, but at this point the effect of this noise or error will be lost.

1. Static estimation technique. The first attempt at the estimation of β_ρ and li/2 was a static estimator. This is based on the assumption that the control system is working well and that there is very little error in the plasma position. The vertical magnetic field supplied is assumed to equal the required equilibrium field.

$$B_v = B_{eq} \tag{59}$$

Using equation (1), poloidal beta and internal inductance are equal to:

$$\beta_p + li/2 = \frac{4\pi R B_{eq}}{\mu_o I_p} - \ln 8R/a + 3/2 \qquad (60)$$

The vertical magnetic field can be determined from measurement of the EF coil current which gives:

$$\beta_p + li/2 = \frac{4\pi R K_z K_{ei} I_v}{\mu_o I_p} - \ln 8R/a + 3/2 \qquad (6i)$$

A simple analysis shows that this estimation technique is stable during the flat top region of the burn cycle and unstable during the shutdown. Taking out constants,

$$\beta_p + li/2 \sim RI_v/I_p - \ln 8R/a \qquad (62)$$

During the steady state flat top region, $\dot{I}_v = \dot{I}_p = 0$, so that:

$$\Delta(\beta_p + li/2) \sim \Delta(R - 8R/Ra) \sim \Delta R \qquad (63)$$

A positive (outward) disturbance in R gives a positive increase in the estimate of $\beta_p + li/2$, which leads to a larger vertical field that will tend to bring the plasma back in to the center. But during the area of greatest interest, shutdown, I_p is not constant and:

$$(\beta_p + li/2) \sim \Delta R/\Delta I_p \qquad (64)$$

A decrease in the plasma current leads to an increase in the estimate of $\beta_p + li/2$. This will lead to increase in the vertical field when the vertical field should actually be decreasing with a decrease in the plasma current.

This prediction was verified with the computer model. The static estimation technique was used for all three shutdown cases. In each instance, an initially small error in the estimate of $\beta_p + li/2$ (less than 1%) made the system unstable and the plasma was driven into the reactor wall by the

feedforward control current in less than 15 msec. The feedback does not have enough time to correct for the error in the estimate of the variables.

One way to improve the static estimator would be to weight the estimate of $\beta_p + li/2$ by the magnitude of the error signal on the feedback signal. This can be done with the following equation:

$$\beta_p + li/2 = \frac{4\pi R K_z K_{ei} (I_{vff} - 10\ I_{vcmd})}{\mu_o I_p} - \ln 8R/a + 3/2 \qquad (65)$$

However, this estimation technique is also unstable during shutdown. The control system gives the plasma a exponentially increasing oscillation that drives the plasma into the wall. During a normal shutdown, this occured in 120 msec and in an abort shutdown this occured in 20 msec. Some form of dynamic estimation technique is clearly needed for $\beta_p + li/2$.

2. Dynamic Estimation. A dynamic estimate of β_p ends up being a function of particle energies and densities and their time derivatives. A dynamic estimate of $li/2$ is a function of the radial distribution of current density and magnetic flux surfaces. At the present time there is no way of obtaining this information in a real time manner that is suitable for use in a plasma position controller. This information can only be obtained by using extensive post shot data analysis. Even then the uncertainty in the values is quite large and, in the case of ALCATOR, the error in β_p may be as high as 100%. This problem is discussed in detail in chapter 5.

3. Constant Error. At this point it was decided that the best way to test the CSDL candidate plasma position controller would be to assign a constant error in the feedforward system that simulates an error in the dynamic estimation of $\beta_p + li/2$, without specifying what the estimation technique was.

An abort shutdown was run with a constant error of 10% of the feedforward current magnitude in the feedforward system. The plasma parameters at the start of the shutdown were: $n_i = 6.8 \times 10^{19}$ ion/m^3, T_i = 6.93 kev, $\beta_p = 2.58$, and plasma energy = 133 MJ. As shown in figure (15), a 10% error in the nominal vertical field value corresponds to a 25% error in the estimate of $\beta_p + li/2$. Figure (36) shows the results. The error in the plasma position increases to over 14 cm in .8 seconds. The perturbation feedback control is slowly decreasing from 8.5% of the feedforward current to 6.5% of the feedforward current while the rate of plasma motion is increasing to a maximum value of .55m/s.

The main reason for this unsatisfactory performance is that the system has an infinite steady state actuating error for a ramp input. The static velocity error coefficient for a ramp input is defined as:[16]

$$K_v = \lim_{s \to 0} \; s\, G(s)\, H(s) \qquad (66)$$

for this system:

$$K_v = \lim_{s \to 0} \frac{s\, 7.66 \times 10^{14}}{(s-.44)\,(s^2 + 49.56s + 3.349 \times 10^6)(s^2+1010s+3.949 \times 10^5)} \cdot \frac{1000}{s + 1000} \qquad (67)$$

$$K_v = 0$$

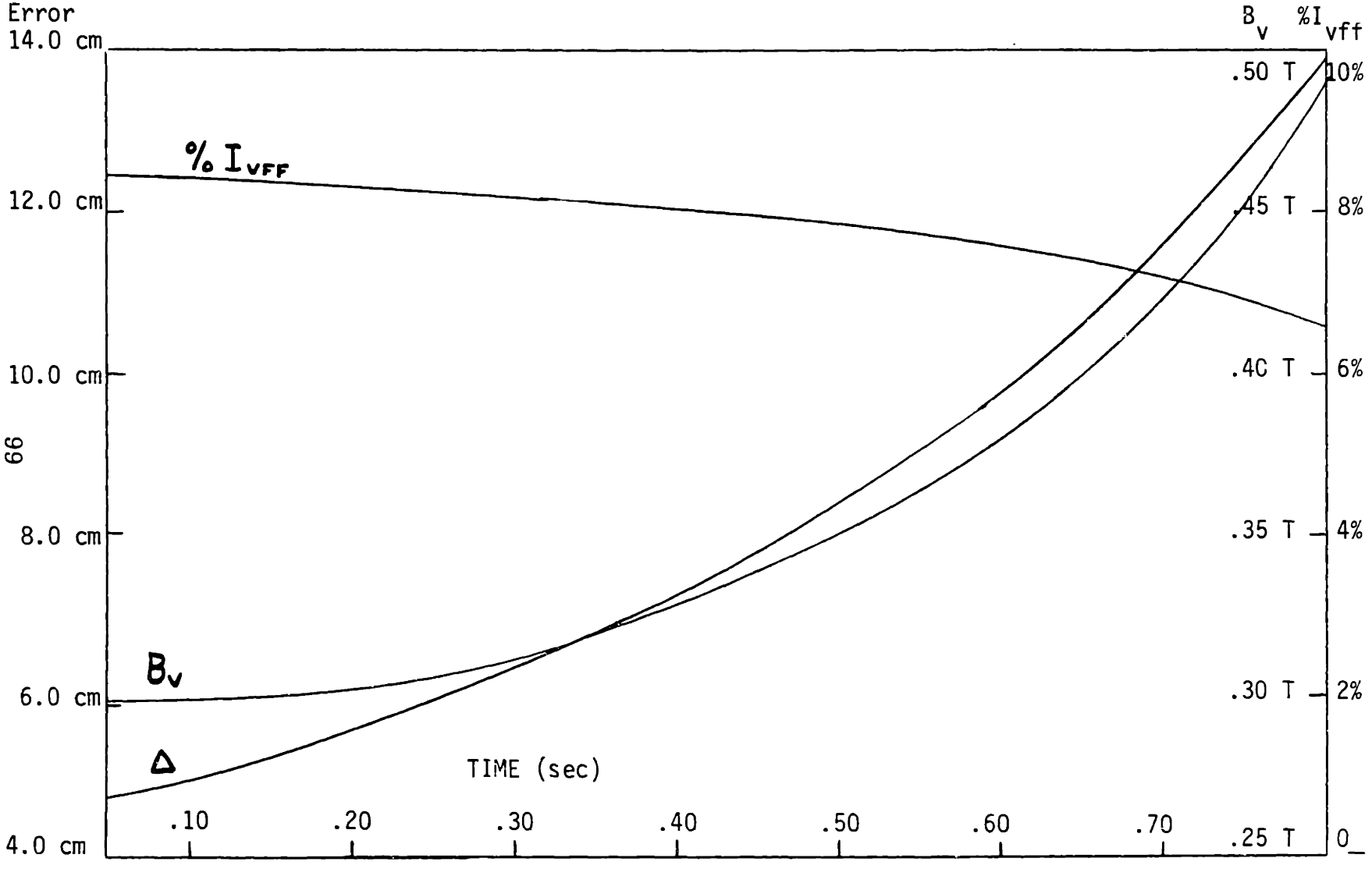

Figure 36 ABORT SHUTDOWN WITH 10% FEEDFORWARD ERROR

The steady state error for a ramp input is;[16]

$$e_{ss} = 1/K_v = \infty \tag{68}$$

This means that the system is incapable of following a ramp input in the steady state. Figure (36) shows that the vertical field required during shutdown approximates a ramp input. The control system needs a pole at the origin.

4. The addition of an integrator. One possilbe solution to the infinite static velocity error is to add an integrator in the feedback system. The integrator must be added so that it does not destabilize the control system during any part of the operating cycle. This can be accomplished by using a constant gain on the integrator and placing it before the scheduled gain parameter is evaluated. The integrator's position is shown on Figure (37). An integrator in the feedback system adds a pole at the origin of the root-locus plot which leads to a finite steady state actuating error for a ramp input. A gain of .5 on the integrator insures that there will be no loss of stability in the system throughout a nominal burn cycle. The difference equations for the integrator are:

$$I_{int}(k) = K_i R_{err}\, T + I_{int}(k-1) \tag{70}$$

$$I_{vcmd} = K_r(R_{err} + I_{int}(k)\ ) \tag{71}$$

A transient response was first done with the integrator to see how it effected the system response. As in figure (29) a 1 cm step input was given to the system. The plot in figure (38) was done under the same conditions as curve 3 in figure (29). Both the feedback and feed-

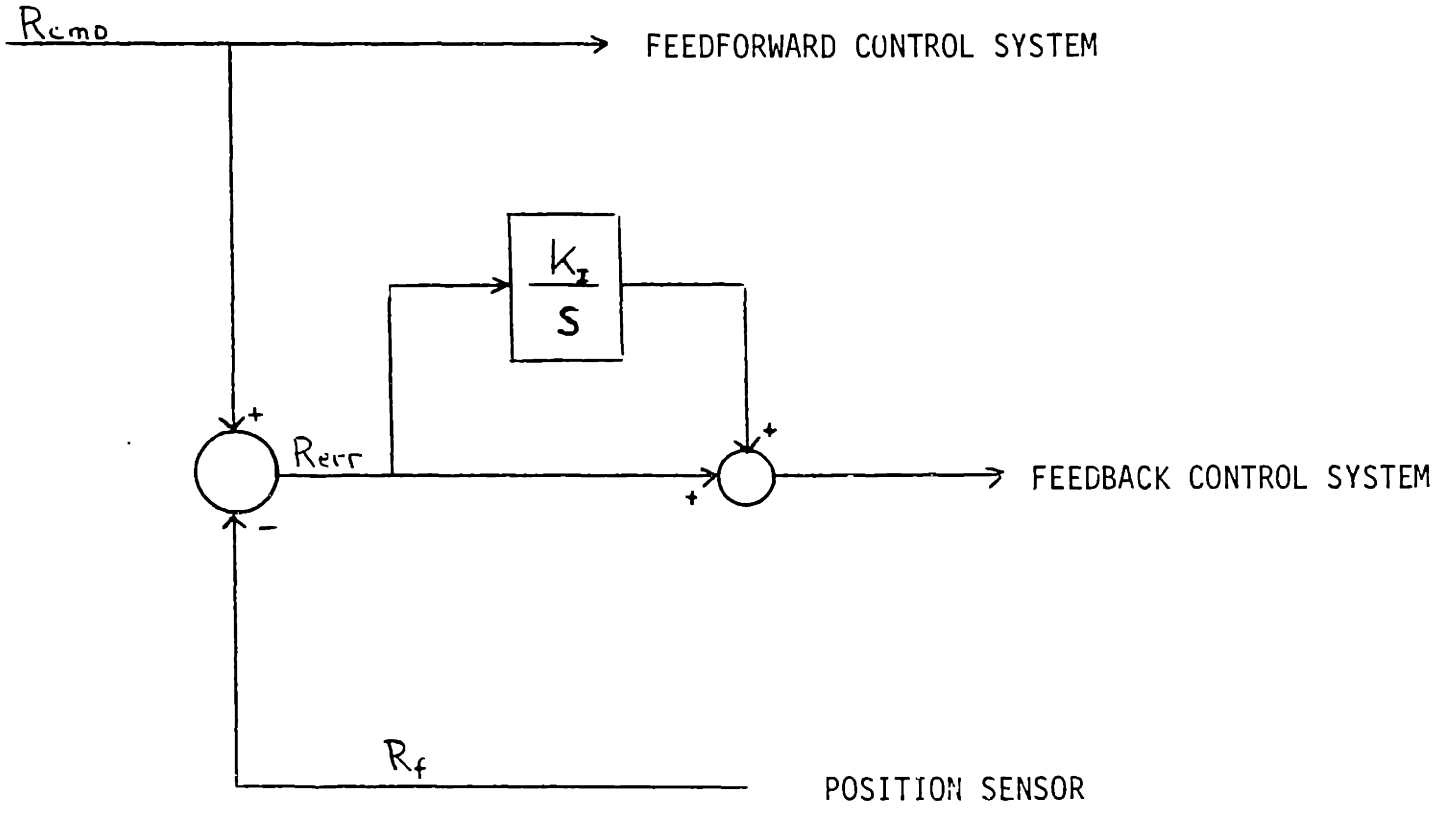

Figure 37 INTEGRATOR LOCATION IN PLASMA POSITION CONTROL SYSTEM

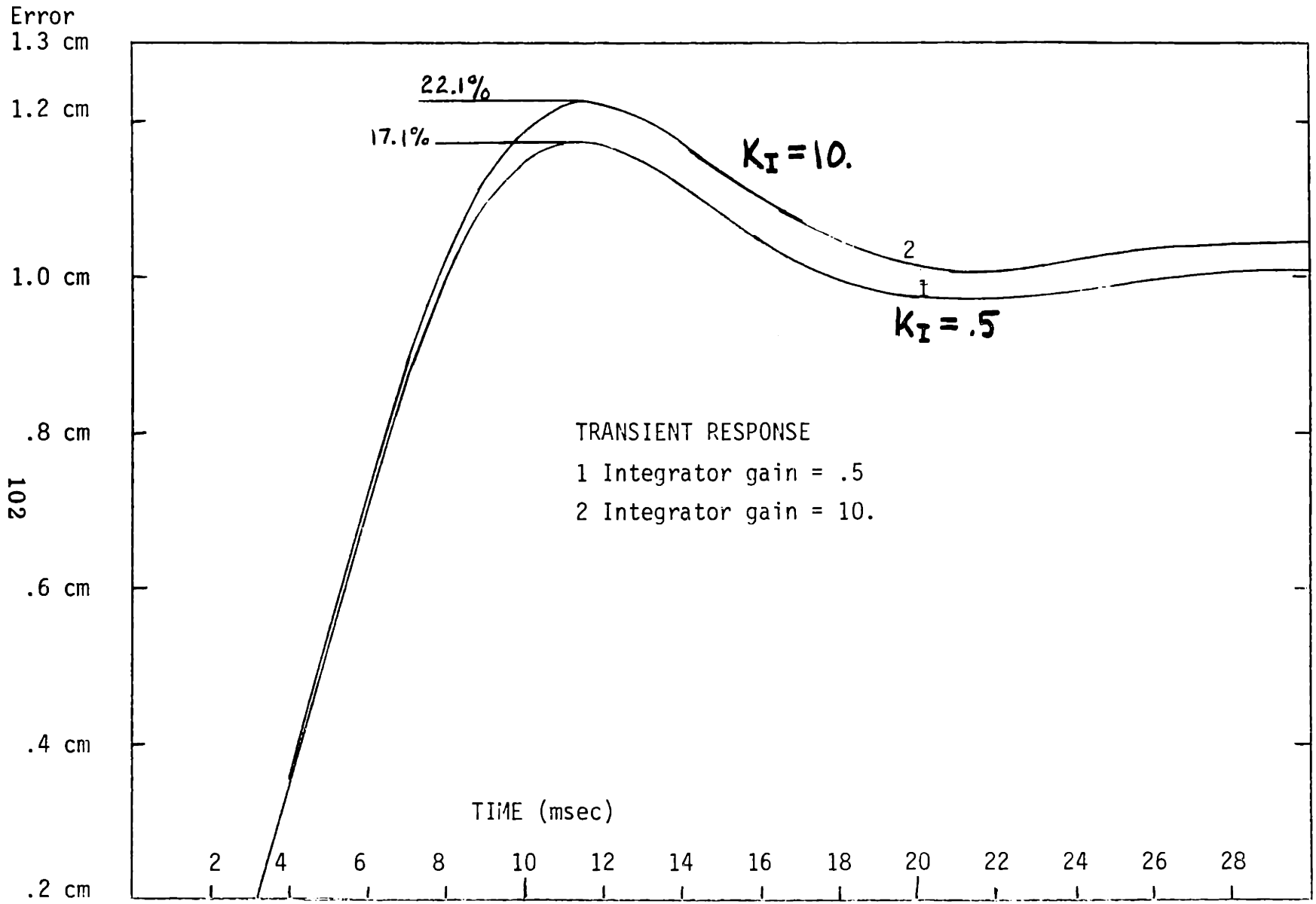

Figure 38 TRANSIENT RESPONSE WITH INTEGRATOR ADDED

forward systems were used to respond to the step input. The integrator is shown to have a very slight effect on the system response. The maximum overshoot has increased only slightly from 16.8% to 17.1% and the rise time is unchanged. The integrator does introduce a .2% steady state error in the plasma position. Giving the integrator a gain of .5 allows it to build up its value slowly and keep from destabilizing the system.

The control system was then used to try and control an abort shutdown. During normal operation of the control system, the integrator would have the correct value stored when a shutdown occured. Any steady state error would have been nulled out by the integrator during the flat top region. With a gain of .5 on the integrator, the computer model would have to simulate about fifteen seconds of flat top burn cycle time in order to build up the correct value on the integrator before shutdown started. However, by calculating the amount of feedback current needed to correct a given error in the feedforward system, an initial value can be placed on $I_{int}(k-1)$ on the first cycle through the control system. At the start of the controller operation, 30 msec before shutdown starts; there will be zero error in the plasma position, but a finite error on the feedforward system. There will be no feedback (no position error) to counterbalance this feedforward error. The correct initial value of $I_{int}(k-1)$ will exactly compensate for the feedforward error. Any transients should die out in the 30 msec preceding the start of the shutdown. This will allow a true evaluation of the control system during shutdown without any interference from an un-

corrected steady state error that existed because the control model was not run long enough preceding shutdown. An example calculation is shown for a 10% error in the feedforward system. The EF coil current required is approximately 7500 Amps and a 10% error in the feedforward component means the feedback current must be 750 Amps. At the start of shutdown, I_p is 4.5 MA and the gain schedule shows a feedback gain of 84.66 db. Since R_{err} is initially zero, equation (71) shows that:

$$I_{int}(k-1) = \frac{I_{vcmd}}{K_r} \qquad (72)$$

Substituting appropriate numbers gives:

$$I_{int}(k-1) = \frac{750}{10^{(84.66/20)}} = .04384 \text{ A} \qquad (73)$$

In the actual computer run, this initial condition gives a plasma position error of only .6 cm after 30 msec.

Figure (39) shows the results of applying four different magnitudes of error in the feedforward system when the controller is used in an abort situation. Curves 1,2,3 and 4 represent the error in the plasma position during an abort shutdown when the integrator constant is .5. Keeping the gain at .5 may have insured control system stability, but it also leads to poor results. A 10% error in the feedforward system has caused a 27 cm error in plasma position. Feedforward errors of 15% and greater led to a position error greater than 30 cm, which was considered a failure. The feedback system is actually doing quite a bit to impede the motion of the plasma towards the reactor wall. Without the feedback

system, a 10% error in the feedforward system drives the plasma into the reactor wall in less than 20 msec with a final plasma velocity greater than 250 m s^{-1}, Figure (40) shows the plasma parameters during the shutdown. The value of β_p has increased to more than 44. This clearly would cause a disruptive instability in the plasma long before shutdown were completed. These plasma parameters give extreme operating conditions for the system to try and control. The magnitude of the required vertical field has more than doubled in less than 1 second. Using the integrator gain of .5 caused the long delay ($\sim$3 seconds) in nulling out the position error after the plasma current has reached a steady state value.

One way to improve the controller performance is to increase the gain on the integrator. However, as an integrator adds 90^{o} phase shift to the system response, the 0 db crossover point must be less than the marginally stable frequency. Using an integrator gain of 10 should keep the system just slightly on the safe side of mariginal stability. The upper curve in figure (38) shows the transient response with an integrator gain of 10. The performance is only slightly degraded. The maximum overshoot has increased from 17.1% to 22.1% and the steady state error has increased to 2%.

Curve 5 on figure (39) shows the increased integrator gain system applied to an abort shutdown with a feedforward error of 10%. The maximum position error has been decreased to 15.5 cm from 27 cm. The time required to null the error has been decreased to 15.5 cm from 27 cm. The time required to null the error after the plasma current has leveled

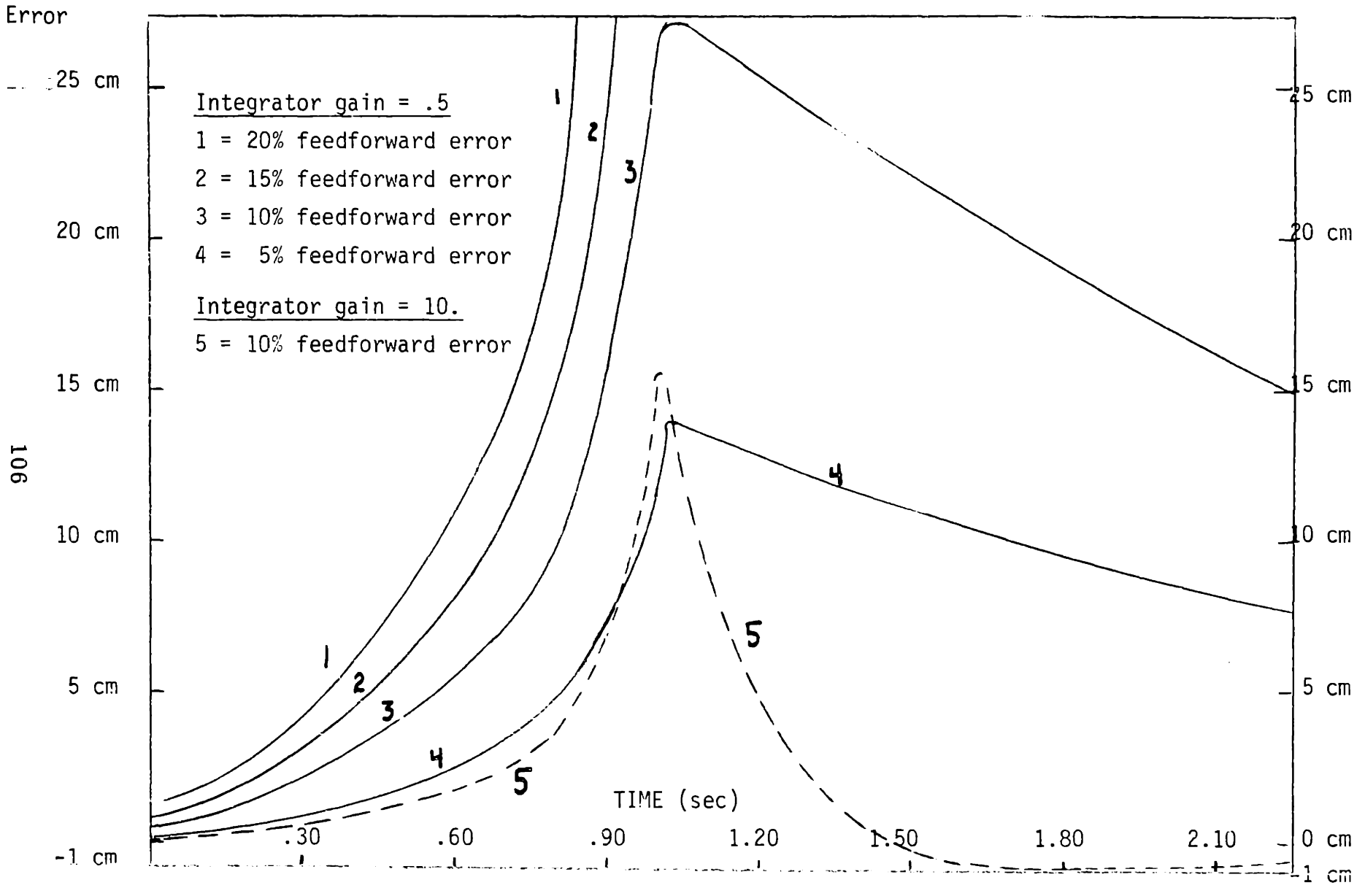

Figure 39 ABORT SHUTDOWN WITH FEEDFORWARD ERROR AND INTEGRATOR

out has been reduced to .5 seconds. Notice that there is now an overshoot in the plasma position correction process. This is an indication that the system is less stable than before.

The improved plasma position controller was now applied to a normal shutdown operation. The results are shown in figure (41). Even a 20% error in the feedforward path is corrected to within 2 cm of the commanded plasma position. This corresponds to a 50% error in the estimate of $\beta_p + li/2$. The lessened stability of the system is shown here by the overshoot that occurs after the plasma current has leveled off. The same shutdown was later run with a 40% error in the feedforward system and the maximum plasma position error was only 4.4 cm. Figure (42) shows the plasma parameters that occured during the normal shutdown.

Most of the error produced is artificial. The error at the beginning of the run is caused by an inaccurate initialization error. But the control system corrects for this very quickly. The transient error at about t = 1 second is caused by the sudden change in plasma current from a ramp input to a steady state value. In reality, a plasma current regulator would make the change in plasma current continuous and a much smaller error would actually occur.

This concludes the test sequence of the CSDL candidate plasma position control system on a zero dimensional plasma physics code. The discussions of the results and conclusions drawn are in the following chapter. This control system has been put through an evaluation under very severe plasma parameters that probably far exceed the actual plasma parameters.

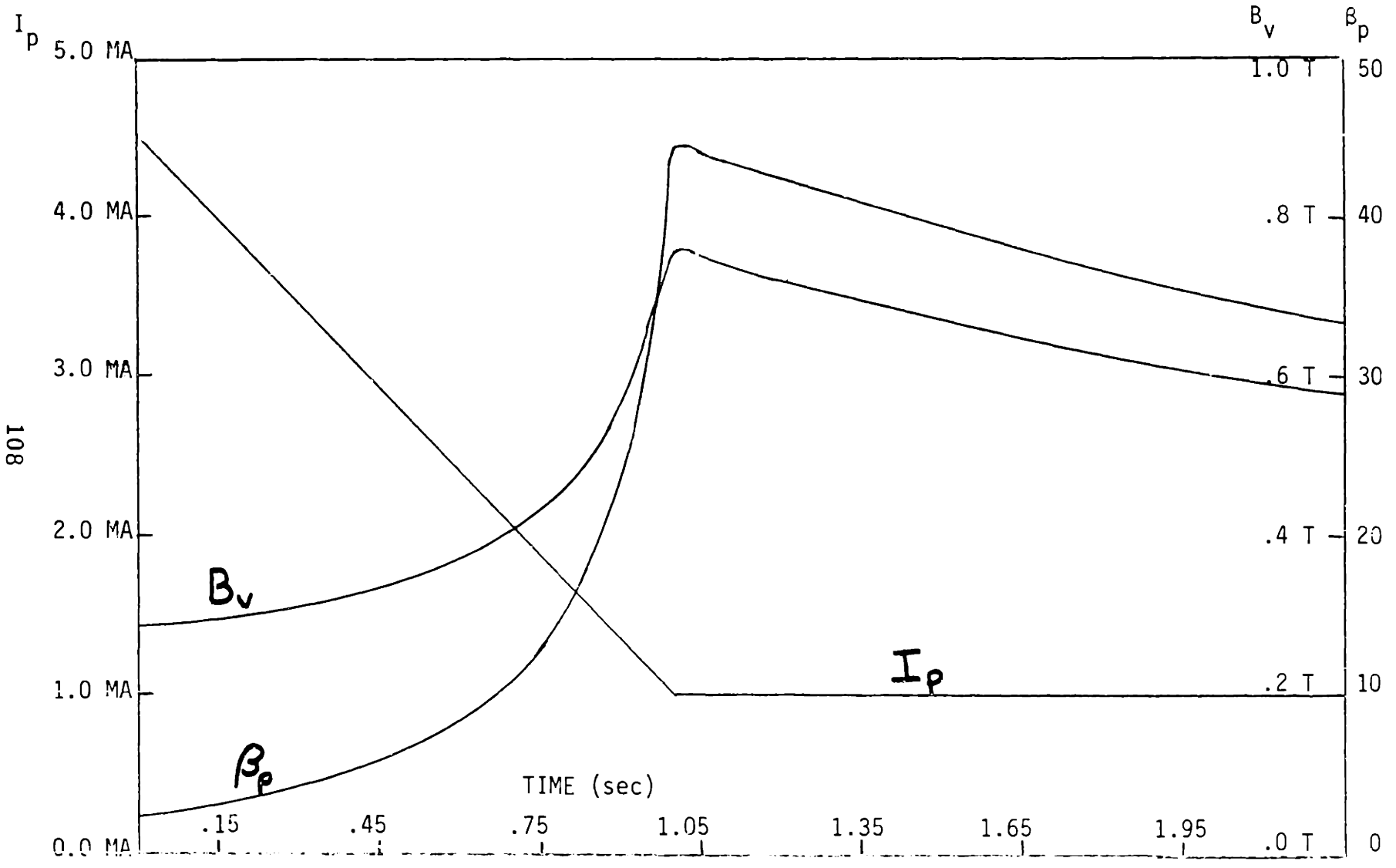

Figure 40 ABORT SHUTDOWN PLASMA PARAMETERS

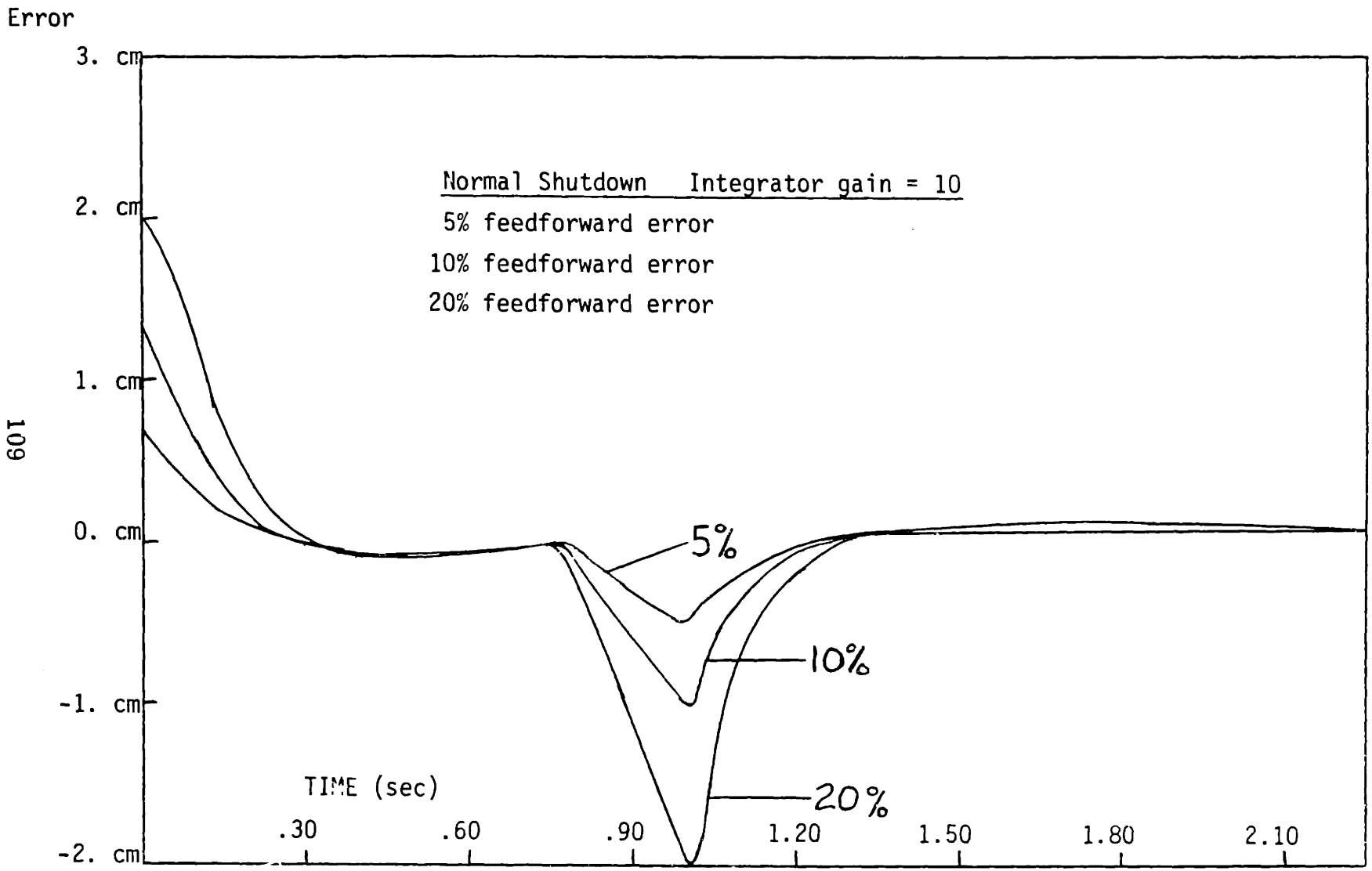

Figure 41 NORMAL SHUTDOWN WITH ERROR AND INTEGRATOR

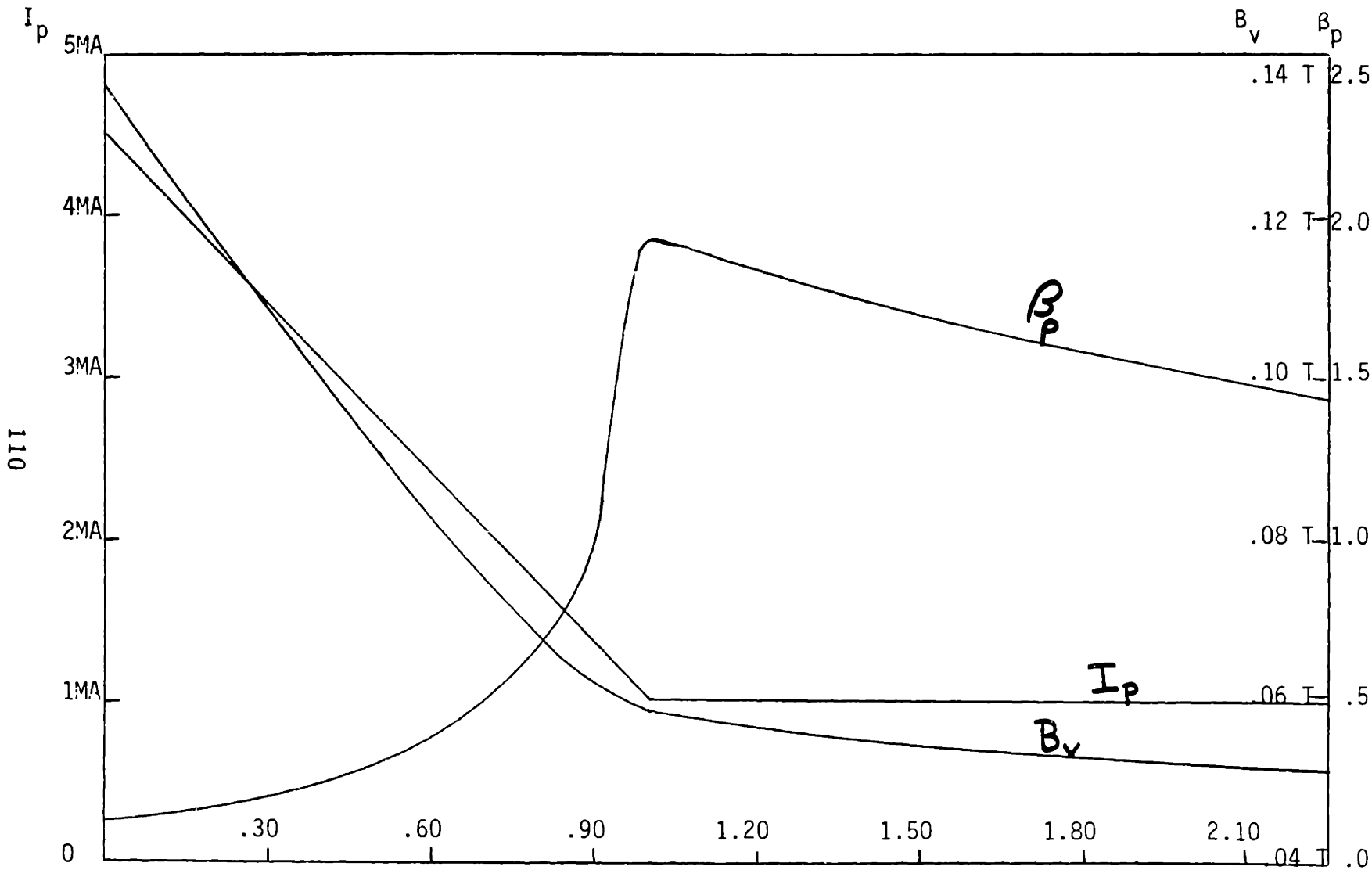

Figure 42 NORMAL SHUTDOWN PLASMA PARAMETERS

Chapter 5. Results and Conclusions

A. Introduction

The results from chapter 4 serve to identify more problems than they solve. The results, nevertheless, indicate the feasibility of a nominal feedforward and perturbation feedback control system for the control of plasma radial position in a large scale tokamak fusion reactor over a wide range of plasma parameters. The operating conditions the control system was subjected to in the "abort" case are probably much more severe than actual operating conditions wil be. However, the results show that the CSDL candidate plasma position controller gave acceptable results for a prototype design. The problems identified fall into two main categories: plasma physics and further controller design.

B. Plasma Physics

Almost every aspect of tokamak reactor design seems to hinge on what the actual particle and energy loss rates will be. The type of confinement determines everything from reactor size to whether the reactor can be operated as an ignition or beam-driven device. Chapter 4 showed the wide variation in plasma parameters that result from different assumptions of particle and energy loss rates. It is necessary to know the type of confinement that exists in order to determine what the different normal and abort scenarios should be. It is usually thought that any enhancement of confinement is good. But during a normal or abort shutdown, enhanced confinement may mean that it is necessary to inject impurities, or a nuetral gas blanket, to increase the energy loss rate. Other-

wise, very high poloidal betas will result with presently indeterminant results. The plasma physics code used to model the reactor and position control system should include a physically accurate description of the interaction of injected particles with the plasma. Putting realistic limits on the plasma parameters will give a realistic limit to the conditions the control system must satisfy.

Another important question that must be answered before further modification of the control system is attempted is the question of high poloidal beta equilibria. As mentioned previously, the high poloidal beta situation during shutdown is different from the conditions of Clarke and Sigmar.[15] But there are indications from other sources[17,18,19] that high poloidal beta's can exist during a sudden plasma current decrease. It has been observed[19] that the value of $\beta_b + \ell i/2$ can be as high as 7 in some experiments on the ST tokamak. The drop in plasma current occured faster than the energy confinement time and the poloidal skin time. This is the same type of situation that occured in the "abort" mode, except that β_p became much higher than 7.

A relationship between β_p and particle and energy confinement time would extend the usefulness of the zero-dimensional code. The classical aspect ratio limit to β_p is based on maintaining the plasma in MHD equilibrium. While the internal structure (magnetic flux surfaces) of a plasma can only change slowly (equation 14), the onset of a disruptive instability propogates through the plasma with a velocity in the vicinity of the Alfven wave velocity. Once this disruption has started, there is no control mechanism to stop the instability. Any such control

mechanism would need a bandwidth in excess of the ion cyclotron frequency ($\sim 1.3 \times 10^8$ rad s^{-1}). It is not intuitively appealing to think that the particle and energy confinement times will remain constant up to a fixed β_p - and then suddenly the plasma will fall apart. Further experimental studies should indicate how "hard" or "soft" this MHD limit to β_p is. A "soft" limit to β_p would mean that the particle and energy losses are greatly enhanced as the limit to β_p is approached, while retaining the plasma in a stable configuration. This would be a stabilizing influence on the plasma as the plasma would dump more and more energy to retain its' configuration. This is a very important factor in control studies of the plasma during shutdown operations. A zero dimensional plasma model could be very useful in exploring the sensitivity of control requirements to the degree of enhanced loss rates as some β_p limit is approached. The results in chapter 4 show that the assumption of constant loss rates (i.e, $\tau_e \sim$TIM, $\tau_e \sim 5 \times$ TIM, etc) lead to unrealistically high β_p's. Further experimental studies show also indicate how the MHD β_p limit varies as a function of how fast the limit is approached during shutdown (i.e, $\beta_{pmax} \stackrel{?}{=} f(\dot{I}_p)$).

Another important phenomenon to be studied and modeled is the rate of current diffusion into the plasma during shutdown. It would seem reasonable to expect the current diffusion time to be of the same order of magnitude as the time it takes to change the magnetic flux surface distribution. Since this is slow, a fast ramp down of the plasma current could conceivably lead to reverse skin currents on the plasma. While Rogowski coils might still give accurate measurements of the total plasma current, they would tell nothing of the internal current distribution. Since li/2 is a function of the current

distribution, this information is important to the operation of the control system. The magnitude of li/2 varies from .5 to 1.8 if the current distribution varies from a flat profile to a Gaussian profile.[26] A modeling of this process, whatever it may be, could also be used in a zero-dimensional plasma model and help in the design of the controller.

The plasma equilibrium problem can be attacked by using a combination of previous approaches to the problem. First, the general equilibrium equations developed by Shafranov[1] and Artsimovich[20] are fine for a steady-state, low poloidal beta ($\beta_p \sim R/a$) device. The equations are good for a zero dimensional model as long as β_p does not increase above R/a and cause serious internal deformations of the plasma and, possibly, the creation of a magnetic separatrix within the plasma. The equations that describe the macroscopic plasma motion need to be greatly expanded to describe the dynamics of the magnetic flux surface motion within the plasma. Reference (19) is an equilibrium study of a plasma within two conducting shells. This represents a possible way to describe the reactor vessel as a distributed parameter current source instead of a single lumped parameter model. Hosea, et.al., broke the structure into essentially two regions; a fast wall constant thin shell and a slower wall constant vessel structure. What is needed in conjunction with this approach to magnetic field diffusion, is a free boundary solution method for MHD equilibria similar to the method used by Cenacchi and Taroni.[21] In reference (21), the MHD equilibria equations were solved numerically on a 50 x 50 grid that computed axially symmetric stable plasma configurations. This method gives detailed information about the magnetic

flux surfaces in stable equilibria. What is needed here is some way of describing the magnetic flux surface dynamics within the plasma while the plasma is not in a stable equilibria; i.e., during either a normal or abort shutdown.

All this should be able to describe the internal and external dynamics of the plasma. The present controller test has brought the zero dimensional code to an area where it is no longer valid. The so called abort shutdown is probably violently unstable at a certain β_p after some poloidal skin current time. But it can not be said with any certainty whether or not the limit to β_p is 5 or 15 and whether the skin time is .2 or 2 seconds. This further development of plasma MHD equilibria and dynamic equations is a prerequisite for further position control studies.

C. Controller Design

The most important aspect of the plasma position controller that needs further study and implementation is the dynamic estimation technique for $\beta_p + li/2$. There are two possible directions to pursue to try and develop a dynamic estimation technique.

One possible method is to infer the value of $\beta_p + li/2$ by measuring the response of the plasma to a perturbation in the vertical magnetic field. This is similar to the static estimation techniques of chapter 4, except that a better dynamic model of the plasma motion is needed. The perturbation on the vertical magnetic field could be a step impulse during the shutdown period. There are several problems with this. Figure (38) shows that the 2% settling time for a transient response is on the order of 25 msec. This is during a stable equilibrium and the question

is how long this settling time is during an unstable dynamic shutdown when all variables are changing. There will be at least a 30 msec lag introduced in the estimate of $\beta_p + li/2$. The control system response can be quickened by increasing the gain on the integrator. But further increase of the integrator gain will degrade its performance (increase overshoot) unless the bandwidth of the EF coil current regulator is increased. An increase in the regulator bandwidth means that a larger power supply is needed. There is also a limit on how fast the EF coils can be charged and not lose superconductivity. Presently the peak power required during the first 10 msec of the transient response is 120 MW_e when $\dot{I}_v = 12{,}300A\ s^{-1}$. This gave a peak field rise of 9KG/sec. in the superconductor. Trying to reduce the lag further when using a perturbation technique will necessitate even larger power supplies - and that is an expensive trade off.

Another big problem with the perturbation method is the fact that the estimate is strongly dependent on the dynamic model of the plasma motion. It will be very difficult to separate model error from noise and disturbance error. The "abort" shutdown already has a large position error and the size of the magnetic field perturbation required for estimate information may degrade the performance even further.

The other possible method for estimating $\beta_p + li/2$ is to develop passive and/or active diagnostics to measure density, temperature and current distribution within the plasma and calculate poloidal beta and internal inductance directly. It would seem that an integrated density

measurement and an average temperature estimate could give a reasonable estimate for β. Magnetic loops can measure a total β_p and a value of β_p could then be calculated using equation (56).

The actual current distribution must be known to evaluate $l_i/2$. Probably some type of interactive laser or microwave interferometry techniques can be developed to give this information. This will require extensive data analysis to get this information in real time.

Between the two methods, it would seem that the diagnostic method holds more promise. The information obtained would also be needed for any interactive control system that will control burn cycle parameters.

The problem of ramping the plasma current down in a smooth, controlled manner will not be a trivial one. As mentioned in a previous section, the questions of current diffusion into the plasma is significant. Building a current regulator for the OH coils is a small problem compared to the questions of plasma stability. The Rogowski coils used to measure the total plasma current are a well developed state-of-the-art diagnostic. Maximum requires sampling rates will be on the order of .5 - 1 MHz[22] to insure sufficient information about the plasma current during all phases of the burn cycle. This does not present a significant problem.

Reference (14) indicates that the x-ray position detector being developed by AS&E has the possibility of providing fast, accurate information about the plasma position. Figure (43) shows a prototype being developed for ALCATOR C. The extension of this to an EPR is not without problems. The plasma parameter profiles in a large Tokamak may end up

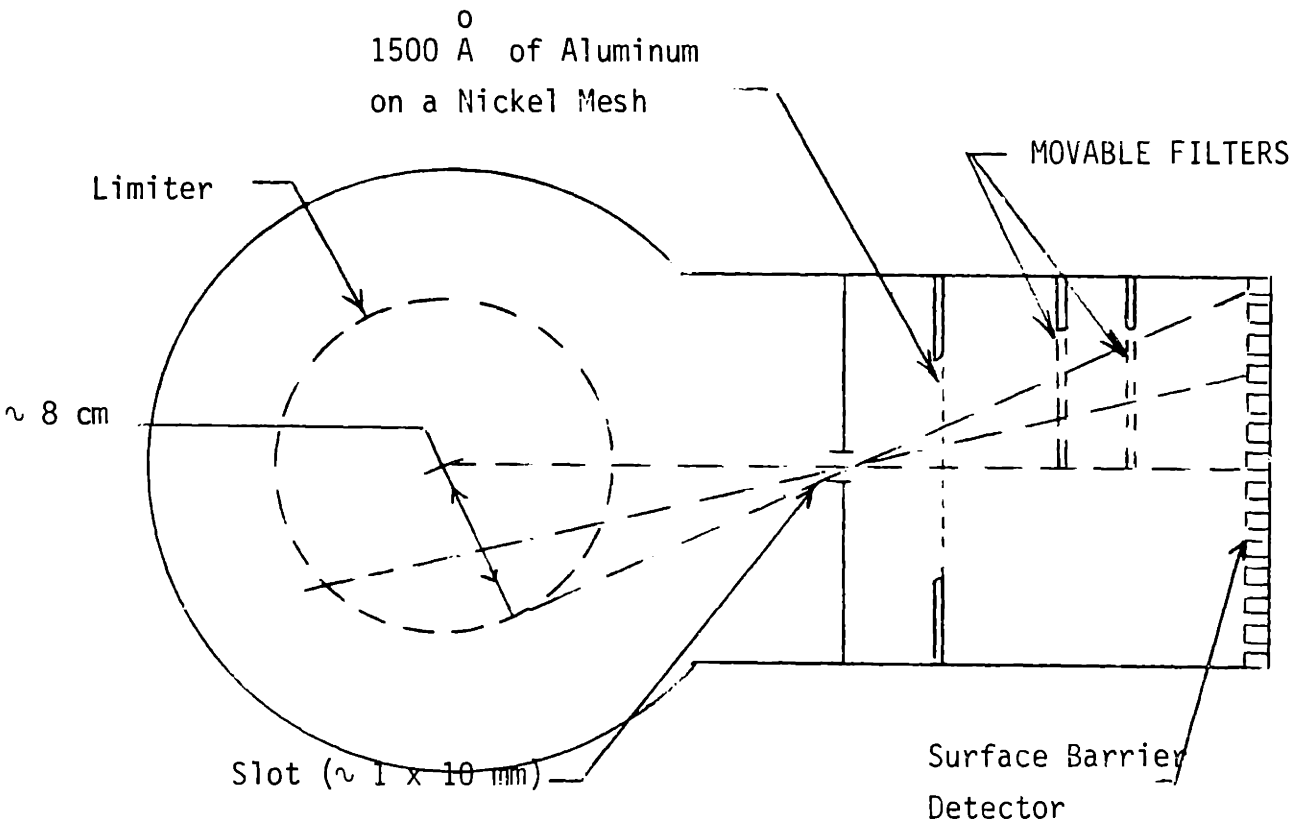

Figure 43 PROPOSED X-RAY POSITION SENSOR FOR ALCATOR C

being very broad peaks. This will make it difficult to resolve a particular point on the profile. There will be radiation frommany sources with a very wide spectral range. The detector will have to operate in an environment of intense radiation. These problems are not overwhelming, but they deserve care in their treatment.

With these tools to test and improve the plasma or position controller, it may be desireable to use a digital synthesis technique instead of a continuous time synthesis technqiue with basic controller design. A digital synthesis will more accurately show the effect of a digital controller implementation on the real control system. The difference equations of Chapter 4 just "digitize" the analog equations that describe the system dynamics. This model will not show the true effect of differences in sampling rates and computational time. Using a digital synthesis from the very beginning may lead to a different control design. An analog synthesis is sufficient for this study with the use of a zero dimensional computer code and lumped parameter equations. Analog synthesis techniques make it easy to visualize how the plasma is responding to different situations.

An optimization process should be carried out in parallel with the design synthesis. Just what criteria is to be optimized will depend on many questions of plasma physics and shutdown modes.

Another important question to be answered about future generation position control systems is the problem of interaction of the position con. ol system with the remainder of the reactor control system. Proposals such as MIMICS[25] envision integrated reactor control system that

may try and control several different plasma parameters at once. There must be knowledge of the interference one control system has on another.

This study has shown the basic feasibility of the CSDL candidate controller. The synthesis and test procedure is a good method for designing and testing the control system. This study represents the first generation of a plasma position control system that does not use a preprogrammed feedforward nominal EF coil current. A zero dimensional computer code can verify the basic operation of the control system, but a one dimensional code with appropriate physics is necessary for further progress on the plasma position control system.

List of References

1 V.S. Mukhovatov, V.D. Shafranov,"Plasma Equilibrium in a Tokamak", Nuclear Fusion, 11 (1971) p. 605.

2 J.M. Greene, J.L. Johnson, and K.E. WEimer, "Tokamak Equlibrium", Phys. Fluids, 14 (1971) p. 671.

3 S. Yoshikawa, "Application of the Virial Theorem to Equilibria in Toroidal Plasmas", Phys. Fluids, 7 (1964) p. 278.

4 W.M. Stacey, et al.,"Tokamak Experimental Power Reactor Studies", ANL/CTR-75-2, National Tevhnical Information Service, Springfield,

5 Ibid., p III-5.

6 Ibid., p II-33

7 T.N. Edelbaum, P.A. Madden, R.E. Var,"Fusion Reactor Control Study", First Annual Report, Charles S. Draper Labratories, Inc. (to be published)

8 G.H. Miley, et al.,"Fusion Cross Sections and Reactivities", University of Illinois, COO-2218-17, June 1974.

9 R.V. Miskell, "A Control Strategy For Plasma Equilibrium in a Tokamak", Oak Ridge Report No. Y-1988. August 1975

10 R.J. Collins, et al., "Feedback Control for Plasma Equlibrium in ORMAK", ORMAK Technical Memo No. 203, Oak Ridge National Labratory, September 1975.

11 J. Hugill and A. Gibson, "Servo-Control of Plasma Position in CLEO-TOKAMAK", Nuclear Fusion, 14 (1974) p. 611.

12 P. Madden, "1976 APS Conference", CSDL Internal Memo,Dec 1, 1976

13 L.T. Anderson, et al.,"Feedback Control for Plasma Position in ORMAK", Nuclear Fusion, 16 (1976) p. 629.

List of References (Continued)

14 M.M. Pickerell, "Radial Equilibrium of Toroidal Plasmas", S.B. Thesis, Department of Physics, Massachusetts Institute of Technology, June 1976.

15 J.F. Clarke and D.J. Sigmar, "Global Properties of High Flux Conserving Tokamak Equilibria",ORNL/TM 5599, August 1976.

16 K. Ogata, "Modern Control Engineering", Prentice-Hall, Inc., Englewood Cliffs, New Jersey. 1970.

17 S.V. Mirnov,Zh.Eksp.Teor.Fiz.Pis'ma Red 12,92 (1970) (JETP Lett 12,64 (1970))

18 C. Bobeldijk, D. Dimock, and J.C. Hosea, Bull. Am. Phys. Soc 16, 1232 (1971).

19 C. Bobeldijk and J.C. Hosea,"Equilibrium of a Toroidal Plasma inside Two Cocentric Conducting Shells", Phys Fluids, 16 (1973) p 1329.

20 L.A. Artsimovich "Tokamak Devices", Nuclear Fusion, 12 (1972) p215

21 G. Cenacchi, A. Sestero, and A. Taroni,"Numerical Solutions of the MHD Equilibrium Equation for an Axially Symmetric Free-Boundary Plasma in a Torus with Arbitrary Cross-Section" Il Nuovo Cimento, 25B, (1975) p. 279.

22 CSDL Report R-967, "Review of Princeton Large Scale Torus (PLT) Instrumentation and Control System", Charjes S. Draper Labratory, Inc. February 1976

23 G.W. Stuart and C.E. Wagner, "Tokamak Reactor Modelling", paper presented at ANS meeting, November 1976.

List of References (Continued)

24 N.A. Krall and A.W. Trivelpiece, "Principles of Plasma Physics", McGraw-Hill, Inc., New York, 1973

25 A Study of the Applications of Advanced Control Systems to Fusion Experiments and Reactors. Interim Report AEC Contract No. AT (11-1)-2418, C.S. Draper Laboratory, May 1974

26 M. Roberts, et al.,"Oak Ridge Experimental Power Reactor Study Reference Design", ORNL-TM-5042, Oak Ridge National Labaratory, November 1975.

27 S.M. Selby, "Standard Mathematical Tables",CRC Press, Inc., Cleveland, Ohio, 1974